# Targeting amyloidogenic immunoglobulin light chain aggregates with small molecules

Inaugural-Dissertation
to obtain the academic degree
Doctor rerum naturalium (Dr. rer. nat.)

submitted to the Department of Biology, Chemistry and Pharmacy
of Freie Universität Berlin

by
Young-In Ko
from Frankfurt a. M.
January, 2017

Die Arbeit wurde im Zeitraum von Oktober 2012 bis Dezember 2015 unter der Leitung von Herrn Prof. Dr. Erich E. Wanker am Max-Delbrück-Centrum für Molekulare Medizin in der Helmholtz-Gemeinschaft in Berlin-Buch angefertigt.

1. Gutachter: Prof. Dr. Erich E. Wanker

2. Gutachter: Prof. Dr. Markus Wahl

Disputation am 11.05.2017

# Danksagung

Ich danke Herrn Professor Erich E. Wanker für die Bereitstellung des Themas, für die finanziellen Mitteln, um an Konferenzen, Workshops und Retreats teilzunehmen und für die Begutachtung der Arbeit.

Bei Herrn Professor Markus Wahl möchte ich mich für das Gutachten dieser Arbeit bedanken.

Für die Betreuung der Arbeit danke ich ganz besonders Dr. Annett Böddrich. Vor allem danke ich Ihr für die zahlreichen Meetings und für die Unterstützung beim Planen und Koordinieren der Experimente.

Vielen Dank an Dr. Ute Hegenbardt und Dr. Stefan Schönland von der Universitätsklinik Heidelberg für die Bereitstellung der Patientenmaterialien.

Bei Daniela Kleckers und Nancy Neuendorf bedanke ich mich für die tatkräftige Unterstützung bei den experimentellen Arbeiten. Desweiteren danke ich Alexandra Redel für all die zahlreichen Tipps im Laboralltag und für den großen Erfahrungsschatz, den sie mit mir geteilt hat. Auch Gerlinde Grelle, Kirstin Rau und Lydia Brusendorf danke ich für die Hilfe im Labor und für das Beantworten aller technischen Fragen.

Außerdem bedanke ich mich bei Dr. Bettina Purfürst von der EM-Corefacility am MDC. Mit ihrer Unterstützung wurden die Elektronenmikroskopie-Bilder erstellt.

Dr. Alex Buntru, Dir danke ich für die unzähligen Hilfestellungen insbesondere in der Anfangszeit, für das Korrekturlesen der Arbeit und nicht zu vergessen für all die wundervollen gemeinsamen Urlaube.

Ich bedanke mich bei Dr. Philipp Trepte für die Hilfsbereitschaft und für das Korrekturlesen der Arbeit.

Dr. Thomas Wiglenda danke ich für die Hilfe an der HPLC und für alle Fragen zu den compounds.

Christian Hänig danke ich für die Hilfe bei allen Problemen mit Computern und Laborgeräten.

Bei meinen Mitdoktoranden Konrad Klockmeier, Nadine Strempel, Anne Steinhof, Carmen Lorenz, Anup Arumughan und bei meinem Office-Buddy Franzi Hesse bedanke ich mich für ein angenehmes Arbeitsklima und nicht zu vergessen auch für die gute Zeit außerhalb des Labors. Lisa Diez, danke für eine unfassbar schöne Zeit in Amsterdam und für die zahlreichen Stunden, die du mir zugehört hast. Danke, Simon Berberich, für eine lustige Zeit in Berlin.

Mein besonderer Dank gilt meiner Familie ohne die diese Arbeit nicht möglich gewesen wäre. Danke, Michel, für die gemeinsame Zeit.

## Zusammenfassung

Die Leichtketten (AL) Amyloidose ist durch die Ablagerung von extrazellulären Amyloidfibrillen im Gewebe charakterisiert. Kranke Plasmazellen im Rückenmark sind dafür verantwortlich, dass Leichtketten-Proteine überproduziert werden, die im Blut aggregieren und zur systemischen Infiltration von Organen und Geweben mit Leichtketten-Aggregaten führt. Das Herz und die Niere sind dabei am häufigsten betroffen. In über 50% der Fälle ist das Herz so stark infiltriert, dass es zu einer massiven Verdickung der Herzwände führt, was eine Herzinsuffizienz zur Folge hat. Die Behandlung der AL Amyloidose basiert auf der Zerstörung der verantwortlichen Plasmazellen mittels Chemotherapie, um die Vermehrung des Amyloids zu reduzieren. Diese Therapie stellt jedoch eine sehr aggressive Art dar, die für die instabilen Patienten nur schwierig zu tolerieren ist. Es gibt keine Therapie, die AL Amyloidose heilen kann. Daher werden dringend neue Therapie-Strategien gebraucht. Ein vielversprechender Ansatz ist das Amyloid mit kleinen Molekülen anzugreifen. Um dies zu realisieren, ist es notwendig, die pathogenen Leichtketten-Aggregate aus Patienten zu isolieren. Dazu wurden in dieser Arbeit Leichtketten-Aggregate aus dem Herzen eines Amyloidose-Patienten mittels Wasser-Extraktionsmethode aufgereinigt und systematisch charakterisiert. Die aus der vorliegenden Arbeit generierten Ergebnisse repräsentieren die erste detaillierte Studie, in der Leichtketten-Aggregate aus dem Herzen eines AL Amyloidose Patienten präpariert und sowohl biochemisch als auch biophysikalische charakterisiert wurden. Thioflavin T (ThT)- und Congo Rot (CR)-basierte Fluoreszenzassays zeigten, dass die präparierten Leichtketten-Aggregate aus β-Faltblatt-reichen Strukturen bestehen. Mittels Filtertests und Blau nativer Polyacrylamid-Gelelektrophorese (BN-PAGE) konnte gezeigt werden, dass diese Aggregate hochmolekulare lambda Leichtketten-Proteinkomplexe sind. Die Analysen mittels Natriumdodecylsulfat-Polyacylamid-Gelektrophorese (SDS-PAGE) und Western Blot ergaben, dass die Leichtketten-Aggregate unter denaturierenden Bedingungen nicht stabil sind. Desweiteren wurde mittels Elektronenmikroskopie (EM) gezeigt, dass Leichtkettenaggregate sowohl fibrilläre also auch amorphe Strukturen bilden. Untersuchungen an HeLa-Zellen ergaben, dass die Behandlung mit den isolierten Leichtketten-Aggregaten zu einer signifikanten Reduktion der metabolischen Aktivität der Zellen führte, was auf einen potentiell cytotoxischen Effekt hinweist.

Der zweite Fokus dieser Arbeit liegt darin, die präparierten Aggregate einer Wirkstofftestung zu unterziehen. Um wirksame Modulatoren zu identifizieren wurden die isolierten Leichtketten-Aggregate mit kleinen Molekülen behandelt und mittels ThT Assays analysiert. Dabei wurde Apomorphin als dasjenige Molekül identifiziert, das den β-Faltblatt-Anteil der Aggregate am effektivsten reduzierte. Weiterhin wurde der Effekt von Apomorphin mittels verschiedener biochemischen und biophysikalischen Methoden im Detail charakterisiert. Es konnte eine

zeitaufgelöste Veränderung im β-Faltblatt-Anteil und in der SDS-Stabilität der Leichtketten-Aggregate gezeigt werden. Desweitern deuten die Ergebnisse darauf hin, dass sich die Größe, die Oberflächenhydrophobizität und die Morphologie der Leichtketten-Aggregate in Gegenwart von Apomorphin verändern. Außerdem weisen Toxizitätsassays in HeLa-Zellen darauf hin, dass die durch die Leichtketten-Aggregate induzierte Reduzierung der metabolischen Aktivität durch Apomorphin möglicherweise aufgehoben wird. Damit konnte gezeigt werden, dass ein Wirkstoff-Screening gegen Leichtketten-Aggregaten aus Patientenmaterial eine mögliche Strategie darstellt, um neue potente Wirkstoffe zu identifizieren.

Darüber hinaus wurde die Aggregation des Volllängen-Leichtketten Proteins AL01 analysiert. Die Leichtketten Aggregate wurden mittels biochemischen und biophysikalischen Methoden charakterisiert. Die daraus resultierenden Ergebnisse zeigten, dass das Leichtketten-Protein AL01 β-Faltblatt-reiche, hochmolekulare Strukturen ausbilden, die SDS-löslich und amorph in der Struktur sind. Um den Effekt von Apomorphin auf Patienten-Aggregate zu bestätigen, wurden zusätzlich die rekombianten Leichtketten-Aggregate mit Apomorphin getestet. Dabei deuten die Resultate darauf hin, dass Apomorphin nicht nur Aggregate aus Patientenmaterial sondern auch *in vitro* generierte Leichtketten-Aggregate modellieren kann.

Zusammenfassend lässt sich sagen, dass im Zuge dieser Arbeit Leichtketten-Aggregate aus dem Herzen eines AL Amyloidose Patienten isoliert und charakterisiert werden konnten. Durch ein direktes Wirkstoff-Screening konnte ein potentieller Modulator gegen pathogene Leichtketten-Aggregate identifiziert werden und stellt damit einen wichtigen neuen Ansatzpunkt für weiterführende Studien dar.

## Summary

The deposition of amyloid fibrils has long been implicated as a pathological hallmark of immunoglobulin light chain amyloidosis (AL). In this devastating disease monoclonal plasma cell clones in the bone marrow overproduce immunoglobulin light chain proteins which form aggregates in the blood stream ultimately leading to the systemic infiltration of organs and tissues. The heart and the kidney are the two most affected organs. Cardiac involvement represents over 50% of all cases where the wall of the heart is heavily enlarged due to the immense load of amyloid deposition which causes cardiac arrhythmia and finally death. Current treatment is predominantly based in destroying the underlying B-cell clone using chemotherapy which is often too aggressive for the debilitated patients. Consequently, new therapeutic strategies are utterly needed. One promising approach is to target the amyloid deposition with small molecules. Targeting amyloid deposits requires the isolation of the latter from the affected organ. In this study, light chain aggregates were prepared from the heart of a patient with AL amyloidosis and were systematically characterized in terms of β-sheet content, size, SDS-stability and morphology. The results obtained from this study represent the first detailed biochemical and biophysical characterization of light chain aggregates isolated from the heart of a patient with AL amyloidosis. For purification, the water-extraction method established by Pras and coworkers was applied. Water-extracted material was analyzed by biochemical and biophysical methods. Thioflavin T (ThT) and Congo red (CR) assays showed that patient-derived light chain aggregates have a high β-sheet content. Results from the analysis by filter retardation assays (FRAs) and blue native polyacrylamide gel electrophoresis (BN-PAGE) indicate that patient-derived light chain aggregates contain high molecular weight lambda light chain structures. Furthermore, SDS-PAGE followed by Western blotting revealed that patient-derived light chain aggregates are non-SDS-stable structures. In addition, electron microscopy (EM) suggests that patient-derived light chain aggregates are fibrillar as well as amorphous in structure. Moreover, the investigation of patient-derived-light chain aggregates with the MTT assay showed reduced cell viability of HeLa cells, indicating a cytotoxic effect. The preparation of patient-derived light chain aggregates enables the evaluation of the targetability of patient-derived light chain aggregates in order to identify small molecules with a potential to remodel light chain aggregates which is another focus of this study.

In order to identify potent modulators against purified patient-derived light chain aggregates a small molecule screening was performed. Therefore, a ThT-based fluorescence assay was developed. Using

this assay the drug apomorphine was identified to be most effective in reducing the β-sheet content of patient-derived light chain aggregates. The effect of apomorphine was further characterized using a set of biochemical and biophysical techniques (CR assays, FRAs and 8-Anilino-1-naphthalenesulfonic acid (ANS) assays). These assays indicated that apomorphine may remodel the biochemical properties of heart-derived light chain aggregates and potentially affects their β-sheet content, SDS-stability, size, surface hydrophobicity and morphology. Furthermore, MTT assays provided experimental evidence that the metabolic activity of HeLa cells exposed to light chain aggregates could be rescued in presence of apomorphine, suggesting a rescuing effect of mitochondrial dysfunction.

In addition, the aggregation of a light chain protein was studied using the recombinant full-length light chain protein AL01 produced in *E. coli* and derived from a patient with excessive cardiac involvement. To this end, a ThT-based fluorescence assay was established for monitoring light chain AL01 aggregation. Recombinant light chain aggregates were further analyzed using a set of biochemical and biophysical techniques. The full-length light chain protein AL01 formed β-sheet rich, high molecular weight, SDS-soluble, amorphous aggregates *in vitro*. Subsequent studies with small molecules and preformed light chain aggregates showed that apomorphine is not only effective in remodeling patient-derived light chain aggregates but remodels also *in vitro* generated light chain aggregates.

Taken together, the preparation and characterization of patient-derived light chain aggregates enables the identification of novel agents opening up new routes for developing effective therapeutic strategies to combat AL amyloidosis.

# Content

## List of Figures

## List of Tables

## List of Abbreviations

| | |
|---|---|
| °C | degrees Celsius |
| Å | Angstrom |
| aa | amino acids |
| Aβ | amyloid-beta |
| AFM | atomic force microscopy |
| AHTC | anhydrotetracycline |
| AL | light chain amyloidosis |
| ANS | 1-anilino-8-naphthalenesulfonate |
| APO | apomorphine |
| ApoE | apolipoprotein E |
| a.u. | arbitrary units |
| α-syn | alpha-synuclein |
| β-MeEtOH | beta mercaptoethanol |
| BN | blue native |
| BSA | bocine serum albumin |
| *C. elegans* | *Caenorhabditis elegans* |
| CL | light chain constant domain |
| CR | Congo red |
| DNA | desoxyribonucleine acid |
| cDNA | complementary DNA |
| DTT | dithiothreitol |
| *E. coli* | *Escherichia coli* |
| EGCG | (–)-Epigallocatechin gallate |
| EGC | (–)- Epigallocatechin |
| EC | (–)- Epicatechin |
| EM | electron microscopy |
| FCS | fetal calf serum |
| FRA | filter retardation assay |
| GndHCl | guanidine hydrochloride |
| GST | glutathione S-transferase |
| HCl | hypochloride |
| HD | Huntington's disease |
| Htt | huntingtin |
| IAPP | islet amyloid polypeptide |
| IB | inclusion body |
| IPTG | isopropyl β-D-1thiogalactopyranoside |
| KCl | potassium chloride |
| kDa | kilodalton |
| LB | Luria Betani |
| MES | 2-(*N*-morpholino)ethanesulfonic acid |
| mg | milligram |
| min | minutes |

| | |
|---|---|
| mL | Milliliter |
| µg | microgram |
| µl | microliter |
| µM | micromolar |
| mRNA | messenger RNA |
| MTT | 3-(4,5-dimethylthiazol-2-yl)-2,5-diphenyltetrazolium bromide |
| MWCO | molecular weight cut off |
| NaOAc | sodium acetate |
| ng | nanogram |
| nm | nanometer |
| OD | opical density |
| PAGE | polyacrylamide gel electrophoresis |
| PBS | phospate buffered saline |
| PCR | polymerase chain reaction |
| PVDF | polyvinylidene difluoride |
| ROS | reactive oxygen species |
| rpm | revolutions per minute |
| RT-PCR | reverse transcriptase PCR |
| SAP | serum amyloid P component |
| SDS | sodium dodecyl sulphate |
| TAE | tris-acetate buffer containing EDTA |
| ThT | Thioflavin T |
| Tris | Tris(hydroxymethyl)aminomethane |
| VL | light chain variable domain |
| $ZnCl_2$ | zinc chloride |

# 1. INTRODUCTION

## 1.1 Protein folding, misfolding and aggregation

Proteins play a role in virtually every biochemical process and are essential for the existence of all living organisms[1]. Being the most abundant macromolecules in living systems, they are involved in a lot of different biological functions, such as catalyzing metabolic reactions as enzymes, DNA replication in form of transcription factors and giving the cell a structure as cytoskeletal proteins[1]. Different proteins are distinguished primarily by the specific order of amino acids in the polymeric sequence, which is dictated by the nucleotide sequence of their corresponding genes. Approximately 100 000 different types of proteins within our bodies are generated from a pool of overall 20 amino acids[2]. Proteins rapidly fold into a well-defined functional three-dimensional structure during or after synthesis in the cytoplasm or in the endoplasmatic reticulum (ER) of a cell (Fig. 1.1). This is essential in order to achieve the functionally active form. However, under destabilizing conditions proteins do not fold correctly into their native structure. Destabilization can be mediated by intrinsic or extrinsic factors, such as mutations[3-6] or exposure to heat[7,8], high pressure[9,10] and low pH[11,12], respectively. When a soluble peptide or protein becomes misfolded or partially folded, hydrophobic regions previously buried in the interior are exposed to the surface eventually resulting in the assembly of multiple misfolded proteins into larger, often insoluble complexes. This process is known as protein aggregation[13].

Protein aggregation leads to two major forms of aberrant aggregates: amyloid fibrils and amorphous aggregates[14]. Amyloid fibrils are characterized by a unique structural organization resulting in a filamentous or fibrillar cross β-sheet structure with high thermodynamic stability[15,16]. They are strongly associated with severe disease as discussed in further detail below. Conversely, amorphous aggregates are formed by non-specific aggregation of proteins into complexes without ordered intermolecular interactions. This type of aggregate is, for instance, mostly responsible for the precipitation of proteins when changing buffer conditions during recombinant protein purification. Amorphous aggregates are also formed when amyloidogenic proteins fail to form amyloid fibrils, and are associated with diseases, such as light chain deposition disease (LCDD)[17,18] or age-related nuclear (ARN) cataract[19].

Nature has evolved a biological machinery to orchestrate protein folding in order to maintain protein homeostasis, or proteostasis[20]. This is essential since the cytoplasm of a living cell is a crowded environment with a protein concentration ~300-400 mg/ml, a condition in which misfolding and

aggregation is favored[21,22]. The quality control machinery consists of an integrated network of several hundred proteins, including molecular chaperones, the ubiquitin-proteasome system (UPS) as well as the autophagy system[23]. Chaperones are proteins that assist newly synthesized polypeptide chains to acquire its functional folding. One of the many members is the family of heat shock proteins (HSPs), such as HSP40, HSP60, HSP70, HSP90 and the small HSPs, classified according to their molecular weight[20]. When the activity of chaperons is insufficient to ensure proteostasis, the UPS or the autophagy systems mediate the removal of irreversibly misfolded and aggregated proteins[24]. Misfolded proteins recognized by the UPS are ubiquitinated and safely degraded by the proteasome or in case of autophagy-mediated proteolysis by the lysosome[25,26]. Despite these efforts to maintain protein homeostasis, the ability of the cell's control system can be defective, impaired or overwhelmed, especially with ageing[13]. The resulting accumulation of misfolded protein is strongly linked to the development of protein misfolding diseases which will be introduced below.

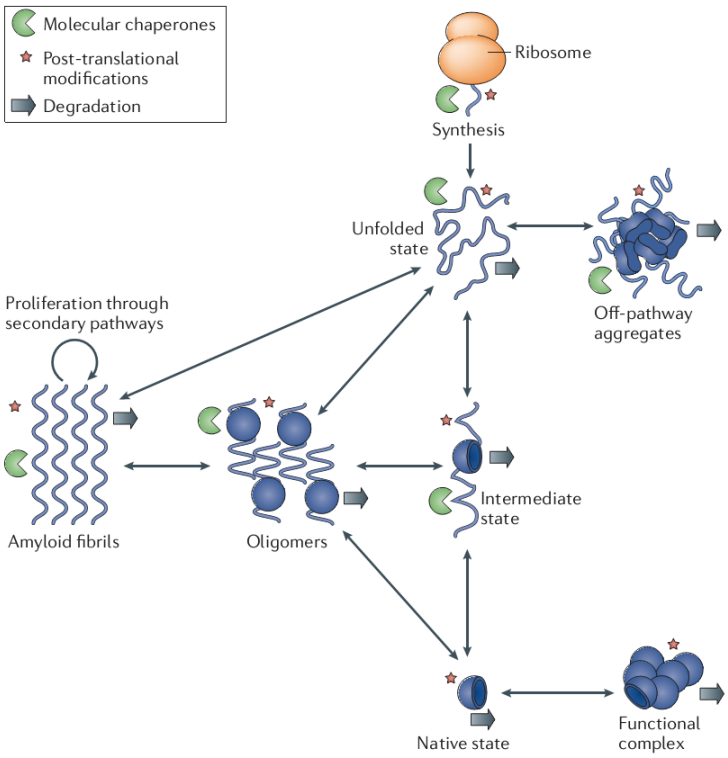


**Fig. 1.1 Transition of natively folded protein to amyloid.**

In cells soluble peptides or proteins are folded during or after synthesis on the ribosome in order to convert into their functional native state. Under destabilizing conditions, however, peptides or proteins can undergo misfolding leading to the formation of misfolded or partially folded conformers. These protein structures become prone to self-association that ultimately leads to the formation of protein aggregates. These aggregates can have a highly ordered conformation with a β-sheet structure and are known as amyloid fibrils. Aggregates without ordered structures are called disordered, amorphous or off-pathway aggregates. (Scheme taken from Knowles et al., 2014[27]).

## 1.2 Protein misfolding diseases and amyloidosis

Protein aggregation has long been associated with several diseases collectively known as protein misfolding diseases, including systemic amyloidoses and neurodegenerative diseases[28,29]. These disorders are characterized by the misfolding of a specific protein that renders the native state to a more amyloidogenic conformation by exposing intrinsically buried hydrophobic amino acid side chains to the surface. Hence, these partially unfolded proteins become prone to self-association that eventually leads to the formation of protein aggregates.

A group of protein misfolding diseases, referred to as amyloid diseases or amyloidoses, is characterized by the extracellular deposition of insoluble protein aggregates, resulting in progressive damage of the structure and function of the affected tissue or organ ultimately leading to death[30]. The amyloid diseases are a heterogeneous group of pathologies that can derive from a lot of different amyloidogenic proteins. At present, over 30 different amyloid proteins have been identified. A selection of these amyloid proteins and the corresponding diseases are listed in Tab. 1.1

Amyloidoses can be either localized or systemic depending on the synthesis of the precursor proteins and the affected organs or tissues[31]. Neurodegenerative disorders, such as Alzheimer's, Huntington's and Parkinson's disease, belong to the localized amyloidoses where the amyloid deposits occur exclusively in the organs or tissues of precursor protein synthesis[32]. In contrast, in systemic amyloidoses the amyloidogenic proteins are solely produced at a site distant from the infiltrated organ[33]. Thus, many different organ systems can be involved. The types of systemic amyloidoses are categorized as primary (AL), secondary (AA) and hederitary (ATTR, ApoA (I, II, IV)). The nomenclature of the various forms of amyloidoses derives from the composition of the letter A for amyloid, followed by a suffix that is an abbreviated form of the amyloidogenic protein name[34]. For instance, AL is the amyloid derived from immunoglobulin light chain protein and AL amyloidosis is the respective disease.

**Tab. 1.1 Different types of amyloidoses.**

| Disease | Aggregating protein or peptide |
|---|---|
| *Neurodegenerative diseases* | |
| Alzheimer's disease | Amyloid β peptide (Aβ), tau |
| Huntington's disease | Huntingtin (HTT) with polyQ expansion |
| Parkinson's disease | α-synuclein |
| Spongiform encephalopathies | Prion protein (PrP) |
| Amyotrophic lateral sclerosis | Superoxide dismutase 1 (SOD1), Transactive response DNA binding protein 43 kDa (TDP43) |
| *Nonneuropathic systemic amyloidoses* | |
| Immunoglobulin LC amyloidosis (AL) | Immunoglobulin light chains or fragments |
| Reactive amyloidosis (AA) | Serum amyloid A protein fragments (SAA) |
| Hemodialysis-related amyloidosis | β2-microglobulin ($\beta_2$m) |
| Familial amyloidosis (ATTR) | Mutant transthyretin (TTR) |
| Senile systemic amyloidosis | Wild-type transthyretin |
| ApoA(I, II, IV) amyloidosis | N-terminal fragments of apolipoprotein A(I, II, IV) |
| *Nonneuropathic localized diseases* | |
| Type 2 diabetes | Islet amyloid polypeptide (IAPP) |
| Injection-localized amyloidosis | Insulin |
| Cataract | γ-crystallin |

## 1.3 Amyloid fibrils - history, structure and properties

First described by Rokitansky in 1842 as a homogeneous, eosinophilic, extracellular material, the term “amyloid” was introduced by the German physician Rudolph Virchow[35]. He investigated the corpora amylacea of a patient brain and found small round deposits that changed the color form brown to blue when stained with iodine and sulfuric acid[36]. This tinctorial properties reminiscent of starch lead to the term amyloid, derived from the Latin word “amylum” and the Greek “amylon” for “starch-like”. Virchow expanded his studies and included tissues corresponding to what is nowadays known as systemic amyloidosis of the AA type and found similar staining properties as had been observed with corpora amylacea. Despite the misleading association to starch, the term is still used.

## 1.4 Preparation and characterization of amyloid fibrils

Preparation and biochemical as well as biophysical characterization of amyloids from biological tissues, together with their histological and immunohistochemical analysis are important in studies of the pathogenesis of amyloidoses particularly because they revealed the properties of amyloid fibrils that are formed *in vivo*[37]. Early works by Shirahama and Cohen were restricted to the analysis of the fibril morphology due to the fact that the highly insoluble amyloid could not be prepared in a soluble form[38,39]. Pioneering work has been done by Pras and coworkers who introduced the water-extraction method for purifying amyloid fibrils in a water soluble form[40]. Since then this method has been universally used for the extraction of almost all types of amyloids, except Aβ[41,42], Htt[43] and PrP[44], opening new routes of analyzing amyloids[45,46]. The method is based on the observation that amyloid fibrils precipitate under physiological conditions but are soluble in distilled water. Repeated homogenization of amyloid-laden tissue and centrifugation steps first in saline remove salt soluble proteins[40]. The same procedure in water then leads to supernatants containing amyloid fibrils in a water-soluble form. Using this method new amyloid proteins, such as AA-type amyloid fibrils[47] and TTR amyloid fibrils[48], could be identified and studies were initiated to characterize fibrils more precisely, in terms of physical, chemical and ultrastructural properties. Furthermore, it enabled the comparison of amyloid preparations derived from different organs and patients[49,50]. Pras and coworkers, for instance, described comparative studies of nine patients with amyloidosis[49]. Amyloids were prepared from spleen, liver, lymph node, tongue and kidney. These studies suggested that amyloid fibrils from different individuals resemble each other but are not identical. Differences in the chemical composition, in the ultrastructure, as well as in the antigenic properties were observed. In another investigation, Gliozzi and coworkers have described the ultrastructural organization of *ex vivo* amyloid fibrils isolated from the transplanted hearts of two patients affected by systemic amyloidosis caused by the Leu174Ser apolipoprotein A-I variant[51]. Using a modified version of the water-extraction method in combination with AFM, they showed that the purified material consists of fibrils and globular aggregates. Moreover, fibril diameters obtained for both patients were comparable. For AL amyloidosis, however, no detailed systematic biochemical characterization of isolated amyloid fibrils from affected heart tissue has been described so far.

## 1.5 Ultrastructure of amyloid fibrils

Over the past five years there have been remarkable advances in our understanding of the structure of amyloid fibrils using different sophisticated techniques such as electron microscopy (EM), atomic

force microscopy (AFM) and solid-state nuclear magnetic resonance (NMR) spectroscopy[52-54]. Despite the differences in size, structure and function of their precursor proteins, amyloid fibrils share a common ultrastructure[32]. In general, amyloid fibrils are straight, rigid and unbranched with diameters ranging from 6-12 nm in width, around 2 nm in diameter and up to several micrometers in length[55]. Typically, there are two to six protofilaments per fibril twisted around each other in a rope-like structure (Fig. 1.2)[56,57]. X-ray diffraction analysis has led to the description of the ordered core of amyloid fibrils as a cross-beta sheet structure (Fig. 1.2 d), where each protofilament results from a double row of beta-sheets whose strands run parallel to each other and perpendicular to the main fibril axis. Cross-beta structure is the main structural hallmark of amyloids and is thought to be responsible for the tinctorial properties typical for these assemblies[30].

Amyloid deposits also contain minor nonfibrillary constituents, including serum amyloid P component (SAP), apolipoprotein E (ApoE), connective tissue components, such as glycosaminoglycans (GAGs) and collagen[58-60]. Basic membrane components such as fibronectin and laminin are also integrated.

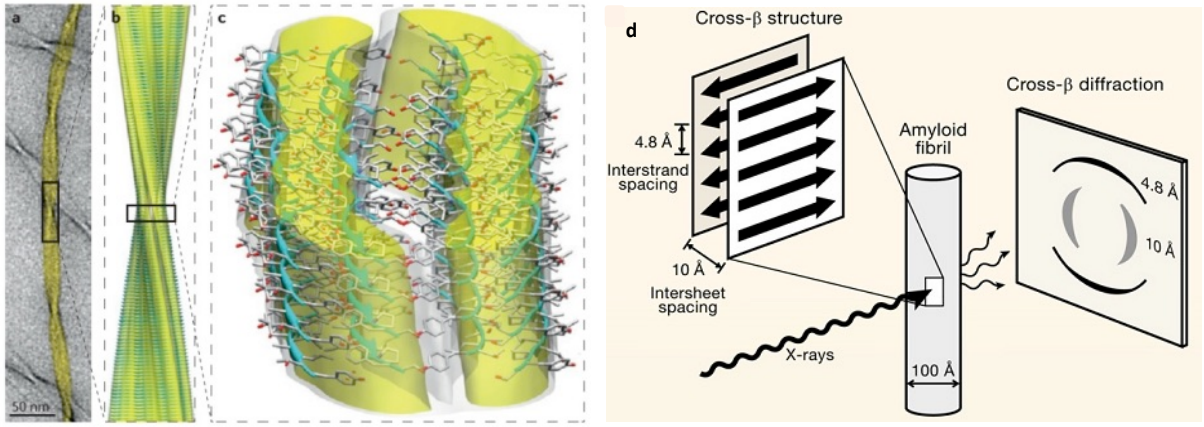


**Fig. 1.2 Structure of an amyloid fibril.**

(**a**) Cryo-electron microscopy image of an amyloid fibril formed from a transthyretin fragment[53]. (**b**) Solid-state NMR analysis of (a) resulted in the atomic resolution of the fibril. (**c**) A more detailed view of the amyloid fibril in (b). Fibril surfaces are shown as electron density maps, and the β-sheets in ribbon representation. Oxygen, carbon, and nitrogen atoms are shown in red, gray, and blue, respectively. (Images taken from Knowles et al., 2014[27]). (**d**) Amyloid fibril with a cross-beta sheet structure exposed to X-ray exhibits a characteristic cross-beta diffraction pattern. (Illustration taken from Eisenberg and Jucker, 2012[61]).

The specific, highly ordered cross-β ultrastructure of amyloid fibrils enables their identification using dyes such as Congo red (CR) and Thioflavin T (ThT) that both change their fluorescent properties upon binding to such structures. CR (Fig. 1.3 A), a diazobenzidine sulfonate dye, stains amyloids red and produces green birefringence when viewed under cross-polarized light[36]. Since 1920, this dye is the histological gold standard for confirming the presence of amyloid in tissue samples[62]. *In vitro*

quantification of amyloids can be performed using absorption spectroscopy[63-65]. However, CR is not well suited for monitoring aggregation *in vitro*, since the dye interferes with the process of protein misfolding and aggregation, and is reported either to inhibit or enhance amyloid fibril formation for several amyloidogenic proteins[66-70].

Naiki and LeVine have demonstrated in 1959 that, upon binding to fibrils, the benzothiazole dye ThT (Fig. 1.3 B) displays a dramatic shift in its excitation maximum (from 385 nm to 450 nm) and the emission maximum (from 445 nm to 480 nm)[71-73]. This is accompanied by a strong enhancement in its fluorescence. Based on these changes in its fluorescence properties upon binding to amyloid fibrils that do not occur on binding to the precursor polypeptides or amorphous aggregates, ThT is widely used in order to monitor fibril formation kinetics *in vitro*[74-77]. Since ThT does not remarkably affect the fibrillation kinetics, the aggregate formation can be probed by monitoring the increase in fluorescence as a function of time using a fluorescence plate reader[70]. Furthermore, it is one of the standard methods used to address the question whether compounds interfere with amyloid formation[78-86]. Furthermore, ThT is used to detect the presence of amyloid fibrils extracted from tissue samples[71]. Despite its extensive use as a molecular probe, the exact mechanism underlying the interaction of ThT with amyloid fibrils remains unresolved[87]. Positive ThT fluorescence is generally complemented by transmission electron microscopy and/or atomic force microscopy to confirm the presence of amyloid fibrils.

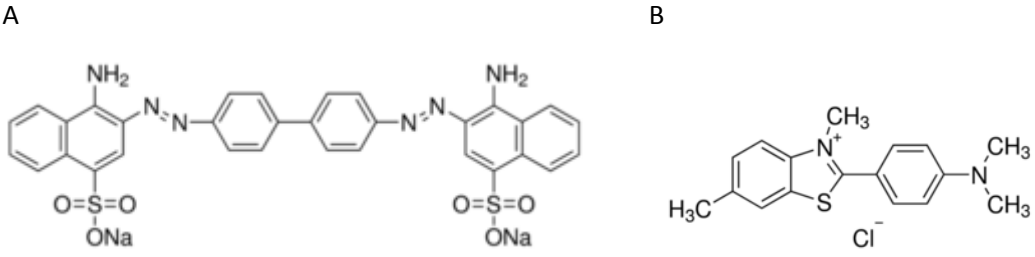


**Fig. 1.3 Chemical structure of Congo red and Thioflavin T.**

**A** CR is the sodium salt of 3,3′-([1,1′-biphenyl]-4,4′-diyl)bis(4-aminonaphthalene-1-sulfonic acid) and is typically used to confirm the presence of amyloid in tissue. **B** ThT is a benzothiazole dye that increases in fluorescence upon binding to amyloid and is therefore widely used as an *in vitro* reporter of amyloid formation.

## 1.6 The kinetics of fibril formation

Kinetic studies of amyloid formation are essential for understanding the molecular mechanism of the aggregation process underlying fibril growth[88]. It is also important in order to develop a systematic approach to explore strategies that inhibit or delay the process of fibril formation[27].

Fibril formation follows a nucleation-dependent process which mostly consists of three steps and follows a typical sigmoidal reaction time course (Fig. 1.4)[89]. The initial step is usually characterized by the presence of a lag-phase, corresponding to the time required for the conversion of monomers into critical nuclei that likely are small oligomers. This phase is a thermodynamically unfavorable process and, therefore, known to be the rate-limiting step. If preformed nuclei (seeds) are added to a solution of monomers, the lag-phase is shortened or abolished, a phenomenon known as seeding[90]. The lag-phase is followed by an exponential growth or elongation phase which is characterized by the rapid association of further monomers to the nuclei forming more complex structures such as protofibrils and mature fibrils. Finally, when all soluble molecules are depleted the reaction rate declines and the process reaches the plateau phase[91,92].

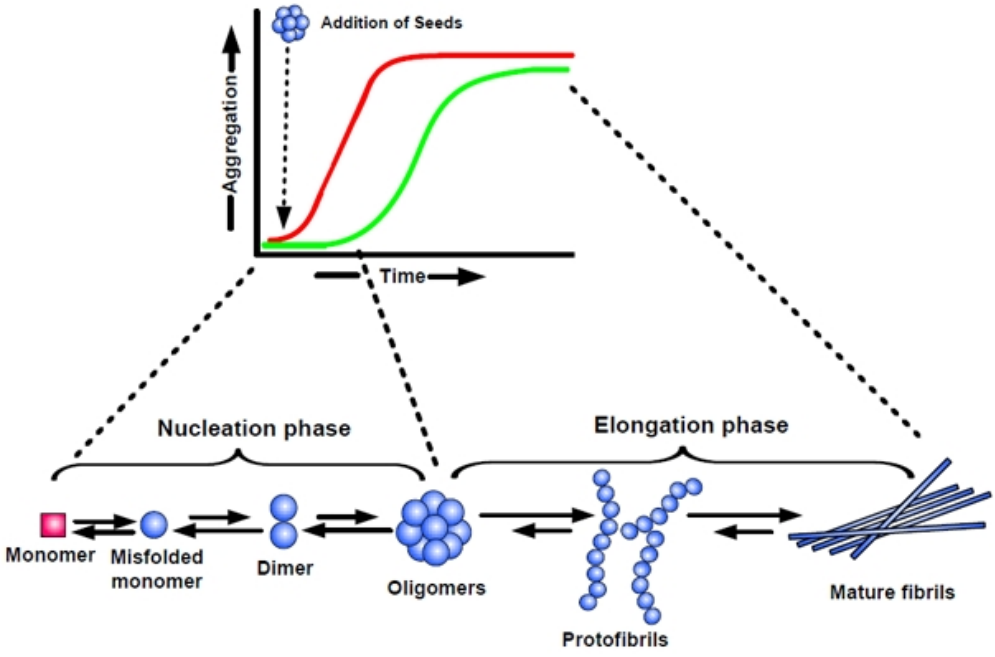


**Fig. 1.4 The sigmoidal growth profile of fibril formation.**

Fibril formation consists of three phases: nucleation/lag phase, elongation phase and saturation/plateau phase. In the lag-phase monomers undergo a conformational change and associate to form oligomeric nuclei. These nuclei rapidly grow in the elongation phase by further addition of monomers and form protofibrils and mature fibrils. When all monomers are depleted from solution the process reaches the plateau phase. Fibril formation follows a sigmoidal growth curve as the nucleation phase is thermodynamically unfavorable compared to the elongation phase which processes more quickly (green curve). The addition of seeds shortens the lag time resulting in faster aggregate formation (red curve). (Scheme taken from Kumar et al., 2011[93]).

## 1.7 AL amyloidosis

Among all systemic amyloidosis immunoglobulin light chain (AL) amyloidosis is the most common form with an annual incidence of 10 cases per million in the Western world[94]. In this disease, monoclonal immunoglobulin light chain proteins or light chain protein fragments are overproduced due to the excessive proliferation of an abnormal bone marrow plasma cell clone[32]. Light chain proteins are secreted into the blood stream and undergo misfolding, leading to the formation of insoluble amyloid fibrils that can deposit in the extracellular space of almost all organs except the brain (Fig. 1.5). AL amyloidosis is usually a systemic disease characterized by multiple organ and tissue involvement. The kidney is the most frequently affected organ followed by the heart and the liver[95-97]. Gastrointestinal tract, peripheral nerve, tongue, salivary glands, skeletal, muscle, joints, ligaments and skin can also be affected[98]. A selection of phenotypes of AL amyloidosis is shown in Fig. 1.7. The deposits may be present in the parenchyma of the viscera of tissues as well as in the walls of blood vessels throughout the body. AL amyloidosis is characterized by non-specific symptoms, i.e. loss of appetite, fatigue, weakness and weight loss making the diagnosis and typing very difficult. The median age of onset in AL amyloidosis is after the age of 40 and both genders are equally affected[99]. Patients with AL amyloidosis have a very poor median survival of around 6-15 months after diagnosis and a 10 year survival rate of <5% [96,100,101].

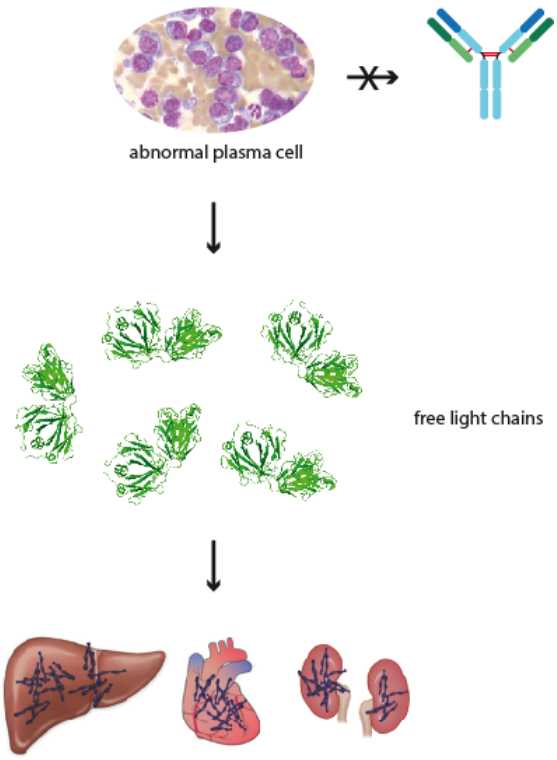


**Fig. 1.5 Schematic representation of fibril deposition in AL amyloidosis.**

Abnormal plasma cells (image taken form bloodjournal.org) in the bone marrow are not able to produce intact antibodies. Instead, free immunoglobulin light chains (image taken from ebi.ac.uk) are overproduced which promotes the formation of insoluble amyloid fibrils that infiltrate multiple organs and tissue, such as liver, heart and kidney (Image modified from Blancas-Mejias et al., 2013[32]).

Over 50% of the patients exhibit a cardiac involvement, the leading cause of morbidity and mortality not only in AL amyloidosis but also in both wild-type and hereditary transthyretin amyloidosis[102]. Amyloid fibril deposition causes stiffness of the myocardium and is a major cause of a cardiac dysfunction and arrhythmia[103] leading to a rapidly progressive form of cardiomyopathy and heart failure. The wall thickening can be monitored by recording an echocardiogram, a cardiac ultrasound. A typical echocardiogram from a patient with amyloidosis, in comparison with a healthy control, is shown in Fig. 1.6. In the AL amyloidosis patient (right), the walls of the heart are markedly thickened due to amyloid infiltration, resulting in a reduced size of the left ventricle (LV), the main pumping chamber, and a stiff heart, eventually with poor pumping function.

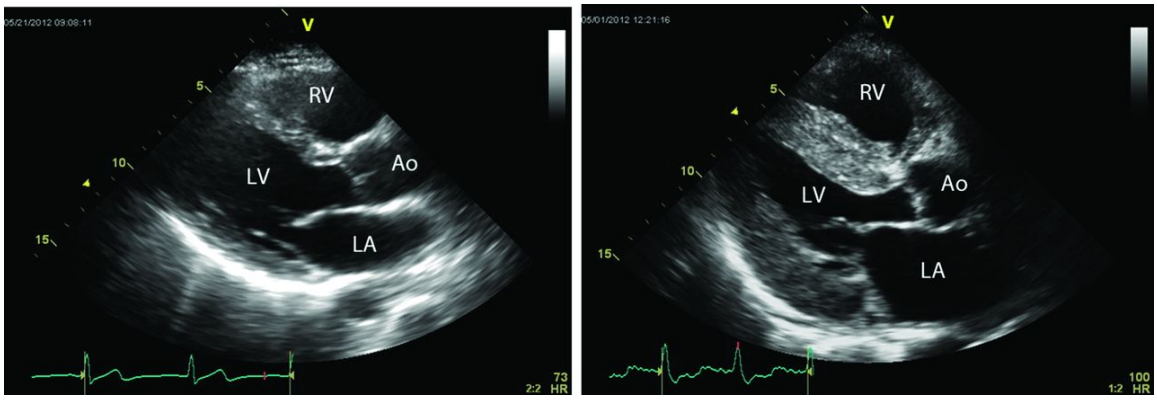


**Fig. 1.6 Echochardiogram of a healthy subject (left) and a patient with cardiac AL amyloidosis (right).**

The size of the left ventricle (LV) is markedly reduced in size due to the wall thickening resulting from amyloid deposition. Septum separating the LV from the right ventricle (RV) is thicker in the patient compared to the healthy heart. RV, Ao and LA indicate right ventricle, aorta and left atrium, respectively. (Images taken from Quarta et al., 2012[104]).

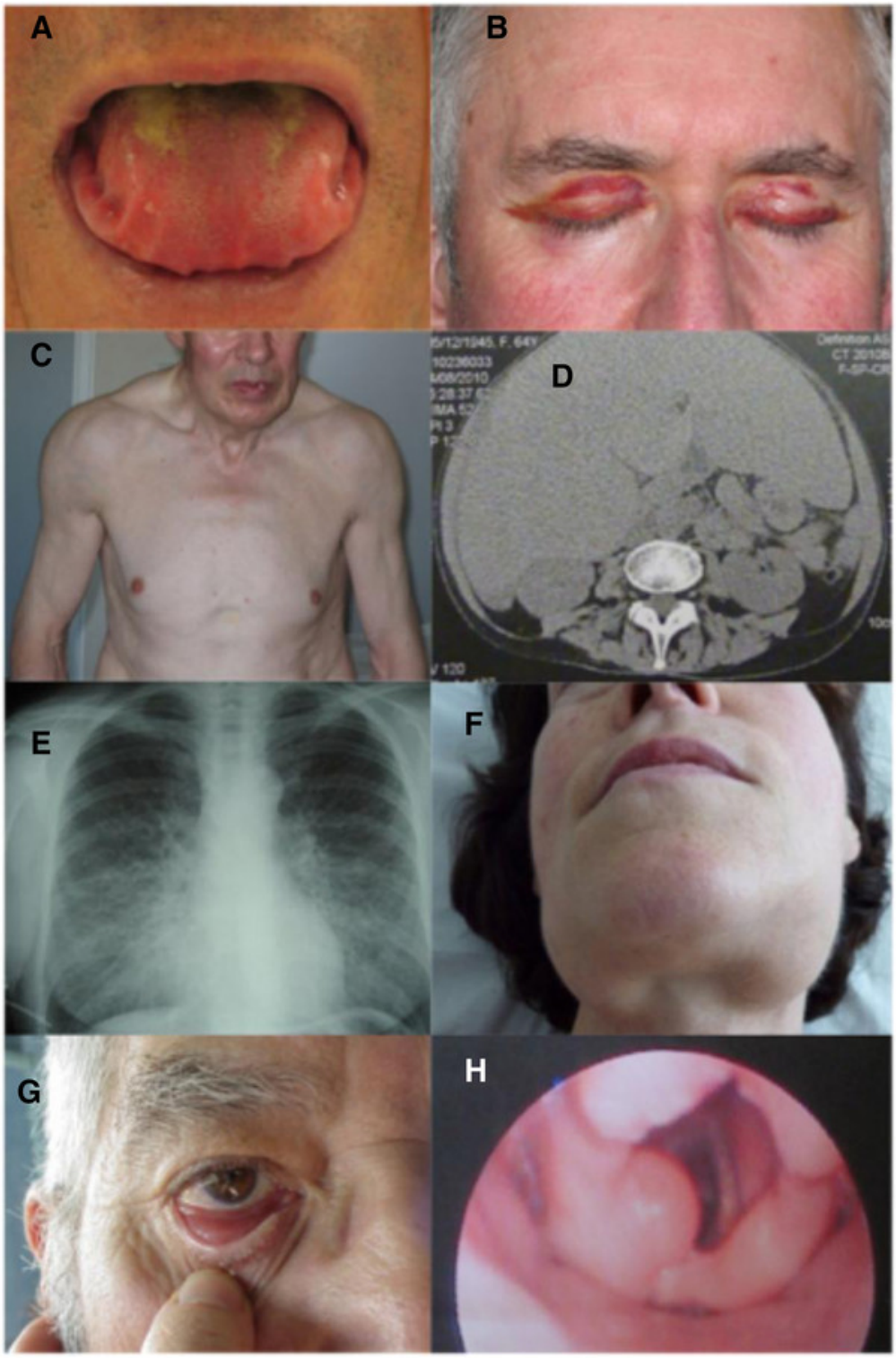


**Fig. 1.7 Phenotypes of systemic AL amyloidosis.**

**A** Macroglossia with lateral scalloping of the tongue. **B** Bilateral periorbital purpura. **C** Pseudo athletic appearance secondary to diffuse muscular infiltration. **D** Voluminous hepatomegaly due to primary hepatic amyloidosis. **E** Diffuse bilateral interstitial lung disease. **F** Submandibular gland enlargement. **G**-**H** Localized AL amyloidosis. **G** Nodular conjunctival amyloidosis. **H** Laryngeal supraglottic amyloid lump (Image taken from Desport et al. 2012[105]).

### 1.7.1 Immunoglobulins - structure and functions

Antibodies or immunoglobulins (Igs) consist of four polypeptides, comprising two identical heavy and two identical light chains joined to form a Y-shaped molecule (Fig. 1.8 A)[106]. Each chain is composed of structural domains called immunoglobulin domain. These domains contain ~70-100 amino acids and have a variable (V) domain at its amino terminus, which contributes to the antigen-binding site, and a constant (C) domain, which determines the isotype. Both Ig domains possess a characteristic immunoglobulin fold in which two antiparallel β-sheets create a β-sandwich, held together by interactions between two conserved cysteins and charged amino acids (Fig. 1.8 B). The V region is further subdivided into hypervariable (HV) and framework (FR) regions (Fig. 1.8 C). The HV region has a high ratio of different amino acids and is thus responsible for the diversity among antibodies. Within light and heavy chains, three hypervariable regions exist, which comprise three loops (Fig. 1.8 D), referred to as complementarity determining regions 1-3 (CDR1-3), which is important for antigen binding. Four conserved FR regions separate the HV regions and serve as a scaffold to hold the HV regions in position to the antigen.

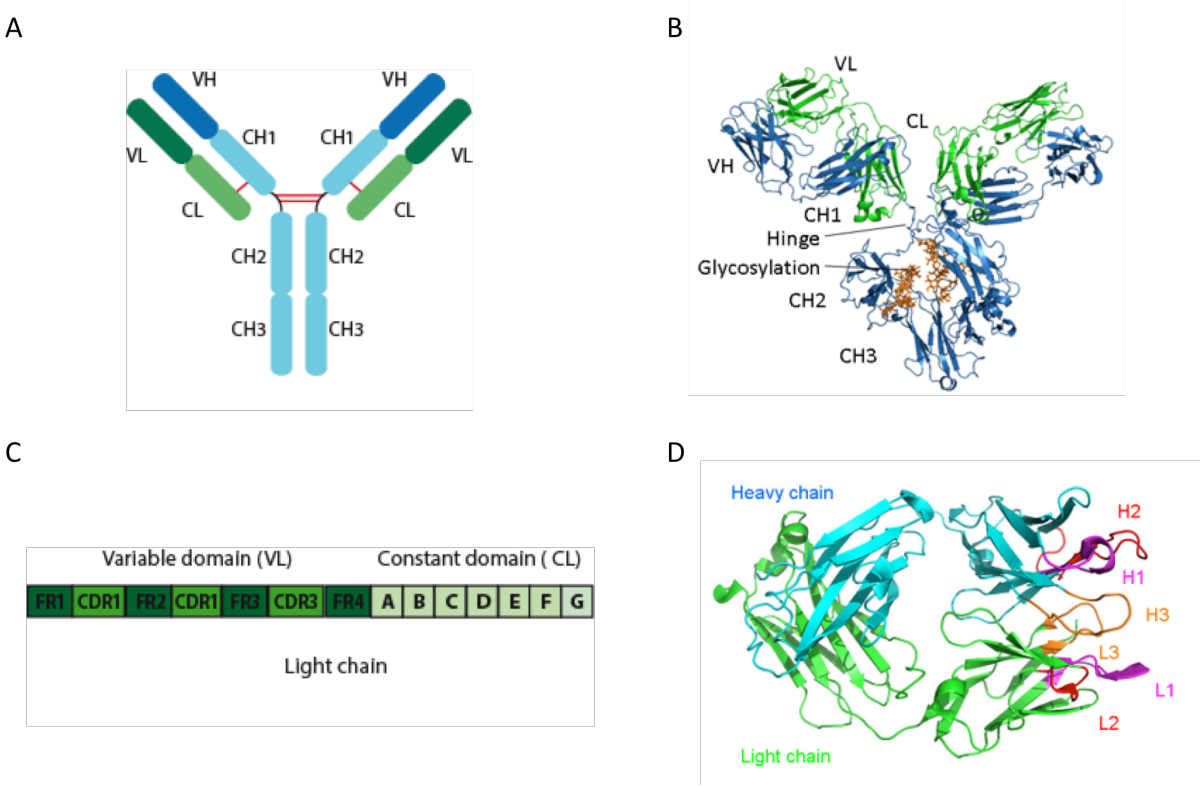


**Fig. 1.8 Structure of immunoglobulins.**

**A** Schematic representation of an immunoglobulin (Ig). A Y-shaped Ig molecule (~150 kDa) consists of two identical heavy chains (blue) and two identical light chains (green). Both chains are subdivided into a constant domain (light blue and light green) and a variable domain (dark blue and dark green). The constant domain of a

heavy chain consists of three different domains CH1, CH2, CH3. A disulfide bond (red line) interconnects heavy and light chain. The heavy chains are joined together by two disulfide bridges at the hinge region between CH1 and CH2. Antigen binding occurs at VH and VL. **B** Crystal structure (ribbon model) of an IgG1 antibody. Both Fab arms, each formed by a heavy and a light chain (~50 kDa), are attached by a flexible hinge region to the stem of the antibody, the Fc domain (~50 kDa). Glycosylation sites are shown in brown. (Image taken from http://absoluteantibody.com (PDB: 1IGY[107]). **C** Schematic representation of light chain domains. VL consists of three hypervariable complementarity determining regions (CDR1-3), evenly distributed between four less variable framework regions (FR1-4). CL is subdivided into seven units A-G. **D** Ribbon model of VH and VL comprising three hypervariable loops, providing a specific antigen recognition site on the surface of the antibody. CDR1 (magenta), CDR2 (red) and CDR3 (orange) of the heavy chain and light chain are represented as H1-3 and L1-3, respectively. (Schematic representation taken from http://dunbrack2.fccc.edu/PyIgClassify/).

In mammals there are only two types of Ig light chains, lambda (λ) and kappa (κ). The gene encoding the λ light chain is located on chromosome 22, the gene locus for κ light chain is found on chromosome 2. The approximate length of a light chain is 211 to 217 amino acids with a molecular weight of ~25 kDa[106,108]. Only one type of light chain, λ or κ, is present in one antibody. The ratio of the two light chain isotypes varies from species to species. In mice, the average κ to λ ratio is 20:1, whereas in human it is 2:1. Light chains are formed by random recombination of multiple gene segments (Fig. 1.9). They are constructed from over 30 potentially functional $V_\lambda$ and $V_\kappa$ light chain gene combined with four $J_\lambda$ (joining) or five $J_\kappa$ genes[109,110]. The random selection of V, J, C genes contributes to the diversity of light chains, resulting in the generation of ~3000 possible light chain variants[111]. In addition, somatic mutations lead to further sequence variation[112].

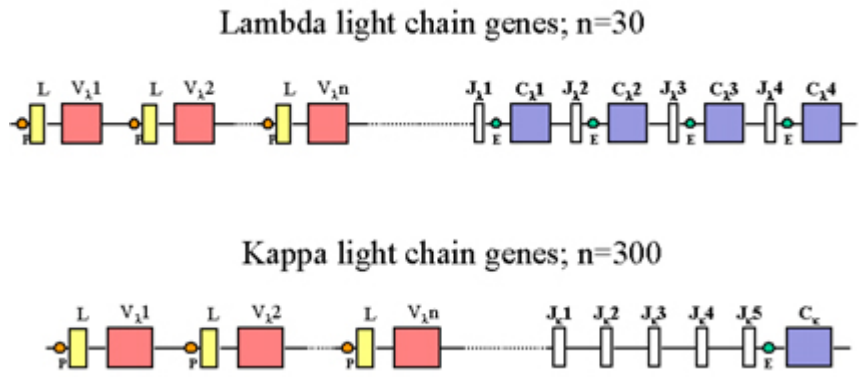


**Fig. 1.9 Organization of lambda (λ) and kappa (κ) light chain genes in the germ line.**

The lambda light chain gene family is composed of 4 C (violet) and 30 V (red) region genes. Each of the V genes is composed of two exons, one (L, yellow) that encodes for a leader sequence and the other (V) for most of the variable region. Upstream of each C gene a joining (J, white) gene is located. The kappa light chain gene family contains only one C region gene, but 300 V genes. 5 exons coding for J are located between V and C genes. Schematic representation taken from http://www.microbiologybook.org/mayer/IgGenetics2000.htm.

## 1.8 In search of the toxic amyloid species

Despite the longstanding knowledge that there is a close association of the appearance of amyloids with disease, the molecular mechanisms of how exactly amyloids lead to dysfunction and cytotoxicity are still elusive[113]. For most of the systemic diseases the simple presence of large quantities of amyloid deposits that disrupt the tissue structure and organ function seems likely to be the primary cause of clinical symptoms[27]. Thus, amyloids may well be the predominant toxic entity *per se*[61]. However, it cannot be excluded that other mechanisms also contribute to toxicity. In other cases, particularly the neurodegenerative diseases, mature amyloid fibrils are often considered to be less toxic, benign, or even protective with respect to cellular health[114]. In Alzheimer's disease, for instance, soluble Aβ species, including oligomers and prefibrillar assemblies, correlate better with the degree of dementia than the Aβ plaque load[61,115]. Evidence for cytotoxicity in systemic amyloidosis in general remains less well characterized compared to what has been shown for AD or PD. But in case of transthyretin-associated amyloidosis toxic oligomeric species have recently been identified[116]. No studies have been shown yet that light chain oligomers induced toxicity in AL amyloidosis patients. However, it has been reported that soluble light chain proteins isolated from the urine of patients can induce increasing oxidative stress and apoptosis in cardiomyocytes in the absence of detectable amyloid fibril formation[117,118]. Moreover, infusion of circulating light chains isolated from AL amyloidosis patients cause diastolic dysfunction in isolated mouse hearts and in a zebra fish model[119]. Recently, Wall and coworkers have demonstrated that *in vitro* generated light chain fibrils cause metabolic dysfunction in human cardiomyocytes[114]. Until now, no *in vitro* study has investigated the direct effects of patient-derived AL fibrils in cell culture. Clearly, addressing the role of purified amyloid fibrils from patients in cell-based assays should lead to a deeper understanding of toxicity.

## 1.9 Diagnosis of systemic amyloidosis

All forms of amyloid stain positively with CR, which is why CR staining of biopsied tissue remains the gold standard for detection of amyloid deposits since 1920[120]. Invasive organ biopsy is not required because amyloid deposits can be found in bone marrow biopsy or subcutaneous fat aspirate in ~85% of patients[121-124]. Deposits of amyloids stained with CR typically have a red color in bright-field microscopy and display a characteristic green birefringence when viewed under cross-polarized light[125,126]. CR is a planar aromatic dye and is known to intercalate between β-strands thereby changing its fluorescence intensity[63]. However, nonspecific reactions can sometimes lead to false-

positive results. Therefore, CR birefringence has been combined with immunohistochemistry (IHC) which remains the most widely available and routinely used method for amyloid typing[127]. However, certain drawbacks of antibody-based methods in amyloid typing indeed exist[128]. For instance, commercially available antibodies are typically raised against the native protein and may not recognize the protein in the amyloid state[129]. Recently, a novel antibody-independent technique for diagnosis and typing of amyloidosis was developed using laser microdissection combined with mass spectrometry[130,131]. Biopsy tissue specimens, positively stained with CR, are laser microdissected and subjected to trypsin digestion. The resulting peptide fragments were analyzed using liquid chromatography mass spectrometry (LC-MS). This method is based on the presence of high quantities of peptides from the amyloidogenic protein compared to apolipoprotein E and serum amyloid P component, which are both known constituents of amyloid. Using this proteomic approach amyloid types, such as AA, AL and ATTR, can be convincingly identified[128,132].

## 1.10 Current treatment options for amyloidosis

A reduction in the supply of amyloid precursor protein underpins all current treatment options for amyloidosis in order to arrest the progression of the disease[133,134]. This and other available strategies for amyloidosis in general are introduced bellow.

### 1.10.1 Lowering the amyloid fibril precursor protein production

The continuous production of amyloidogenic precursor protein results in the accumulation of fibrils and in the disruption of tissue structure and function. This can be tackled by the reduction of the supply in precursor protein production. In AL amyloidosis, high-dose chemotherapy in combination with stem cell transplantation is used to destroy the causative clonal plasma cells in the bone marrow and to replace them by blood forming cells[102,135]. However, this treatment strategy has only been successful in patients where only one organ is clinically involved which represents the minority of patients. Options for lowering the protein production of other amyloidosis are listed in Tab. 1.2.

**Tab. 1.2 Treatment options for amyloidoses.**

| Disease | Aim of treament | Example of treatment |
|---|---|---|
| AA amyloidosis | Suppress acute phase response | Immunosuppression in rheumatoid arthritis |
| AL amyloidosis | Suppress production of monoclonal light chains | Chemotherapy for myeloma and monoclonal gammopathy |
| Dialysis-related amyloidosis | Reduce plasma concentration of $\beta_2$M | Renal transplantation |
| Hereditary amyloidosis | Eliminate source of genetically variant protein | Orthotopic liver transplantation for variant transthyretin-associated FAP |

### 1.10.2 Inhibition of amyloid formation

Proteins with a compact, globular structure have to undergo unfolding prior to forming fibrils[136]. One approach for developing new therapies to treat protein misfolding disorders is the identification of agents that bind to an aggregation prone polypeptide and keep it from forming toxic assemblies[137]. Therefore, identifying chemical entities that stabilize the native conformation and thus prevent misfolding represents a promising strategy. The strategy of inhibiting fibril formation via native-state stabilization has been studied extensively for transthyretin amyloidosis in which transthyretin (TTR) represents the amyloidogenic protein[138]. TTR is a soluble tetrameric protein composed of 127 amino acids, primarily synthesized in the liver and serves as a transport protein for the thyroid hormones thyroxine (T4) and retinol (Vitamin A)[139]. The TTR aggregation process starts with tetramer dissociation into monomers leading to the formation of amyloid aggregates[136]. *In vitro* studies identified the compound Tafamidis (2-(3,5-dichloro-phenyl)-benzoxazole-6-carboxylic acid) as being effective in enhancing the stability of the soluble structure of TTR[140]. Tafamidis binds with high affinity to the TTR T4 binding sites thereby effectively stabilizing the dimer-dimer interface and decreasing the tetramer dissociation rate of both wild type and diverse pathogenic TTR variants.

### 1.10.3 Inhibition of SAP binding to amyloid fibrils

Serum amyloid P component (SAP), a plasma glycoprotein, is known to be an universal constituent of most known amyloid fibrils[141]. The universal presence of SAP in amyloids may stabilize the deposits[142]. Thus, promoting the depletion of SAP is a promising therapeutic option. (R)-1-[6-[(R)-2-carboxy-pyrrolidin-1-yl]-6-oxo-hexanoyl]pyrrolidine-2-carboxylic acid (CPHPC), a drug recently discovered through screening assays, cross-links pairs of pentameric SAP molecules and causes their rapid depletion from the circulation[143]. Consequently, new amyloid deposits were formed at lower frequency and the stability of the fibrils was reduced thereby facilitating degradation. Clinical trials using CPHPC are currently in progress for AA amyloidosis, AL amyloidosis, hereditary TTR amyloidosis, apolipoprotein AI amyloidosis, fibrinogen A amyloidosis, gelsolin amyloidosis, lysozyme amyloidosis and Alzheimer's disease[143-147].

### 1.10.4 Targeting amyloid deposits by immunotherapy - Enhancement of amyloid degradation

Amyloid deposits are remarkably stable[148]. Thus, clearance of amyloids is slow, especially in the heart[149]. Since amyloid fibrils do not promote an immune response, growing interest emerges in developing therapeutic antibodies that directly target amyloid deposits[150].

Currently, two promising antibody-mediated approaches are under investigation. Using an anti-light chain monoclonal antibody (mAb), 11-1FA, a neutrophil response in mice bearing human AL amyloidomas was elicited which resulted in a complete elimination of the amyloid tumors[150,151]. Another monoclonal antibody, mAb 2A4, initially described for imaging and therapy of AA amyloidosis, promoted the clearance of the amyloids by macrophage phagocytosis in mouse models of AL amyoidosis[12]. The humanized form of mAb 2A4, NEOD001, is currently investigated in phase 3 clinical trials[152].

The development of a therapeutic monoclonal antibody that is reactive to all types of amyloid is currently being addressed by targeting SAP, since it is found in most amyloid fibrils[141]. As CPHPC treatment does not deplete all circulating SAP molecules, it can be combined with anti-SAP antibody administration. Consequently, these antibodies localize to the residual amyloid-bound SAP thereby triggering the clearance of the deposits[15,16]. This approach recently entered a phase 1 trial and showed promising results with a marked reduction in liver amyloid deposits[135,153].

### 1.10.5 Current preclinical research approaches using small molecules

One important approach in the development of therapeutic agents is the use of small molecules that efficiently inhibit or even reverse the aggregation process[66]. Small molecules are low molecular weight (<500 daltons) organic compounds that bind to a specific biological target, such as proteins or nucleic acids, thereby altering the function of the target[154]. One advantage of small molecules over "large molecules" biologics is that they are generally cheaper and can be administered orally whereas biologics generally require injection.[155]. The small molecule approach is based on early findings that showed that small aromatic molecules, such as ThT and CR, specifically bind to precursor protein conformations and inhibit amyloid formation[66,156-158]. Since then intense research has been done in the field of protein misfolding diseases in order to identify small molecules with the ability to modify amyloid formation.

Interactions between amyloidogenic proteins can be viewed as stable protein-protein interactions and their disruption by small molecules represents a complex challenge[159-161]. Firstly, the contact surfaces involved in protein-protein interactions are large (~1,500-3,000 Å)[162,163] compared to those in protein-small molecule interactions (~300-1,000 Å)[161,164,165]. Thus, for small molecules of limited steric bulk it is difficult to prevent protein-protein interactions. Secondly, unlike enzyme inhibitors that represent the majority of drugs that have been developed over the last few decades, protein-protein interactions do not have natural small molecule partners[166]. Consequently, there is no small natural substrate or ligand as a starting point of drug discovery. In addition, according to the flatness of the contact surfaces of proteins they generally lack deep cavities that are typically associated with tight binding of a small organic compound to an enzyme[167]. Hence, small molecules that function by mimicking and displacing the naturally occurring interacting partner remain unperturbed. For amyloids, these issues are intensified by their exceptional stability, which generally require harsh denaturing conditions, such as 6 M GndHCl, or boiling in SDS to be disrupted[168]. Even more challenging is the ability of amyloidogenic proteins to form multiple aggregate species[169-172].

Despite these daunting challenges, in the last decade promising small molecule candidates were discovered that inhibit[105,173-175] and even reverse amyloidogenesis[159,176,177], although the mechanisms remain largely elusive. The majority of research focuses on Aβ and α-synuclein, but also transthyretin and the prion protein enter the compound screening world. Compounds that have been discovered to inhibit aggregation and to disassemble preformed fibrils are reviewed below.

### 1.10.6 Examples of small molecules inhibitors of amyloid formation

One of the most prominent small molecule in the amyloid world is the polyphenol (–)-epigallocatechin-3-gallate (EGCG) from green tea which has been ascribed to exert antioxidative, antiinflammatory, antitumorigenic and antiviral properties[178-181]. Recently, *in vitro* experiments have demonstrated that this polyphenol very efficiently inhibits the amyloidogenesis of various polypeptides, including Aβ, tau, α-synuclein, Htt, IAPP, TTR and also modulates prions[159,173,174,182-184]. Interestingly, EGCG can also disassemble a wide range of preformed amyloid fibrils[159,183,185-189]. Moreover, EGCG prevents Htt aggregation and toxicity in yeast and fly models of Huntington's disease (HD)[173]. Mereles and coworkers described a patient with systemic light chain amyloidosis who showed impressive cardiac and clinical improvement after therapy with daily ingestion of green tea[190].

Furthermore, other polyphenolic compounds, such as baicalein[78], curcumin[191] and apomorphine[63,159], were shown to be effective in the inhibition of fibril formation and exhibit also disaggregating properties[78,191]. The flavonoid baicalein inhibits the formation of α-synuclein fibrils *in vitro*[78]. In addition, existing fibrils of α-synuclein are disaggregated by baicalein. The phenolic yellow curry pigment curcumin inhibits the formation of Aβ oligomers and fibrils and disaggregates fibrillar $A\beta_{40}$ *in vitro*. *In vivo* studies revealed that curcumin binds to plaques and reduces amyloid aggregates in a mouse model[191]. Apomorphine, a synthetic polyphenol, inhibits α-synuclein and β-amyloid polymerization[82,192].

Although giant strides have been made in recent years in the field of AL amyloidosis, especially in exploring the kinetics and thermodynamics of light chain aggregation[32], very little research has been conducted in identifying compounds that directly target preformed or patient-derived light chain fibrils *in vitro*. In 2015 *in vitro* experiments have shown that EGCG very efficiently inhibits light chain fibrillogenesis[193]. Few months later another study was published in which small molecules were screened for an inhibitory effect on the formation of recombinant light chain fibrils[86]. Eisenberg and coworkers identified sulfasalazine and methylene blue as the two most potent inhibitors out of 27 hydrophobic and aromatic ligands using ThT fluorescence assays and EM analyses. Although recent research has demonstrated that the soluble light chain precursor protein induces cytotoxic effects in cell-based assays[117-119,194-196], in animal models[196-198] and in patient studies[199,200], experimental evidence was obtained that insoluble amyloid light chain fibrils are toxic structures that mechanically perturb organ function[32,114]. Clearly, extracellular amyloid fibrils create a physical barrier around cells that cause tissue damage[32]. In addition, a recent line of inquiry has demonstrated that preformed light chain aggregates formed by recombinant light chain protein induced metabolic dysfunction in

human cardiomyocytes, indicating a cytotoxic effect of light chain fibrils[114]. A key unaddressed issue in the field of AL amyloidosis, however, is whether small molecules can actively disrupt or remodel pathogenic immunoglobulin light chain fibrils in order to reduce or remove the overall amyloid load from affected tissues. A small molecule with this ability is desperately needed, particularly because amyloid deposition is advanced at the time point of diagnosis not only in AL amyloidosis but also in other amyloidoses.

## 1.11 Research objective

Precise identification and extensive characterization of amyloid fibrils are crucial in order to gain a better understanding of the pathogenesis of AL amyloidosis and to target the deposition with small molecules in light of the currently limited repertoire of therapeutic options. To this end, the present work attempts to answer whether light chain fibrils isolated from the heart tissue of an AL amyloidosis patient represent a "druggable" disease target. *En route* to targeting patient-derived light chain fibrils it should be evaluated beforehand whether light chain aggregates can be isolated from the heart which represents the most affected organ after the kidney. To the best of my knowledge light chain fibrils have never been purified particularly from heart tissue of an AL amyloidosis patient so far. Thus, the first question to be posed is whether it is possible to purify light chain fibrils from heart extensively infiltrated with amyloids. The systematic use of biochemical and biophysical methods should generate a detailed characterization of the isolated material to provide a deeper understanding of the biochemical properties of heart-derived light chain aggregates. Furthermore, the question whether patient-derived light chain aggregates induce toxicity should be investigated in a cell-based assay. Moreover, compounds that target light chain aggregates shall be identified *in vitro* using a ThT based assay. To further validate the effects of the most potent compound a set of biochemical and biophysical methods should be performed. The results obtained in this work may provide an important starting point for further small molecule design that may open new routes for tackling AL amyloidosis.

# 2. RESULTS

## 2.1 Diagnosis of AL amyloidosis using Congo red staining and immunohistochemistry

Heart material was obtained from the Amyloidosis Center at Heidelberg University Hospital in order to isolate light chain aggregates from a patient with AL amyloidosis. The heart was a transplant from a 50 year-old female AL amyloidosis patient with extensive cardiac involvement. Fig. 2.1 illustrates that the heart walls were severely thickened. It measured ~2 cm that is approximately 2-3-fold thicker compared to a normal heart (Fig. 2.1 B).

To confirm the presence of amyloids in the heart Congo red (CR) staining of tissue sections was performed in collaboration with the Amyloidosis Center at Heidelberg University Hospital and the institute of pathology in Kiel. CR staining is the gold standard for detecting amyloids and was first described by Puchtler et al. in 1965[201]. Amyloids stained by CR shows a green birefringence in polarized light which is an indication of the presence of amyloid fibrils. Two heart pieces (2.8 x 2.5 x 2.5 cm, 4x 2.7x 2cm) were analyzed in the laboratory of Prof. Dr. med. C. Röcken using CR staining. Fig. 2.1 C shows a microscopic image of a heart section positively stained with CR. As expected, amyloid deposits were stained red with nuclei stained blue. Furthermore, examination of the heart section under polarizing light resulted in the characteristic apple green birefringence of the amyloid using a polarized light microscope (Fig. 2.1 D). Strong staining intensities confirmed the extensive load of aggregated material in the heart.

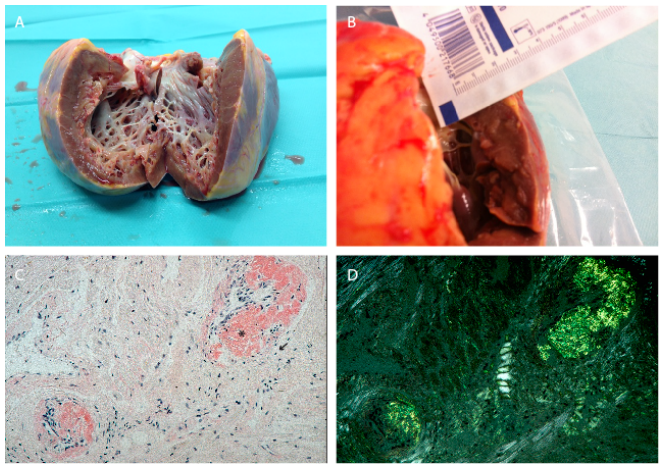


**Fig. 2.1 Congo red staining of the heart tissue of a patient with AL amyloidosis.**

**A** The heart was transplanted from a patient with AL amyloidosis. **B** The wall of the heart is clearly thickened. It measures ~2 cm that is 2 to 3-fold thicker compared to a normal heart. **C** Light microscope image of heart tissue from the AL amyloidosis patient stained with Congo red. Amyloid deposits stains red (asterisk) and the nuclei blue (arrow). **D** Green birefringence under polarized light confirms the existence of light chain amyloid in heart tissue. Pictures are from the Amyloidosis Center at Heidelberg University Hospital.

## 2.2 Isolation of light chain aggregates from the heart of a patient with AL amyloidosis

The extraction of the amyloids from the heart of an AL patient was performed as described by Pras et al.[40] and is shown in the flowchart of Fig. 2.2. The tissue was repeatedly homogenized first in NaCl, solutions, followed by homogenization in distilled water. The protocol is based on the physical characteristic that amyloids precipitate under physiological conditions, but are highly soluble in water. Once all salt soluble proteins are removed through repeated homogenization and centrifugation, amyloids can be finally isolated in pure water (see Materials and Methods section 4.2.2.1 for a detailed protocol). In total, four NaCl and four $H_2O$ supernatants were obtained.

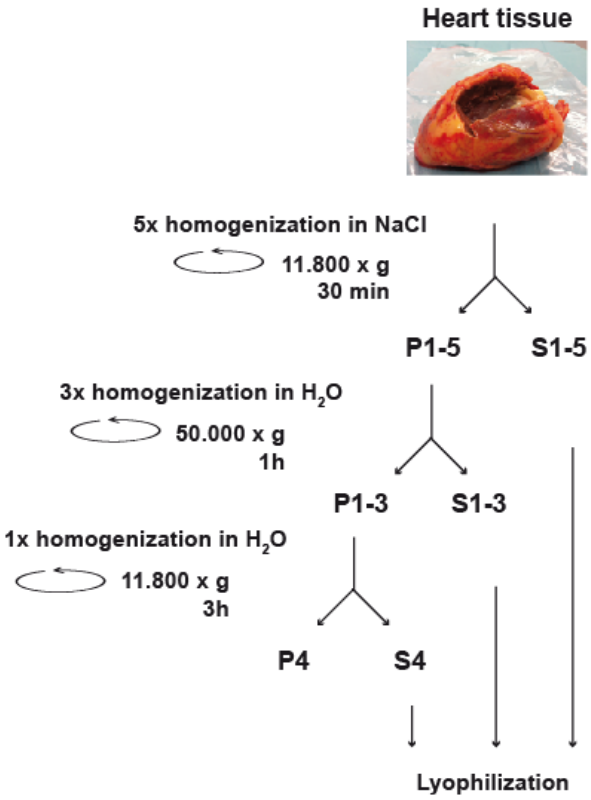


**Fig. 2.2 Extraction protocol of amyloids from the heart of a patient with AL amyloidosis.**

Schematic representation of the purification protocol used to isolate light chain aggregates from the heart of an AL amyloidosis patient according to the water-extraction method published by Pras et al.[1]. Heart pieces (~4 g) were homogenized first in 0.15 M NaCl followed by centrifugation at 11,800 x g for 30 min. The resulting supernatant (S) was decanted and saved for further analysis. The pellet (P) fraction was subjected to further homogenization and centrifugation. This step was repeated 5 times. Next, the pellet was homogenized in $H_2O$ and centrifuged at 50,000 x g for 1 h. This step was repeated 3 times. Finally, pellet 3 was further homogenized in $H_2O$ and centrifuged at 11,800 x g for 3 h. All supernatants were lyophilized at the end and stored at -80°C until further use.

## 2.3 Characterization of patient-derived light chain aggregates

### 2.3.1 Determination of the protein concentrations of $H_2O$ supernatants using BCA assay

To determine the protein concentrations in the prepared NaCl and $H_2O$ supernatants obtained from the amyloid containing heart, a bicinchoninic acid (BCA) assay was performed. The BCA assay, first described by Smith et al., is a method for measuring the total protein concentration in a solution[202]. The assay is based on the reduction of $Cu^{2+}$ to $Cu^{1+}$ by the peptide bonds of proteins and the colorimetric detection of the cuprous cation by BCA. Fig. 2.3 illustrates this reaction. The first step is the chelation of copper with protein in an alkaline environment to form a light green complex. In this reaction, known as the biuret reaction, peptides containing three or more amino acid residues form a complex with cupric ions. In the second step BCA reacts with the $Cu^{1+}$ to a purple reaction product with an absorbance maximum at 562 nm. Since the production of $Cu^{+}$ is a function of the protein concentration and the incubation time, the protein content is determined by comparison with known protein standards.

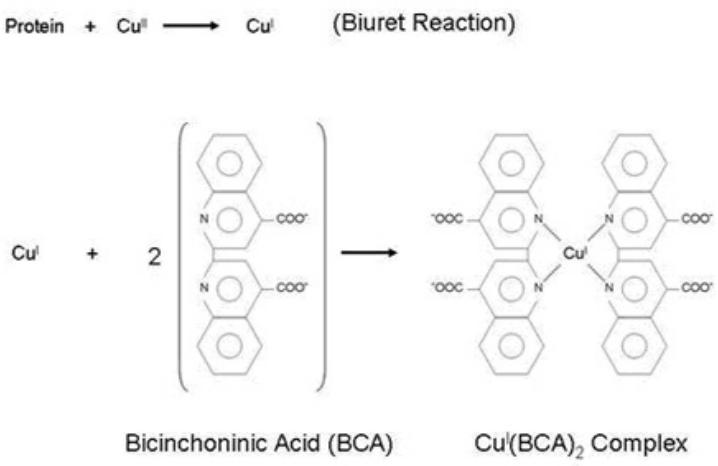


**Fig. 2.3 BCA reaction for protein quantification.**

In presence of proteins $Cu^{2+}$ is reduced to $Cu^{1+}$ which is known as the Biuret reaction. Bicinchoninic acid (BCA) reacts with $Cu^{1+}$ to a purple $Cu(BCA)_2$ complex. This complex strongly absorbs light at 562 nm and can be used for the estimation of the protein concentration by comparison with known protein standards.

In order to determine the protein concentrations of the different supernatants a reference curve using protein bovine serum albumin (BSA) was created. The BCA assay was performed as described in the Materials and Methods section 4.2.2.15 and measured protein concentrations are presented in Tab. 2.1. In total, the $H_2O$ supernatants 1-4 contained ~4 mg of protein, which corresponds to ~0.1% of potentially fibrillary material isolated from ~4 g starting material.

**Tab. 2.1 Protein concentrations of NaCl supernatants 1-3 and $H_2O$ supernatants 1-4 obtained from the extraction of the amyloid containing heart.**

| supernatant | c [mg/ml] |
|---|---|
| NaCl 1 | 7.96 |
| NaCl 2 | 1.52 |
| NaCl 3 | 0.92 |
| $H_2O$ 1 | 0.30 |
| $H_2O$ 2 | 0.89 |
| $H_2O$ 3 | 1.46 |
| $H_2O$ 4 | 1.40 |

### 2.3.2 Analysis of NaCl and $H_2O$ supernatants obtained from the heart of an AL amyloidosis patient using a native filter retardation assay

To assess whether the prepared fractions from the heart extraction procedure contain light chain aggregates NaCl and $H_2O$ supernatants were first analyzed using a native filter retardation assay (FRA)[203]. With this method high molecular weight aggregates can be detected on a cellulose acetate membrane. 2.5 µg of NaCl supernatants 1-3 and $H_2O$ supernatants 2-4 were spotted in triplicates on a filter membrane (0.2 µm pore size) which was then immunoprobed with an anti-lambda light chain antibody (A0101, Dako). As shown in Fig. 2.4 A and B, an enrichment of lambda light chain protein aggregates in the $H_2O$ supernatants 2-4 could be observed. Quantification of the dots in Fig. 2.4 B shows the highest amount of lambda light chain protein in the $H_2O$ supernatant 3. NaCl supernatants 1-3 and $H_2O$ supernatants 2-4 were also filtered through the membrane and analyzed with an anti-kappa light chain antibody (A0100, Dako). On this filter no detection of light chain aggregates could be seen, indicating that light chain aggregates do not consist of kappa light chains (Fig. 2.4 C). These results are in good agreement with the clinical data which diagnosed the patient as lambda positive. Taken together, $H_2O$ supernatants are highly enriched in lambda light chain-containing aggregated material.

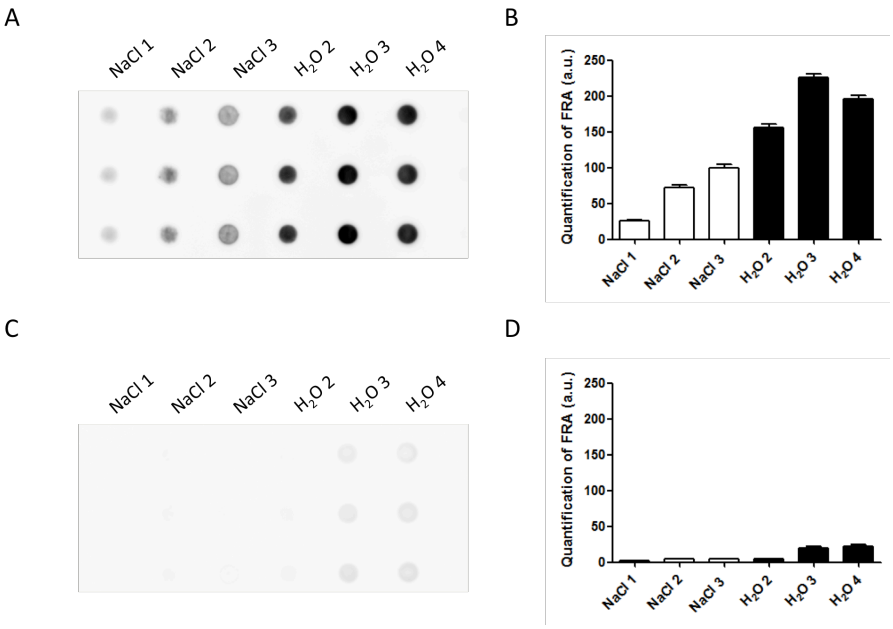


**Fig. 2.4 Characterization of NaCl and $H_2O$ supernatants obtained from the heart of an AL amyloidosis patient using native FRAs.**

**A** Enrichment of patient-derived light chain aggregates monitored by native FRA. 2.5 µg of NaCl supernatants 1-3 and $H_2O$ supernatants 2-4 were filtered through a cellulose acetate membrane and immunoprobed with a lambda (A0101, Dako) specific (**A**) and a kappa (A0100, Dako) specific (**C**) light chain antibody. **B**, **D** Quantification of patient-derived light chain aggregates from native FRAs, as shown in A and C, respectively. The immunoblots detected with the anti-lambda light chain antibody (A0101, Dako) showed that the $H_2O$ supernatant 3 contains the highest amount of lambda light chain aggregates.

### 2.3.3 Analysis of NaCl and $H_2O$ supernatants using native-PAGE and Western blotting

Next, Blue native (BN)-PAGE followed by Western blotting was used to examine the NaCl supernatants 1 -3 and the $H_2O$ supernatants 2-4. With this method the approximate molecular mass of native protein complexes can be estimated[204]. 5 µg of the NaCl supernatants 1-3 and the $H_2O$ supernatants 2-4 were loaded onto a native gel and separated by electrophoresis. Proteins were then transferred to a polyvinylidene fluoride (PVDF) membrane using Western blotting[205]. For immunological detection an anti-lambda light chain antibody (A0101, Dako) and an anti-kappa light chain antibody (A0100, Dako) was used. In Fig. 2.5 A, the immunoblot shows that lambda light chain aggregates were retained in the pockets of the stacking gel, indicating high molecular weight >1048 kDa. Furthermore, the immunoblot revealed that lambda light chain aggregates were enriched in the $H_2O$ supernatants, supporting the results obtained from the native FRA (Fig. 2.4 A). In contrast, no light chain aggregates were detected in the gel pockets when the blot was immunoprobed with an anti-kappa light chain antibody (A0100, Dako) (Fig. 2.5 B), suggesting patient-derived light chain

aggregates do not consist of kappa light chains. This is also in good agreement with the FRA results shown in Fig. 2.4 C.

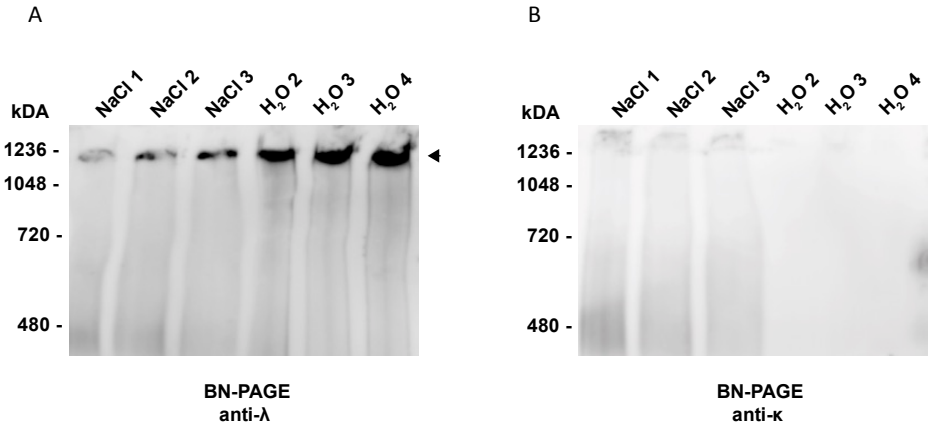


**Fig. 2.5 Analysis of NaCl and $H_2O$ supernatants obtained from the heart of an AL amyloidosis patient using BN-PAGE and Western blotting.**

**A** The NaCl supernatants 1-3 (5 µg) and the $H_2O$ supernatants 2-4 (5 µg) were loaded onto a 4-16% native gel and separated by BN-PAGE. Then, proteins were transferred from the gel to a PVDF membrane by capillary blotting and immunodetected with an anti-lambda light chain antibody (A0101, Dako). The immunoblot displays an enrichment of lambda light chain aggregates in the $H_2O$ supernatants 2-4. Lambda light chain aggregates are retained in the gel pockets, indicating high molecular weight (≥ ~1048 kDa). Arrow head indicates the accumulation of aggregated material in the stacking gel. **B** In the corresponding immunoblot detected with an antibody specific for kappa light chain protein (A0100, Dako) no aggregates were detectable in the stacking gel.

### 2.3.4 Analysis of NaCl and $H_2O$ supernatants using SDS-PAGE and Western blotting

Using sodium dodecyl sulfate polyacrylamide gel electrophoresis (SDS-PAGE) followed by Western blotting the SDS-stability of patient-derived light chain aggregates was investigated. SDS-PAGE is a commonly applied technique first described by U.K. Laemmli with which proteins can be separated according to their molecular weight[206]. Therefore, SDS, an anionic detergent, has to be applied to protein samples in order to linearize proteins and to impart a negative charge to the linearized proteins. The negatively charged proteins migrate in the polyacrylamide gel towards the anode using an electric field, a procedure called electrophoresis. The separated proteins are then transferred from the gel to a membrane where they are stained with antibodies specific for the protein of interest. In order to analyze samples obtained from the heart extraction 5 µg of the NaCl supernatants 1-3 and $H_2O$ supernatants 2-4 were loaded onto a polyacryamid gel, separated using electrophoresis and blotted onto a nitrocellulose membrane. The membrane was analyzed with an anti-lambda light chain antibody (A0101, Dako). Analysis of samples by SDS-PAGE and

immunoblotting showed that no aggregates are retained in the pockets of the gel (Fig. 2.6 A). However, in the $H_2O$ supernatants 2-4 a major protein band migrating at ~25 kDa was detected which corresponds to the size of a light chain monomer. This indicates that patient-derived light chain aggregates are none-SDS-resistant structures. Several additional protein bands were also detected in the $H_2O$ supernatants 2-4 with estimated molecular weights between 10 and 50 kDa, which could represent light chain fragments and dimers. The intensity of these bands is much weaker than that of the monomer, suggesting that the latter is the most abundant species. NaCl supernatants 1-3 and $H_2O$ supernatants 2-4 were also analyzed with an antibody against kappa light chain proteins (A0100, Dako). No light chain monomer band could be detected in the $H_2O$ supernatants 2-4, indicating these supernatants do not contain kappa light chain protein (Fig. 2.6 B). In the NaCl supernatants 1-3 a protein band migrating at ~25 kDa was detected, suggesting that kappa light chain proteins resulting from intact immunoglobulins are present in the NaCl supernatants 1-3.

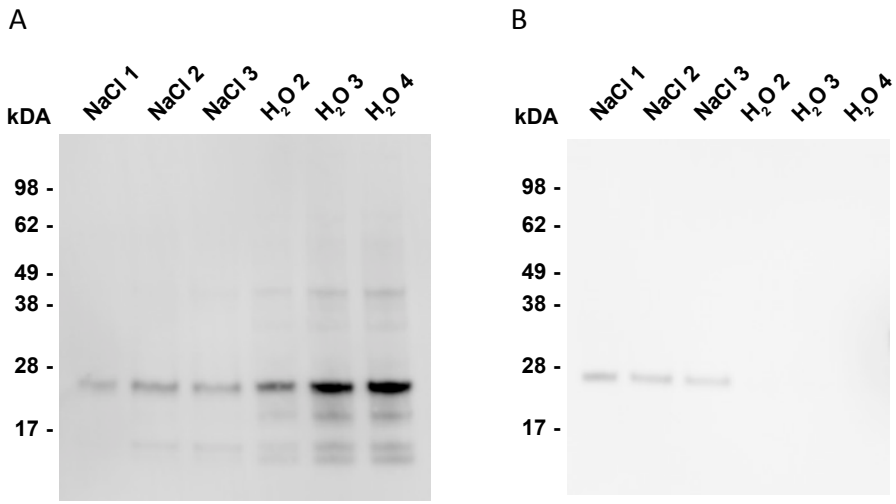


**Fig. 2.6 Characterization of NaCl and $H_2O$ supernatants obtained from the heart of an AL amyloidosis patient using SDS-PAGE and immunoblotting.**

**A** NaCl supernatants 1-3 (5 µg) and $H_2O$ supernatants 2-4 (5 µg) were loaded onto a 4-12% Bis-Tris polyacrylamid gel, separated by SDS-PAGE and transferred to a nitrocellulose membrane by Western blotting. Proteins were immunodetected using an anti-lambda light chain antibody (A0101, Dako). Immunoblotting shows progressively enriched light chain protein in the $H_2O$ supernatants 2-4. A major band appeared at the size of ~25 kDa, corresponding to the size of a light chain monomer. No light chain protein was detected in the pockets of the SDS gel, indicating that light chain aggregates are none-SDS-stable structures. **B** Control experiments with a specific kappa light chain antibody (A0100, Dako) showed kappa light chain protein in the NaCl supernatants but not in the $H_2O$ supernatants.

### 2.3.5 Analysis of NaCl and $H_2O$ supernatants obtained from the heart of an AL amyloidosis patient using a denaturing FRA

To further analyze whether the NaCl supernatants 1-3 and the $H_2O$ supernatants 2-4 contain SDS-resistant light chain aggregates, a FRA was performed under denaturing conditions. Therefore, 2.5 µg of each supernatant was boiled in 4% SDS and 100 mM DTT at 95°C for 5 min and was immediately filtered separately through two cellulose acetate membranes (pore size 0.2 µm) using a vacuum apparatus. Each sample was assessed in triplicate. Both membranes were immunoprobed with an anti-lambda light chain (A0101, Dako) (Fig. 2.7 A) and an anti-kappa light chain antibody (A0100, Dako) (Fig. 2.7 B), respectively. No antibody signal could be detected in any of the tested fractions, indicating that lambda light chain aggregates are not resistant to denaturing conditions This is in concordance with the results obtained from the SDS-PAGE analysis, showing no high molecular weight lambda light chain aggregates retained in the pockets of the gel, but instead monomeric protein migrating at ~25 kDa (Fig. 2.6). Since low molecular weight proteins are too small to be retained on the filter membrane, no lambda light chain protein can be detected on the membrane. The filter membrane immunoprobed with the anti-kappa light chain antibody A0100 (Dako) shows no signal for the tested supernatants, which is consistent with the data from the FRA (Fig. 2.4), the BN-PAGE (Fig. 2.5) and the SDS-PAGE (Fig. 2.6).

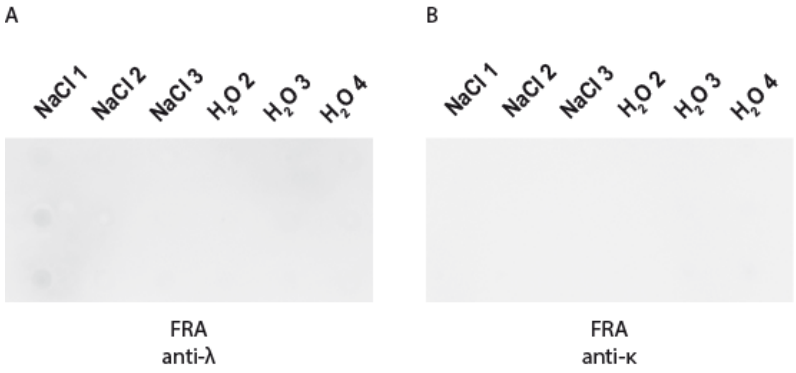


**Fig. 2.7 Analysis of NaCl and $H_2O$ supernatants obtained from the heart of an AL amyloidosis patient using a denaturing FRA.**

The NaCl supernatants 1-3 (2.5 µg) and the $H_2O$ supernatants 2-4 (2.5 µg) were boiled in 4% SDS and 100 mM DTT at 95°C for 5 min, filtered through a cellulose acetate membrane (pore size 0.2 µm) and immunoprobed with a lambda specific (**A**) and a kappa specific (**B**) light chain antibody (A0101, A0100, repectively). No antibody signals were detected, indicating that the light chain aggregates present in the analyzed supernatants are non-SDS-resistant structures.

### 2.3.6 Investigation of the purity of $H_2O$ supernatants obtained from the heart of an AL amyloidosis patient using SDS-PAGE and Coomassie blue staining

To examine the purity of the light chain aggregate containing $H_2O$ supernatants, samples were loaded onto a polyacrylamide gel and proteins were separated by electrophoresis. Finally, the gel was stained with Coomassie Brilliant Blue. This dye has a high affinity for proteins and stains them blue so that they can be detected as blue bands in the gel[207]. The total protein content of the $H_2O$ supernatants 1-4 is shown in Fig. 2.8 A. The $H_2O$ supernatants 1-4 contained multiple other proteins in addition to the light chain proteins. These proteins could either be contaminants or proteins that were coaggregated into the light chain aggregates and might therefore play a role in the pathogenesis of AL amyloidosis. Serum amyloid P component (SAP, ~25 kDa) and apolipoprotein E (ApoE, ~36 kDa) have been identified in all amyloid aggregates examined to date[59,208]. In order to determine whether these proteins are present in the prepared supernatants, the $H_2O$ supernatant 4 was subjected to Western blotting using anti-SAP (EP1018Y, Abcam) and anti-ApoE (AB947, Merck) antibodies. Fig. 2.8 B displays a ~25 kDa SAP and a ~36 kDa ApoE band, indicating that both proteins are present in the $H_2O$ supernatant 4. Taken together, $H_2O$ supernatants contain other proteins in addition to the lambda light chain protein, suggesting that the enriched supernatants contain multiple other proteins, including SAP and ApoE.

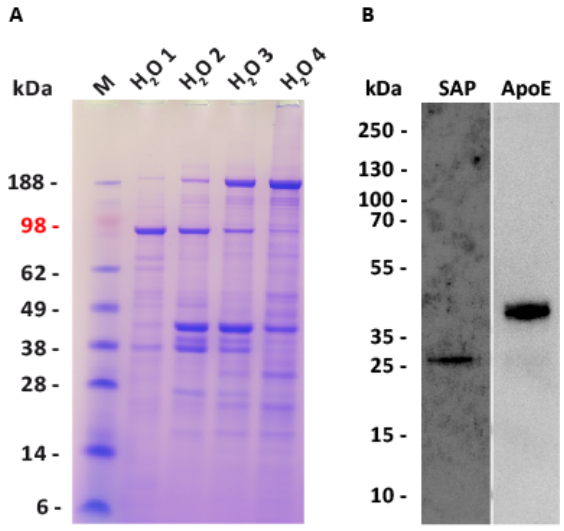


**Fig. 2.8 Investigation of the purity of $H_2O$ supernatants obtained from the heart of an AL amyloidosis patient using SDS-PAGE and Coomassie blue staining.**

**A** The $H_2O$ supernatants 1-4 (5 µg) were loaded onto a 4-12% Bis-Tris polyacrylamid gel, separated by SDS-PAGE and stained with Coomassie blue. The analysis reveals that the $H_2O$ supernatants 1-4 contain multiple proteins. M: SeeBlue plus2 pre-stained protein standard (Thermo Scientific). **B** Western Blot of $H_2O$ supernatant 4 using anti-SAP (EP1018Y, Abcam) and anti-ApoE (AB947, Merck) antibodies, display the presence of the proteins SAP and ApoE, respectively.

### 2.3.7 Investigation of the β-sheet content of proteins in NaCl and $H_2O$ supernatants

The cross β-sheet structure is a characteristic feature of amyloid aggregates[72]. To examine whether heart-derived aggregates are β-sheet-rich structures the NaCl and $H_2O$ supernatants were analyzed using a Thioflavin T (ThT) assay. ThT is a dye that monitors β-sheets by an enhanced fluorescence as well as a red shift of its emission spectrum and is widely used for the identification and quantification of amyloid fibrils i*n vitro*[73,209,210]. Therefore, 50 µg of the NaCl supernatants 1-3 and the $H_2O$ supernatants 2-4 were incubated with 20 µM ThT and the fluorescence was measured at an emission wavelength of 485 nm using an excitation wavelength of 440 nm in a Tecan plate reader. $H_2O$ supernatants 2-4 exhibited strong ThT fluorescence, which was ~6-fold higher compared to the NaCl supernatants 1-3 or NaCl and $H_2O$ solutions alone (Fig. 2.9 A). Synthetic Aβ monomer and *in vitro* produced ThT-reactive Aβ aggregates were used as negative and positive controls, respectively. As expected, Aβ monomer displayed no enhanced ThT fluorescence whereas Aβ aggregates showed an increased fluorescence.

To confirm the presence of β-sheets, another amyloid sensitive assay was performed. The dye Congo red (CR) is also known to bind amyloid, which results in an enhanced fluorescence[63]. 50 µg of the NaCl supernatant 1 and the $H_2O$ supernatant 4 were incubated with 10 µM CR and the fluorescence was measured at an excitation wavelength of 511 nm. An emission spectrum was recorded from 550 nm to 700 nm in a Tecan plate reader. The $H_2O$ supernatant 4 displayed a ~3-fold higher fluorescence than the NaCl supernatant 1 and the buffer control, indicating that the $H_2O$ supernatant 4 contains β-sheet-rich aggregates (Fig. 2.9 B). Preformed *in vitro* Aβ aggregates were used as a positive control. As expected, Aβ aggregates showed an increased CR fluorescence compared to the buffer solution alone. Taken together, heart extracted $H_2O$ supernatants display enhanced ThT and CR fluorescence, indicating that they contain a high content of β-sheet structures.

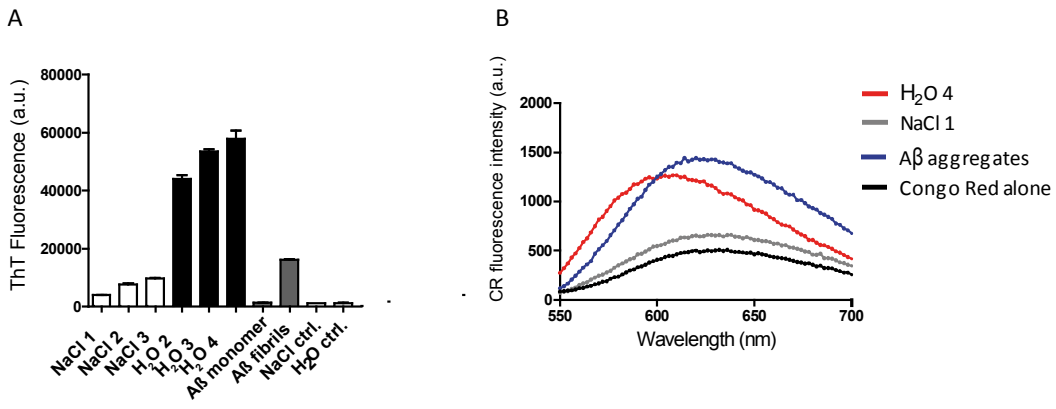


**Fig. 2.9 Analysis of the β-sheet content of light chain aggregates isolated from the heart of an AL amyloidosis patient.**

**A** 50 µg of the NaCl supernatants 1-3 and the $H_2O$ supernatants 2-4 were incubated with 20 µM ThT and the fluorescence was measured at an emission wavelength of 485 nm using an excitation wavelength of 440 nm in a Tecan plate reader. The studies showed an enhanced fluorescence in $H_2O$ supernatants compared to NaCl supernatants and buffer controls. Aβ monomer and aggregates were used as negative and positive controls, respectively. **B** 50 µg of the NaCl supernatant 1 and the $H_2O$ supernatant 4 were incubated with 10 µM CR and an emission spectrum was recorded from 550 nm to 700 nm in a Tecan plate reader. The CR fluorescence was increased in the $H_2O$ supernatant 4 compared to the NaCl supernatant 1 and a buffer with CR alone. Preformed Aβ aggregates were used as a positive control.

### 2.3.8 Morphological investigation of heart extracted supernatants using electron microscopy

Next, the morphology of the isolated proteins and structures in the NaCl supernatant 3 and in the $H_2O$ supernatant 4 was analyzed using electron microscopy (EM). Samples and buffer controls were applied on carbon-coated grids and negatively stained with uranyl acetate. As illustrated in Fig. 2.10 A-B fibrillar structures were observed in the $H_2O$ supernatant 4. The aggregates appear essentially straight, unbranched and fibrillar in structure and they are present as individual fibrils or in bundles. The length of the fibrils measures ~100 nm in average and they are approximately 5-10 nm in width. There are also other structures observed that seem to be attached to the fibrils (Fig. 2.10 B, asterisks). These structures could represent tissue debris or other components, such as fat tissue that tightly binds to the aggregates because no detergent was used in the extraction protocol. These results are in good accordance with the analysis of the samples by SDS-PAGE which revealed various proteins in the $H_2O$ supernatant 4 (Fig. 2.8). In addition to fibrillar structures EM analysis revealed also non-fibrillar amorphous structures (Fig. 2.10 C, arrow), indicating the existence of two aggregate species. In the NaCl supernatant 3 no fibrillar structures were detected. Instead, structures were displayed that may represent residual adipose tissue which is a major component of the heart (Fig. 2.10 D). In buffer controls no fibrillar or amorphous structures were visible (Fig. 2.10 D-F).

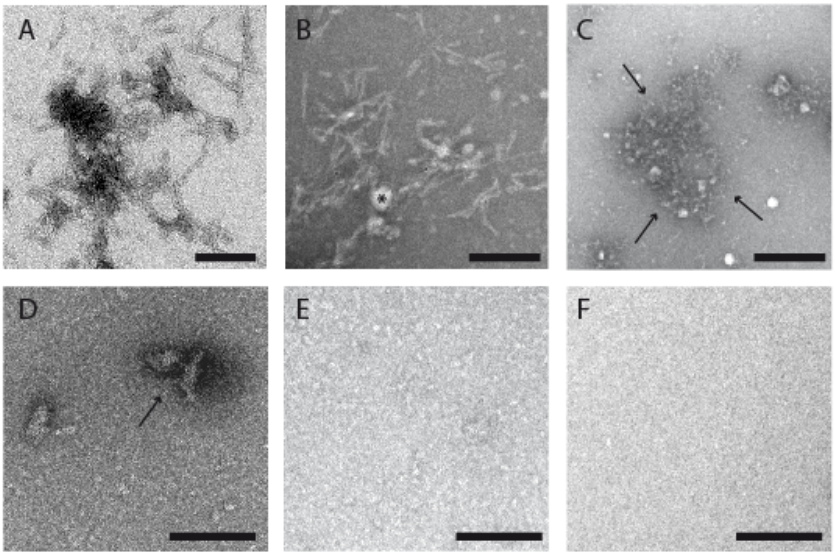


**Fig. 2.10 EM analysis of water-extracted light chain aggregates isolated from the heart of an AL amyloidosis patient.**

The $H_2O$ supernatant 4 and the NaCl supernatant 3 were negatively stained with 5% uranyl acetate and analyzed by EM. **A** EM analysis revealed that the water-extracted light chain aggregates from the heart of an AL amyloidosis patient likely have a fibrillar structure. **B** Many detected fibrils are straight and unbranched but additionally, bundles of fibrils were also observed. Other structures that are attached to the fibrils are indicated by an asterisk. **C** Amorphous structures indicated by arrows could also be observed in the $H_2O$ supernatant 4. **D** In the NaCl supernatant 3 no fibrillar structures were detectable. Instead, structures which may be tissue debris or fat were displayed (arrow). $H_2O$ and NaCl buffer controls are illustrated in **E** and **F**, respectively. The scale bar represents 200 nm for A-C and 300 nm for D-F.

### 2.3.9 Immuno-EM of light chain aggregates using antibody gold-labeling

In order to confirm that the water-extracted supernatants indeed contain immunoglobulin light chains aggregates immunogold labeling of the $H_2O$ supernatant 4 was performed. For immunodetection an anti-lambda light chain antibody (A0101, Dako) was used. Secondary antibodies were conjugated with colloidal gold particles with a diameter of 10 nm. These gold particles can be visualized as black dots when viewed under the EM. The analysis revealed fibrillar aggregates that were decorated with gold particles (Fig. 2.11, arrows), suggesting that the water-extracted aggregates indeed consist of lambda light chain protein. The EM-images also demonstrated that besides fibrils other structures are present in the $H_2O$ supernatant 4.

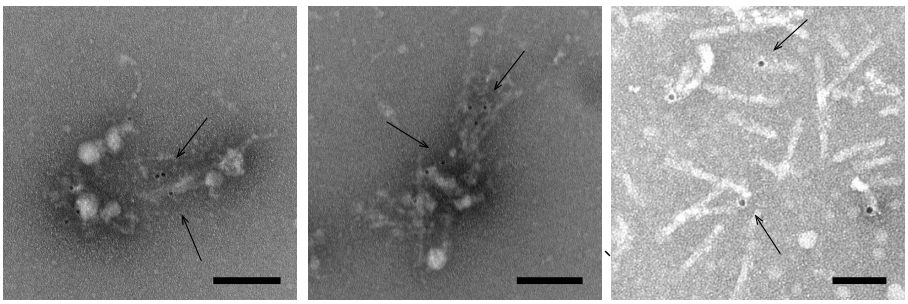

**Fig. 2.11 Immuno-EM analysis of water-extracted light chain aggregates from the heart of an AL amyloidosis patient.**

The $H_2O$ supernatant 4 was subjected to immunodecoration with an anti-lambda light chain antibody (A0101, Dako) and secondary antibodies conjugated with 10 nm gold particles. Arrows indicate gold particles. The scale bar is 200 nm.

### 2.3.10 Purification of patient-derived light chain aggregates using ultracentrifugation

According to the results obtained by SDS-PAGE (Fig. 2.8) and the EM analysis (Fig. 2.10), the $H_2O$ supernatant 4 contains structures other than light chain aggregates. In order to further purify patient-derived light chain aggregates ultracentrifugation experiments were performed. Amyloid aggregates have a higher molecule mass than soluble proteins, such as monomers and oligomers. Consequently, larger aggregates and fibrils precipitate during ultracentrifugation whereas soluble protein remains in the supernatant. Samples were centrifugated at 55,000 rpm (TLA rotor) and 4°C for 40 min. Supernatant was transferred to a fresh tube and pellet was resuspended in 150 µl $H_2O$.To analyze whether ultracentrifugation resulted in an enrichment of light chain aggregates 10 µg of the input, the supernatant and the resuspended pellet fraction were each mixed with 20 µM ThT and the fluorescence was measured in a plate reader. Synthetic Aβ monomers and preformed Aβ aggregates were used as negative and positive controls, respectively. The $H_2O$ supernatant 4 (input sample) exhibited a strong ThT fluorescence, equally to Aβ aggregates, indicating the presence of β-sheet rich aggregates in this supernatant (Fig. 2.12). The ThT fluorescence of the supernatant after ultracentrifugation was dramatically decreased similar to Aβ monomer. In comparison, the pellet fraction exhibited an increased ThT fluorescence compared to the input and the supernatant, indicating that ultracentrifugation indeed resulted in an enrichment of patient-derived aggregates in the pellet fraction.

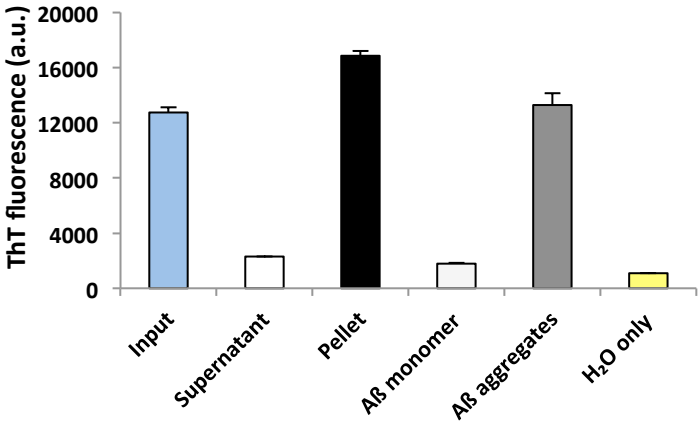


**Fig. 2.12 Analysis of the ultracentrifugated $H_2O$ supernatant 4 obtained from the heart of an AL amyloidosis patient using the ThT assay.**

The $H_2O$ supernatant 4 was ultracentrifugated for 40 min at 55,000 rpm and 4°C (TLA-55 rotor) and the resulting samples were analyzed using the ThT assay. 10 µg of the input, the supernatant and the resuspended pellet fraction were incubated with 20 µM ThT and fluorescence was measured at an excitation and emission wavelength of 440 nm and 480 nm, respectively. The input sample exhibited a strong ThT fluorescence, indicating the presence of β-sheet-rich structures in the $H_2O$ supernatant 4. In comparison, the supernatant after the ultracentrifugation showed a dramatically decreased ThT fluorescence. In contrast, a very high ThT fluorescence was detectable in the pellet fraction. Synthetic Aβ monomers, preformed Aβ aggregates and $H_2O$ only were used as controls.

To further analyze the precipitated patient-derived light chain aggregates obtained after ultracentrifugation, the generated supernatant and pellet fractions were analyzed by SDS-PAGE and Coomassie staining. Coomassie staining showed that the input sample contains multiple protein bands ranging from ~14 to 188 kDa and higher (Fig. 2.13). Several bands (~25 to ~188 kDa) appeared in the supernatant after ultracentrifugation. However, the pellet fraction showed nearly the same pattern of bands as the input sample (Fig. 2.13, lane 3), indicating the presence of other insoluble proteins that may either be associated with patient-derived light chain aggregates or may form other aggregates. Analysis of the samples by Western blotting revealed light chain proteins in the input sample and in the pellet fraction, but not in the supernatant, indicating that $H_2O$ supernatant 4 contains lambda light chain aggregates that precipitate when subjected to ultracentrifugation.

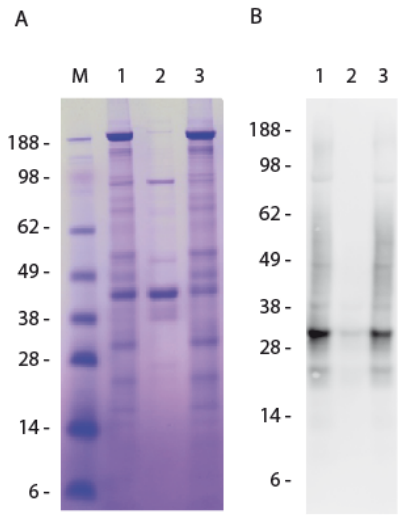


**Fig. 2.13 Analysis of ultracentrifugated $H_2O$ supernatant 4 obtained from the heart of an AL amyloidosis patient by SDS-PAGE and Western blotting.**

The $H_2O$ supernatant 4 was ultracentrifugated at 55,000 rpm (TLA rotor) and 4°C for 40 min and the resulting samples were analyzed by SDS-PAGE and Western blotting. Input (lane 1), supernatant (lane 2) and pellet fraction (lane 3) were boiled in 1xLDS buffer and DTT, loaded onto a polyacrylamide gel and separated by electrophoresis. **A** Coomassie staining of the SDS-gel. The input sample showed multiple bands from the bottom to the top of the gel. The supernatant showed two prominent bands (~40 and ~188 kDa) as well as some weaker bands (~38 kDa, ~55 kDa, ~70 kDa). The pellet fraction showed nearly the same pattern as in the input sample. M: SeeBlue plus2 pre-stained protein standard (Thermo Scientific). **B** Analysis of the samples by Western blotting using an anti-lambda light chain antibody (A0101, Dako). Lambda light chain protein migrating at ~30 kDa was detected only in the input and pellet fraction, but not in the supernatant.

### 2.3.11 Analysis of the $H_2O$ supernatant 4 after ultracentrifugation using EM

In order to further analyze the pellet and the supernatant fractions after ultracentrifugation of $H_2O$ supernatant 4 immunogold-EM was applied. Fig. 2.14 shows the input, the resuspended pellet fraction and the supernatant in two magnitudes each. The analysis of the input sample revealed straight, unbranched fibrils all over the grid which are decorated with immunogold particles (Fig. 2.14 A, B). Such fibrillar structures, however, could not be observed in the resuspended pellet fraction (Fig. 2.14 C, D) or in the supernatant (Fig. 2.14 E, F). Instead, globular structures could be detected in the supernatant which likely represent soluble proteins (Fig. 2.14 E, F). The pellet fraction showed unstructured material which can possibly be tissue components. The absence of fibrils in the pellet fraction was unexpected because input samples indeed showed fibrils (Fig. 2.14 A, B) and the pellet fraction displayed a strong ThT fluorescence (Fig. 2.12). Thus, it may be possible that fibrils were not transferred to the EM-grids. Ultracentrifugation tubes have no protein lobind surface. Therefore it is possible that hydrophobic fibrils strongly adhered to the hydrophobic plastic surface of the tube.

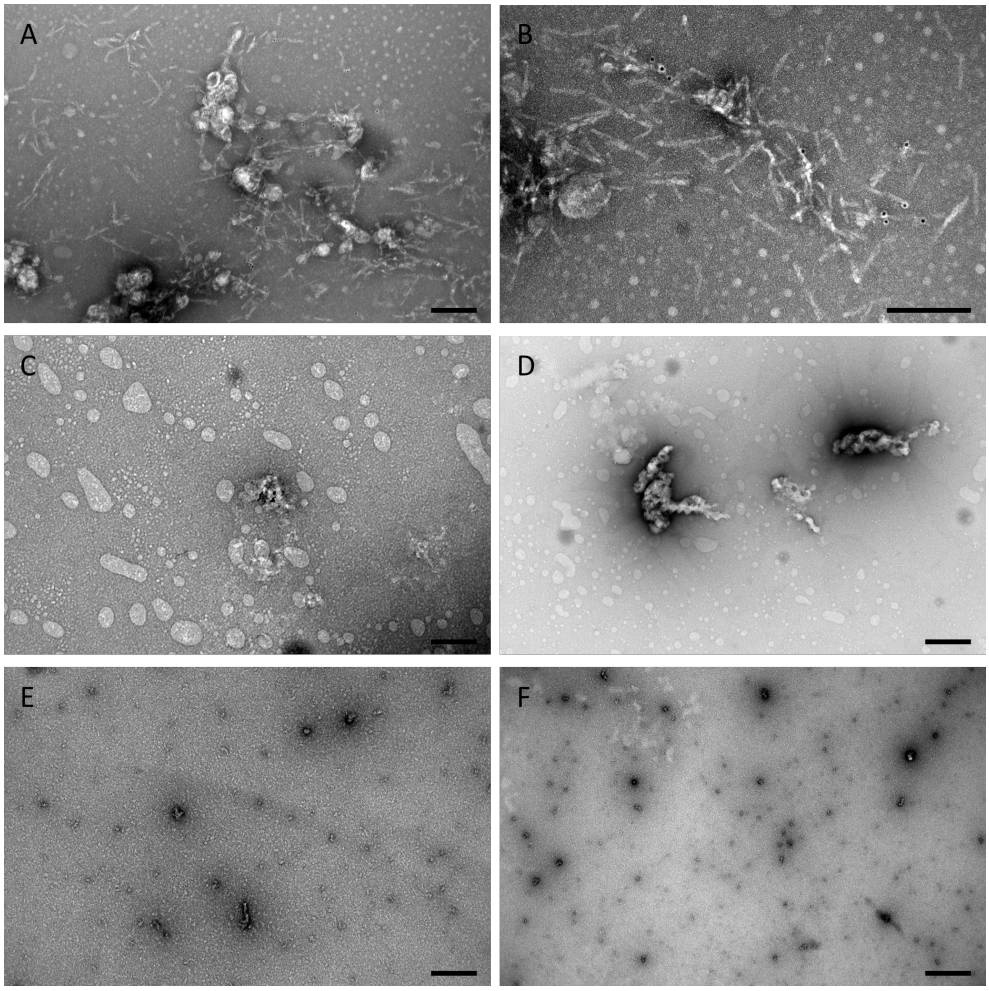


**Fig. 2.14 EM images of $H_2O$ supernatant 4 obtained from the heart preparation of an AL amyloidosis patient after ultracentrifugation.**

**A, B** Immuno-EM analysis of the $H_2O$ supernatant 4 before ultracentrifugation. Input samples were stained with an anti-lambda light chain antibody (A0101, Dako) and with a secondary antibody conjugated with 10 nm colloidal gold particles (Dianova). 25,000x (A), 50,000x (B) **C, D** In the resuspended pellet fraction after centrifugation (55,000 rpm, 40 min, 4°C) no fibrils could be detected. 25,000x (C), 12,500x (D). **E, F** In the supernatant of ultracentrifugated $H_2O$ supernatant 4 globular structures could be detected. 25,000x (E), 12,500x (F). Scale bar 200 nm for A, B, C and E and 400 nm for D and F.

### 2.3.12 Analysis of patient-derived light chain aggregates using size exclusion chromatography

Parallel to ultracentrifugation experiments size exclusion chromatography (SEC) was applied to analyze patient-derived light chain aggregates obtained from the heart of an AL amyloidosis patient. SEC, which is also known as gel filtration, is a technique commonly used to separate proteins based on their apparent molecular size in solution[211]. The column packing material consists of particles that contain pores of a particular size. Proteins with molecular weights that are larger than the exclusion limit of the particular pore size pass by the pores and elute in the void volume of the column. Smaller

proteins, in contrast, can enter the pores and elute at a later time point[211]. Thus, larger proteins flow through the column more quickly and elute first compared to smaller proteins that are retained in the pores. Molecular size estimation is achieved by running protein standards with known molecular weights.

A Superose 6 10/300 column was used to analyze the $H_2O$ supernatant 4 at 4°C with $H_2O$ as the running buffer. SEC was conducted at a flow rate of 0.3 ml/min using an Äkta HPLC system (GE Healthcare). To analyze the resulting SEC fractions Dot blot and ThT assays were performed. In addition, samples were analyzed by SDS-PAGE and EM.

In order to analyze the size of the water-extracted light chain aggregates by SEC, 95 µl of the $H_2O$ supernatant 4 was injected into the column. Three major protein peaks appeared in the SEC profile (Fig. 2.15 A) at 215 nm where the amide peptide bond has a strong absorbance[212]. The first and the second peak eluted between ~5 and 7 ml (fraction 13 and 15), corresponding to the void volume of the column, which was determined in an independent experiment by the elution of blue dextran from the column. Blue dextran is a large molecule with a molecular weight of ~2000 kDa and is commonly used to determine the void volume of SEC columns[213]. The third peak eluted after 10 ml and represents with ~750 mAU the smallest peak.

To confirm that the eluted fractions indeed contain light chain protein, they were analyzed by dot blot assays using an anti-lambda light chain antibody (A0101, Dako). As depicted in Fig. 2.15 B fractions 12 to 23 contained lambda light chain protein with the most intensive antibody signal in fraction 15 which corresponds to the second peak.

In order to assess the β-sheet content of the proteins in the different fractions obtained by SEC, a ThT assay was conducted. The fractions 11 to 16 exhibited increased ThT fluorescence compared to all other fractions, indicating that these fractions contain light chain aggregates with typical β-sheet structures (Fig. 2.15 C).

Taken together, the SEC analysis showed that the $H_2O$ supernatant 4 contains high molecular weight lambda light chain aggregates with a β-sheet structure that are eluted in the void volume of the column.

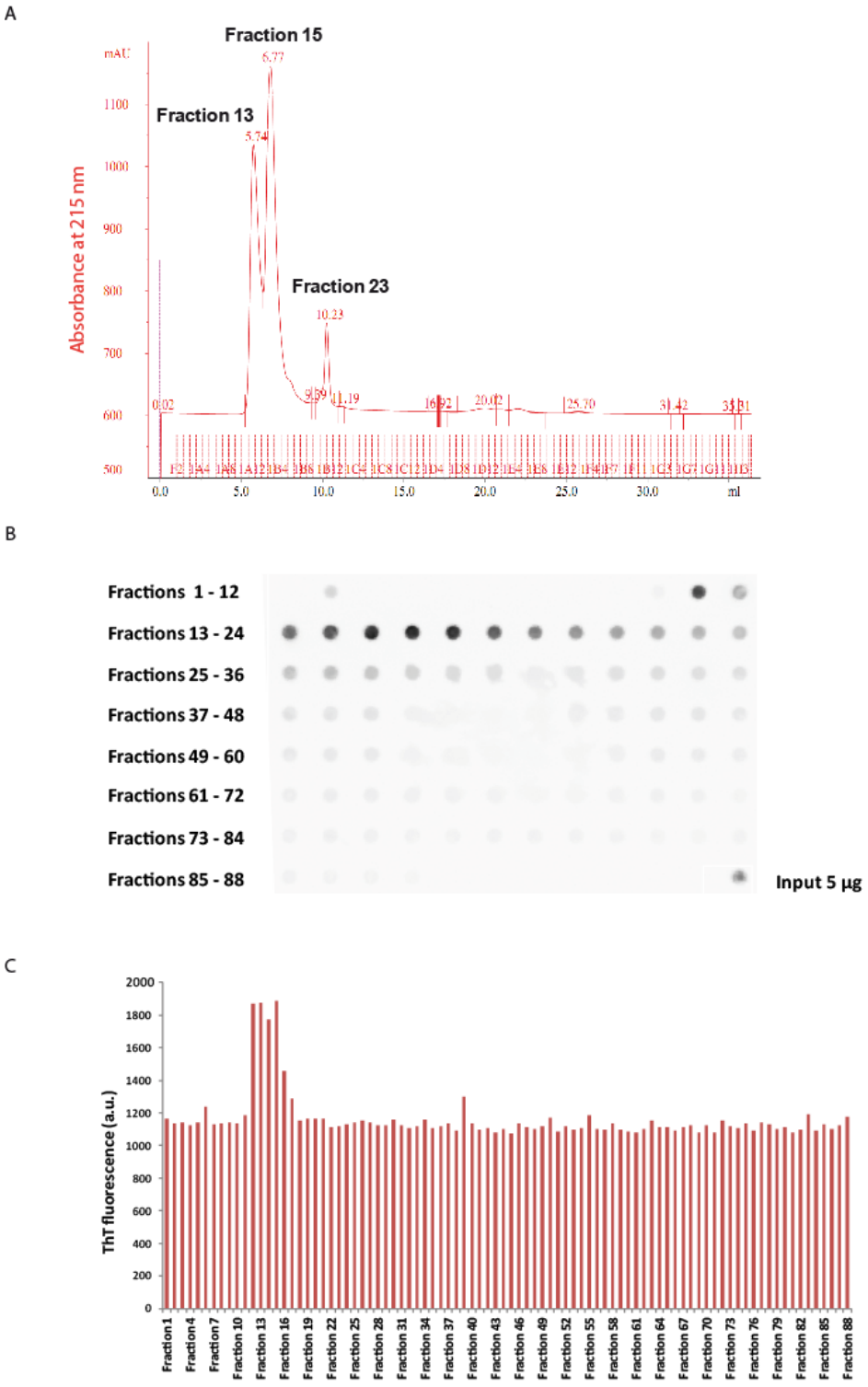


**Fig. 2.15 Analysis of the $H_2O$ supernatant 4 obtained from the heart of an AL amyloidosis patient using size exclusion chromatography.**

**A** The SEC elution profile of the $H_2O$ supernatant 4 obtained from the heart of an AL amyloidosis patient is shown. Sample (95 µl) was analyzed on a Supersoe 6 10/300 column (GE Healthcare) using a mobile phase of $H_2O$. SEC was conducted at a flow rate of 0.3 ml/min with a detection wavelength at 215 nm. SEC profile revealed three peaks. Peak 1 and 2 eluted in the void volume of the column (~5 and 7 ml), peak 3 eluted close to 10 mL. **B** Dot blot analysis of SEC fractions using the anti-lambda light chain antibody A0101 (Dako). Light chain protein was detected in fractions 11 to 24 with the highest antibody signal in fractions 11 to 15. **C** SEC fractions were analyzed using the ThT assay. Increased ThT fluorescence was observed in fractions 12 to 16.

Next, the fractions obtained by SEC were analyzed by EM. EM-images of input samples (Fig. 2.16 A) showed unstructured material, possibly fat tissue, in addition to patient-derived light chain fibrils as described in section 2.3.8. Electron micrographs of fraction 13 (peak 1) from the SEC experiment revealed bundles of aggregates with diameters of ~300 (Fig. 2.16 B-D) and >1000 nm (Fig. 2.16 B). In contrast, fraction 15 contained individual, separated fibrils that were partly connected to bundles with a diameter of ~100 nm (Fig. 2.16 E-F). Large interconnected structures which were seen in the input sample were not observed in the peak fractions after SEC, suggesting that SEC allowed further purification of light chain aggregates.

Taken together, SEC experiments showed that the $H_2O$ supernatant 4 contains β-sheet-rich lambda light chain protein aggregates that are fibrillar in morphology and are present in bundles or as individual fibrils.

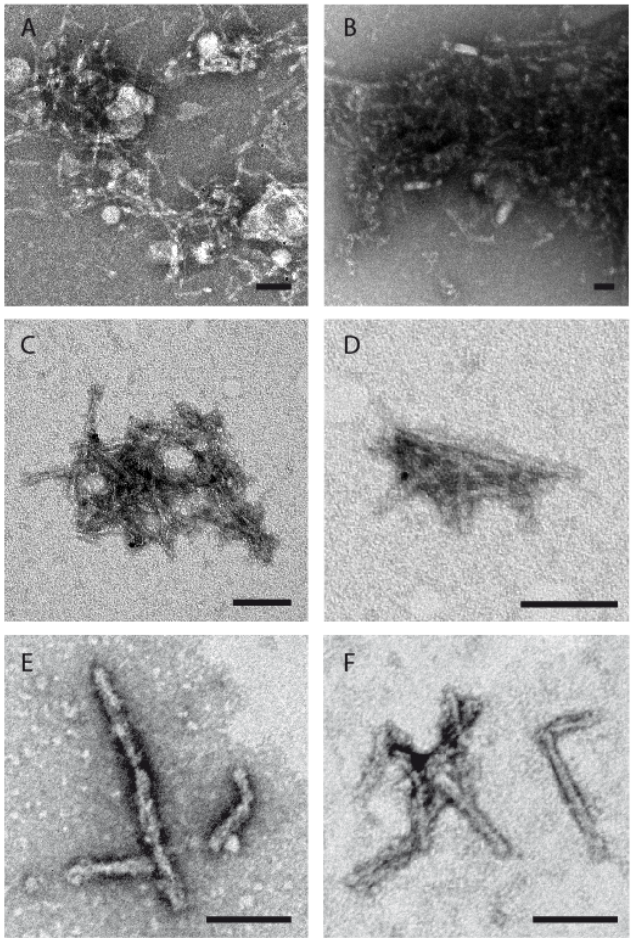


**Fig. 2.16 EM analysis of peak fractions obtained from SEC experiments of a water-extracted fraction of an AL amyloidosis patient.**

**A** Input sample ($H_2O$ supernatant 4) contain unstructured material, possibly adipose tissue, in addition to fibrils. **B-D** Aliquots of peak 1 (fraction 13) from SEC were applied to carbon-coated grids and negatively stained with uranyl acetate. Bundles of fibrillar aggregates with a diameter of ~300-1000 nm were detected. **E-F** Peak 2 (fraction 15) shows straight unbranched fibrils with a length of ~100 nm. They are present in bundles or as individual fibrils. Scale bar represents 100 nm for A-D and 50 nm for E-F.

### 2.3.13 Investigating the toxicity of patient-derived light chain aggregates in a cell-based assay

After patient-derived light chain aggregates were extensively characterized with biochemical and biophysical methods, the next question to be answered was whether these structures are toxic in a cell model system. To answer this question, MTT (3-(4,5-Dimethyl-2-thiazolyl)-2,5-diphenyl-2H-tetrazolium bromide) assays were conducted on HeLa cells. This assay is commonly used to measure the viability of cells in culture and was first described by Mosmann in 1983[214]. It is a colorimetric assay in which the yellow tetrazolium dye MTT is reduced into purple formazan precipitates by mitochondrial dehydrogenases of living cells (Fig. 2.17). The addition of a second reagent containing SDS and DMSO solubilizes the formazan crystals into a homogenous colored solution. The metabolic activity of cells can be quantified by measuring the absorbance at 570 nm using a spectrophotometer. Because reduction of the tetrazolium dye takes only place when mitochondrial reductase enzymes are active, conversion can be directly related to the number of viable cells. Thus the quantified absorbance correlates with cell viability and activity.

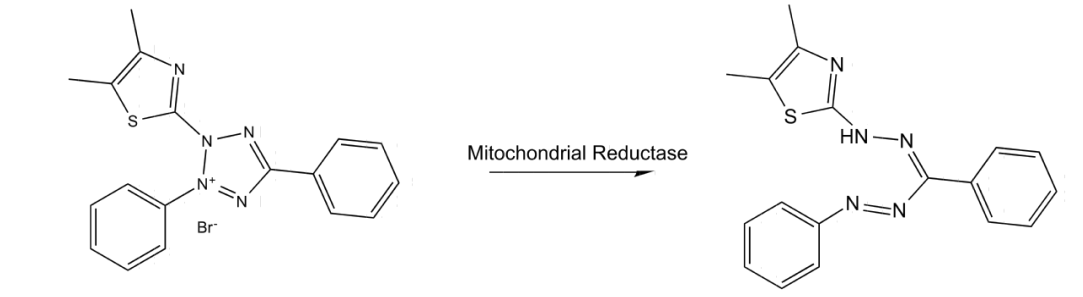


**Fig. 2.17 MTT reduction in living cells by mitochondrial reductases results in the formation of purple formazan characterized by high absorbance at 570 nm.**

MTT, a yellow tetrazolium salt, is reduced to purple formazan precipitates by mitochondrial reductases in mammalian cells. After adding a solubilization solution the insoluble purple formazan product converts into a homogenous purple solution. This conversion can be quantified by measuring the absorbance at 570 nm using a spectrophotometer.

In order to evaluate the cytotoxic effects of patient-derived light chain aggregates HeLa cells were used as a model system. Since the exact concentrations of patient-derived light chain aggregates in the $H_2O$ supernatants could not be determined, MTT assay was conducted in a concentration series with unknown concentrations. Therefore, $H_2O$ supernatant 4 was tested in five dilutions (undiluted, 1:10, 1:50, 1:100 and 1:1000). HeLa cells were treated with the indicated dilutions of patient-derived

light chain aggregates for 48 h at 37°C. Because patient-derived light chain aggregates were extracted in $H_2O$, $H_2O$ was used as a buffer control. Cycloheximid, an inhibitor of protein synthesis in eukaryotic cells, was used as a positive control for a cytotoxic response[215]. 10 µl of MTT was added to each well and incubated for 4 h at 37°C. Then, the solubilization solution was added and the absorbance was recorded at 570 nm in a Tecan plate reader. Fig. 2.18 illustrates that patient-derived light chain aggregates induce a decrease in the viability of HeLa cells in a dose-dependent manner, compared to the control ($H_2O$). Undiluted samples significantly reduced the cell viability by ~50% after 48 h of incubation compared to $H_2O$-treated cells. This result strongly suggests that patient-derived light chain aggregates impair cellular metabolic activities in HeLa cells.

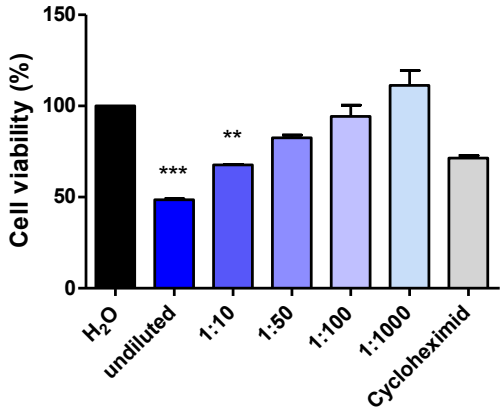


**Fig. 2.18 Patient-derived light chain aggregates reduce the viability of HeLa cells in a concentration-dependent manner.**

HeLa cells were treated with patient-derived light chain aggregates (undiluted, 1:10, 1:50, 1:100 and 1:1000) for 48 h at 37°C and cell viability was assessed using the MTT assay. Patient-derived light chain aggregates reduced the viability of HeLa cells in a dose-dependent manner. A ~2-fold reduction of cell viability could be observed in cells exposed to undiluted $H_2O$ supernatant 4. Statistical analysis was performed using one-way ANOVA followed by Bonferroni's multiple comparison test using GraphPad Prism 5 software. *** $p < 0.0001$, ** $p < 0.001$.

## 2.4 Preparation of NaCl and $H_2O$ supernatants from a pig control heart

As healthy human hearts are difficult to obtain for research, the heart of a feral pig was used as a control. In order to compare the results from the patient preparation with a control, heart pieces from the feral pig were prepared according to the water-extraction method that was applied for the preparation of the patient heart (Fig. 2.2). NaCl and $H_2O$ supernatants were first analyzed by ThT assays. Therefore, 10 µg of NaCl supernatants 1-4 and $H_2O$ supernatants 1-4 were incubated with 20 µM ThT and the fluorescence was measured at an excitation and emission wavelength of 440 nm and 485 nm, respectively. Fig. 2.19 A shows that NaCl supernatants 1-4 did not exhibit a marked ThT

fluorescence. In contrast, $H_2O$ supernatants 2-4 from the control heart displayed a high ThT fluorescence comparable to $H_2O$ supernatant 3 from the patient preparation, indicating that β-sheet-rich structures are present in these fractions. Aβ monomers and preformed Aβ aggregates were used as negative and positive controls, respectively.

For the native FRA 2.5 µg of $H_2O$ supernatants 1-4 was filtered through a cellulose acetate membrane. For the detection the anti-lambda light chain antibody A0101 (Dako) was used. This antibody is also reactive with light chain proteins derived from pig as light chains in NaCl supernatant 1-3 from pig preparation could be detected in the immunoblot (Fig. 2.19 C). The corresponding amount of $H_2O$ supernatant 4 obtained from the patient preparation was also filtered through the membrane. In contrast to patient samples no lambda light chain reactive species in $H_2O$ supernatants 1-4 could be detected in the control preparation (Fig. 2.19 B).

For BN-PAGE analysis followed by Western blotting 5 µg of $H_2O$ supernatant 1-4 was analyzed. In pig $H_2O$ supernatants 1-4 no lambda light chain aggregates were detected in the stacking gel (Fig. 2.19 C, lane 1-4), indicating that no light chain aggregates are present in these samples in contrast to the patient samples (Fig. 2.19 C, lane 5).

Toxicity of the pig-derived $H_2O$ supernatant 4 was assessed using the MTT assay. Therefore, $H_2O$ supernatant 4 was added in two dilutions (undiluted, 1:1000) to HeLa cells and incubated at 37°C for 48 h. To compare the toxicity with patient samples corresponding dilutions of patient-derived $H_2O$ supernatant 4 (undiluted, 1:1000) were used. Fig. 2.19 D shows that pig-derived $H_2O$ supernatant 4 caused no reduction of cell viability. In contrast, $H_2O$ supernatant 4 obtained from the patient heart resulted in a marked impairment of the cell viability.

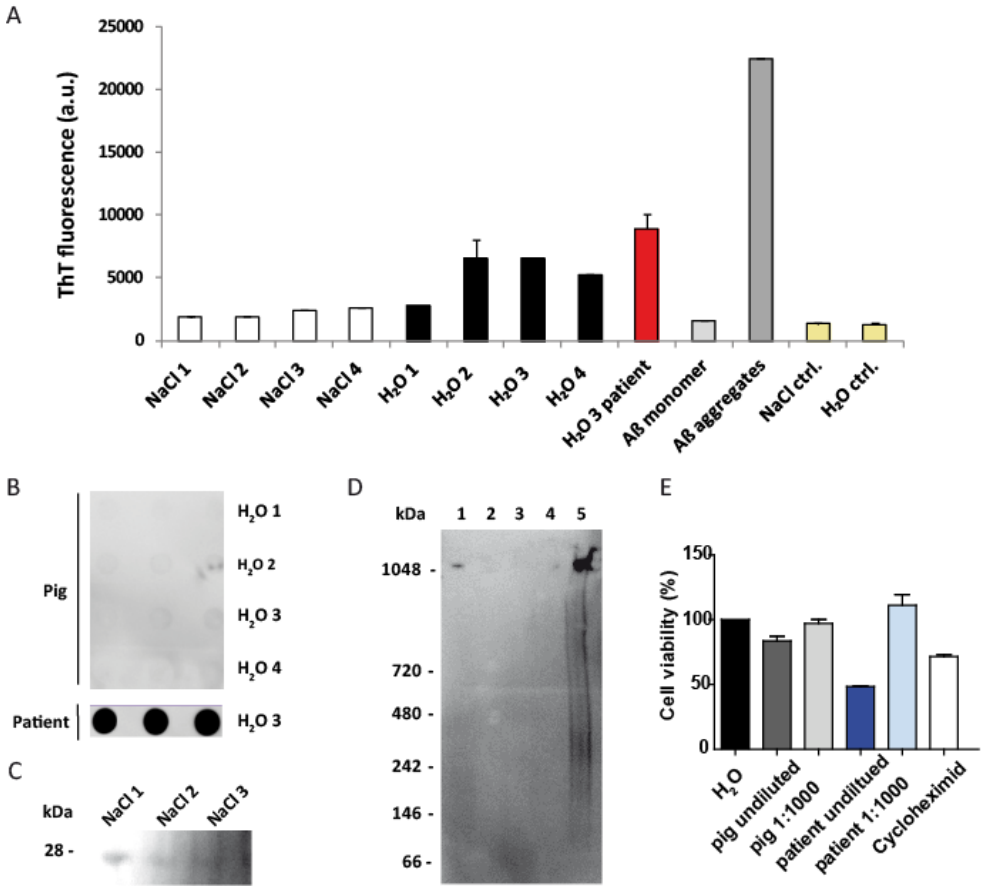


**Fig. 2.19 Analysis of $H_2O$ supernatants obtained from the heart of a pig.**

**A** Pig-derived NaCl and $H_2O$ supernatants 1-4 were analyzed using a ThT assay. 10 µg of each sample was added to 20 µM ThT and ThT fluorescence was measured at an excitation and emission wavelength of 440 nm and 485 nm, respectively using a plate reader. The $H_2O$ supernatant 3 from an AL amyloidosis patient was used to compare the ThT fluorescence with the fluorescence obtained from pig-derived $H_2O$ supernatants 1-4. Aβ monomers and preformed Aβ aggregates as well as NaCl and $H_2O$ solutions were used as controls. No marked differences in the ThT fluorescence between $H_2O$ supernatants derived from pig and patient could be observed. **B** 2.5 µg of pig-derived $H_2O$ supernatants 1-4 and patient-derived $H_2O$ supernatant 3 was filtered through a cellulose acetate membrane and detected with the anti-lambda light chain antibody A0101 (Dako). Native FRA showed no dots on the membrane compared to $H_2O$ supernatant 3 from the patient preparation. **C** 2.5 µg of pig-derived $H_2O$ supernatants 1-3 was analyzed by SDS-PAGE followed by Western blotting. The blot detected with the anti-lambda light chain antibody A0101 (Dako) showed that this antibody also recognizes light chain proteins from intact immunoglobulins derived from feral pig. **D** 5 µg of pig-derived $H_2O$ supernatants 1-4 (lane 1-4 and patient-derived $H_2O$ supernatant 4 (lane 5) was analyzed by BN-PAGE followed by Western blotting. The immunoblot detected with the anti-lambda light chain antibody A0101 (Dako) revealed that $H_2O$ supernatants 1-4 from pig preparation do not contain lambda light chain aggregates in contrast to $H_2O$ supernatant 4 from patient preparation. **E** MTT assay of $H_2O$ supernatant 4 obtained from pig and patient preparations. HeLa cells were treated with $H_2O$ supernatant 4 (undiluted, 1:1000) from pig and patient preparations at 37°C for 48 h. Cycloheximid was used as a control.

## 2.5 Targeting patient-derived light chain aggregates with small molecules

### 2.5.1 Identification of modifiers of patient-derived light chain aggregates using a ThT assay

In order to identify compounds that are able to modify toxic patient-derived light chain aggregates, the $H_2O$ supernatant 4 was incubated with compounds and analyzed by the ThT assay. A reduction of the ThT fluorescence indicates that the binding of ThT to the aggregates is reduced over time as a result of structural changes of the aggregates in the presence of the compound. Thus, using the ThT assay compounds can be identified that potentially modify the toxic conformation of patient-derived light chain aggregates. To test this, a selection of eight compounds (Fig. 2.20) was chosen for their ability to modify patient-derived light chain aggregates. These compounds were previously identified in high throughput screenings (HTS) performed in the laboratory of Prof. Erich E. Wanker and were shown to be effective in Aβ and huntingtin aggregation assays. Thus, they were promising candidates for targeting patient-derived light chain aggregates in cell-free assays. Among these compounds (Fig. 2.20) apomorphine, EGCG, catechin, robinetin and resveratrol belong to the class of polyphenols[66]. Levodopa and Methyldopa are catecholamines that are derived from the amino acid tyrosine[105,216,217]. Quinidine is an alkaloid extracted from the Cinchona tree[218].

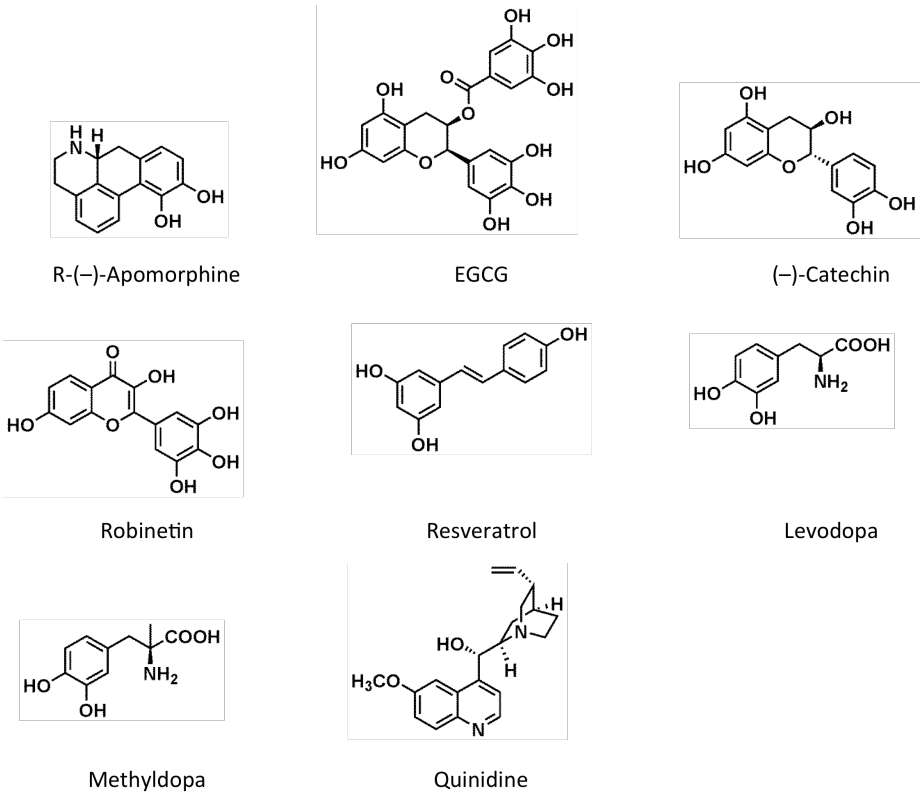


**Fig. 2.20 Chemical structures of selected compounds used in this study.**

In order to test the eight selected chemical compounds, they were dissolved in $H_2O$ to a stock concentration of 20 mM and diluted to an assay concentration of 100 µM. $H_2O$ supernatant 4 (0.7 µg/µl) was incubated in a black 384-well plate with 100 µM of each compound at 37°C and ThT fluorescence was measured after 24 h in a Tecan plate reader. Seven out of eight compounds decreased the ThT signal in the *in vitro* assay (Fig. 2.21). Only quinidine did not reduce the ThT fluorescence compared to the untreated control. The most potent candidates were apomorphine and EGCG, which caused an 8-fold reduction in ThT fluorescence compared to untreated samples. Because apomorphine displayed the stongest reduction in ThT fluorescence and is known to be effective in the inhibition of other amyloidogenic proteins, such as α-synuclein and Aβ, its effect on patient-derived light chain aggregates was studied further.

The polyphenol apomorphine (Fig. 2.21 C ) is a derivative of morphine and its synthesized by heating morphine at 100°C with HCl or $ZnCl_2$[219]. Because apomorphine is a chiral molecule, R-and S-enantiomer can be obtained from synthesis. In clinical practice, the R-apomorphine enantiomer is the only active form. It is a very lipophilic compound which is rapidly autooxidized. Despite being a derivative of the opiod, morphine, it has no opioid analgesic properties, but has a short-acting agonist effect on D1 and D2 receptors[220]. Apomorphine was first discovered by Landsbury and colleagues who investigated the inhibition of α-synuclein, an amyloidogenic protein that is found to accumulate as Lewy bodies in the brain of Parkinson's disease patients[192]. Later, it was also shown by Lashuel and coworkers that apomorphine inhibits Aβ aggregate formation[82].

A control experiment was designed to ensure that the observed decrease in ThT fluorescence is not the result of a quenching effect of the compounds on the fluorescence of ThT. If the reduction of ThT fluorescence is affected by quenching, a concentration-dependent loss of the fluorescence would be observed with increased compound concentration. To test this, $H_2O$ supernatant 4 was incubated with 10 µM ThT for 2 min. Then, apomorphine (0.5, 25 and 50 µM) was added and the fluorescence was immediatly quantified at a wavelength of 440 nm in a Tecan plate reader. No concentration-dependent reduction of the ThT signal upon addition of apomorphine to the assay was detected, suggesting the reduction of the ThT fluorescence is not due to a quenching effect (Fig. 2.21 B). However, it could not be excluded that the compound competitively binds with ThT for β-sheet-rich sites along the fibrils and is able to displace ThT from these sites.

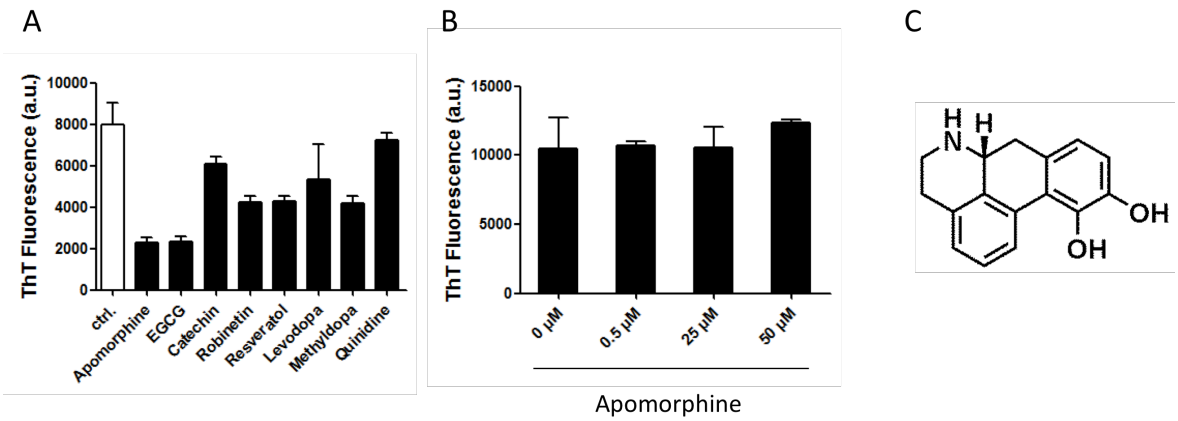


**Fig. 2.21 Identification of chemical compounds that potentially target amyloidogenic patient-derived light chain aggregates using a ThT assay.**

**A** Eight compounds were tested in a ThT-based assay for their ability to modify patient-derived light chain aggregates isolated from the heart of a patient with AL amyloidosis. Aggregates were incubated with 100 µM of each compound in a black 384-well plate at 37°C for 24 h and ThT fluorescence was measured at an excitation and emission wavelength of 440 nm and 485 nm, respectively. **B** In order to exclude potential quenching effects of apomorphine on the ThT fluorescence different concentrations of apomorphine were added to patient-derived light chain aggregates and ThT fluorescence was immediately measured in a Tecan plate reader. Under these conditions no concentration-dependent decrease of the ThT fluorescence was observed. **C** Chemical structure of apomorphine.

### 2.5.2 Effect of apomorphine on patient-derived light chain aggregates using ThT and CR assays

To monitor the effect of apomorphine on patient-derived light chain aggregates $H_2O$ supernatant 4 (0.7 µg/µL) was incubated in the presence of apomorphine (100 µM) in a 1.5 ml LoBind tube at 300 rpm and 37°C. After 24 h aliquots were taken and analyzed using the ThT assay. In presence of apomorphine ThT fluorescence intensity significantly decreased to ~20%, compared to the untreated control, indicating that apomorphine has an effect on the binding of ThT to patient-derived light chain aggregates (Fig. 2.22 A). The reduced ThT fluorescence can have different possible reasons. Apomorphine binds competitively with ThT molecules to the aggregates. Or, apomorphine induces a conformational change in the aggregates. It is also possible that aggregates were disassembled by apomorphine.

To confirm the results obtained from the ThT assay, a CR assay was performed as an alternative assay. Binding of CR to β-sheet rich structures induces a characteristic increase in fluorescence at 614 nm[221]. Patient-derived light chain aggregates were incubated in presence of 100 µM apomorphine at 37°C and 300 rpm in a 1.5 mL LoBind tube. After 24 h 10 µM CR was added and the fluorescence was measured at 614 nm in a Tecan plate reader. In presence of apomorphine CR fluorescence was

significantly decreased to ~40% compared to the untreated control, indicating that apomorphine influences the binding of CR to patient-derived light chain aggregates (Fig. 2.22 B). This result is in good accordance with the aforementioned ThT assay data (Fig. 2.22 A).

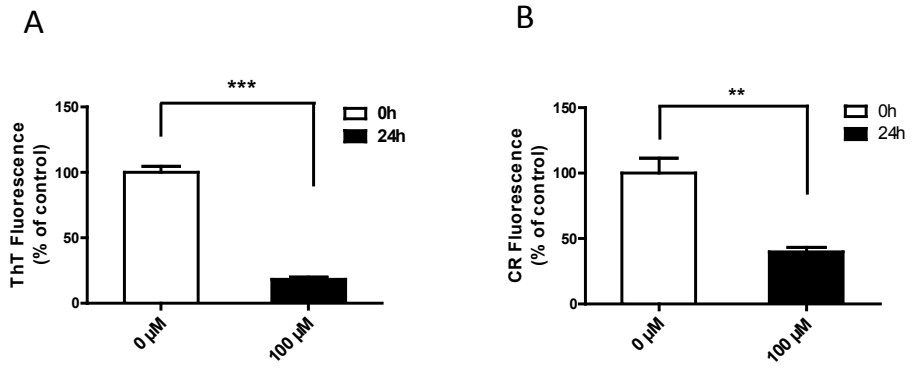


**Fig. 2.22 Effect of apomorphine on patient-derived light chain aggregates using ThT and CR assays.**

**A** Patient-derived light chain aggregates ($H_2O$ supernatant 4) were incubated with apomorphine (100 µM) at 37°C. After 24 h ThT (10 µM) was added and the fluorescence was measured in a Tecan plate reader. Asterisk indicates a statistically significant reduction in ThT fluorescence relative to the control ($p < 0.05$). Error bars represent means of SEM from three independent experiments. Statistical analysis was performed using the t-test and GraphPad Prism 5 software. **B** To confirm the ThT results a CR assay was used in the same experimental setup as described in A. In presence of apomorphine CR fluorescence was significantly decreased ($p < 0.05$), indicating that apomorphine has an influence on the binding of CR to patient-derived light chain aggregates.

### 2.5.3 Effect of apomorphine on patient-derived light chain aggregates analyzed by a filter retardation assay

Next, it was investigated whether apomorphine has the ability to influence the size and the SDS-stability of patient-derived light chain aggregates. $H_2O$ supernatant 4 was incubated in the presence or absence of apomorphine (100 µM) at 37°C and 300 rpm in a 1.5 mL protein LoBind tube. After 24 h samples were analyzed using FRAs under native as well as denaturing conditions.

First, the samples were assessed with the FRA under none-reducing and non-denaturating conditions to maintain the secondary structure. 5 µg of $H_2O$ supernatant 4 was spotted onto a cellulose acetate membrane, filtered through the membrane and immunoprobed with an anti-lambda light chain antibody (A0101, Dako). The analysis of the filer membrane revealed that the antibody signal is reduced in presence of 100 µM apomorphine compared to untreated control (Fig. 2.23 A). This suggests that the compound promotes a disassembly of large light chain aggregates and smaller species are formed that are no longer retained on the filter membrane. SEC experiments or native gels could answer this assumption. Another possible explanation could be that apomorphine

promotes a remodeling of light chain aggregates towards a conformer that shows reduced antibody reactivity due to epitope masking.

To further analyze the effect of apomorphine on the SDS-stability of patient-derived light chain aggregates a denaturing FRA was performed. Therefore, 5 µg of untreated and compound treated $H_2O$ supernatants 4 were boiled in 4% SDS and 100 mM DTT at 95°C for 5 min and subsequently filtered through a cellulose acetate membrane with a pore size of 0.2 µm and immunoprobed with an anti-lambda light chain antibody (A0101, Dako). In the absence of apomorphine, no antibody signal was detected, indicating that patient-derived light chain aggregates are non-SDS-resistant structures and therefore are not retained on the cellulose acetate membrane (Fig. 2.23 B). In contrast, when patient-derived light chain aggregates were incubated with apomorphine a strong antibody signal could be detected on the membrane. These results strongly indicate that the treatment with apomorphine promotes the conversion of patient-derived light chain aggregates from SDS-soluble into SDS-insoluble structures. Strikingly, these results are similar to previous observations with the polyphenolic compound EGCG that was found to convert high molecular weight Aβ aggregates into amorphous SDS-stable structures[185]. Thus, apomorphine could act by a similar mechanism as EGCG when added to amyloidogenic light chain aggregates.

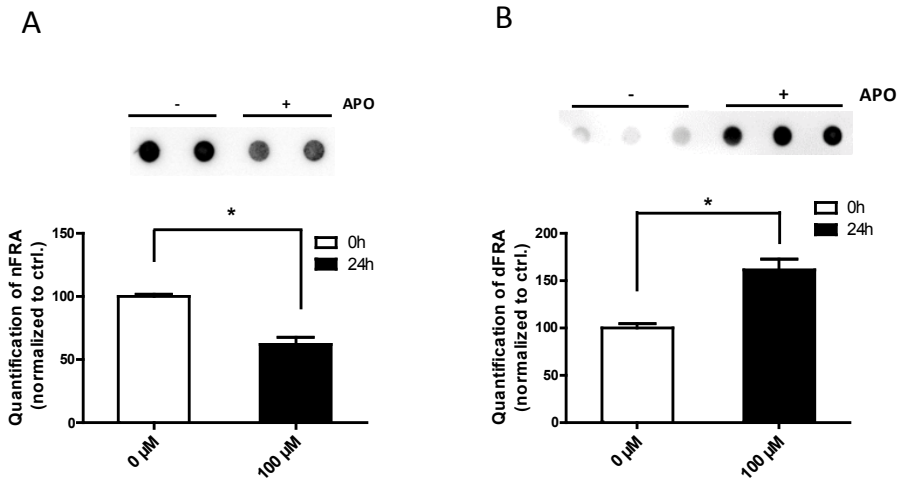


**Fig. 2.23 Effect of apomorphine on patient-derived light chain aggregates analyzed by native and denaturing filter retardation assays.**

Patient-derived light chain aggregates ($H_2O$ supernatant 4) were incubated with and without apomorphine (100 µM) at 37°C and 300 rpm in 1.5 ml LoBind tubes. After 24 h samples were filtered through a cellulose acetate membrane under native (**A**) and denaturing (**B**) conditions and immunoprobed with an antibody directed against the lambda light chain protein (A0101, Dako). Under native conditions the antibody signal decreased ($p < 0.05$) in presence of apomorphine, suggesting that patient-derived light chain aggregates are smaller in size or have an alterd structure so that the antibody could not recognize the epitope. Under denaturing conditions the amount of SDS-stable light chain aggregates was increased in presence of apomorphine ($p < 0.05$). Quantification of dots is shown below the respective filters.

### 2.5.4 Effect of apomorphine on patient-derived light chain aggregates using the ANS assay

Several lines of evidence indicated that amyloidogenic aggregates expose hydrophobic regions on their surface, a feature that has been strongly correlated with cellular toxicity of protein aggregates[222]. It can be hypothesized that along with structural rearrangements apomorphine may also alter the solvent exposed hydrophobic regions. 1-anilinonaphthalene-8-sulfonate (ANS) is routinely used as a dye to efficiently detect hydrophobic regions in proteins upon binding[222]. Both an increase in fluorescence intensity and a blue shift in the peak wavelength of the fluorescence spectrum, $\lambda_{max}$, are usually observed upon binding of ANS to exposed hydrophobic regions on the surface of proteins or protein assemblies[223]. In order to monitor changes in the surface hydrophobicity of patient-derived light chain aggregates upon apomorphine treatment the ANS assay was used. Therefore, ANS fluorescence was measured in apomorphine treated and untreated aggregate samples. $H_2O$ supernatant 4 was incubated with and without 100 µM apomorphine at 300 rpm and 37°C in 1.5 mL protein LoBind tubes. Aliquots were taken after 24 h, transferred to a black 384-well plate and ANS was added to a final concentration of 10 µM. The fluorescence emission spectrum was recorded from 400 nm to 600 nm using a Tecan plate reader. Untreated patient-derived light chain aggregates exhibited a high ANS fluorescence intensity, whereas a decreased fluorescence intensity and a red shift of $\lambda_{max}$ from 480 nm to 540 nm was observed in presence of apomorphine (Fig. 2.24). This suggests that apomorphine treatment decreases the solvent exposed hydrophobic regions in patient-derived light chain aggregates. This observation supports the view that apomorphine modifies the surface hydrophobicity of patient-derived light chain aggregates. Another explanation could be that apomorphine has a higher binding affinity for patient-derived light chain aggregates than ANS. In this case ANS molecules would not be able to bind to the aggregates thereby unable to change its fluorescence properties.

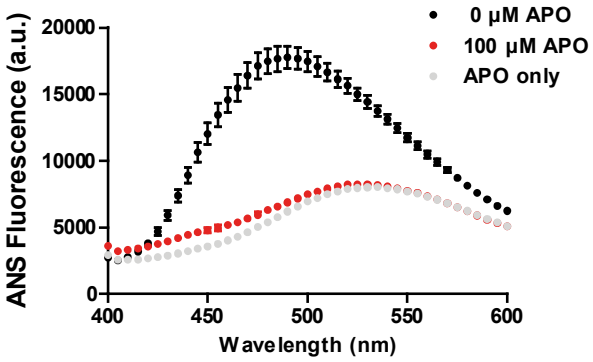


**Fig. 2.24 Effect of apomorphine on the surface hydrophobicity of patient-derived light chain aggregates monitored by the ANS binding assay.**

Patient-derived light chain aggregates were incubated with and without apomorphine (100 µM) at 300 rpm and 37°C for 24 h in 1.5 ml protein LoBind tubes. To monitor changes in surface hydrophobicity 8-Anilinonaphthalene-1-sufonic acid (ANS) was added to the samples and a fluorescence emission spectrum from 400 nm to 600 nm was recorded using a Tecan plate reader. Apomorphine only (100 µM) was used as a control. In presence of 100 µM apomorphine ANS fluorescence dramatically decreased compared to untreated control samples.

### 2.5.5 Concentration- and time-dependent analysis of the effect of apomorphine on patient-derived light chain aggregates

To investigate whether apomorphine alters patient-derived light chain aggregates in a dose- and time-dependent manner 0, 50 and 100 µM apomorphine was added to $H_2O$ supernatant 4 and incubated at 37°C with agitation (300 rpm) in 1.5 ml LoBind tubes. Aliquots were taken after 4 h and 24 h, transferred to a black 384-well plate, mixed with ThT (10 µM final concentration) and the fluorescence was measured in a Tecan plate reader. A concentration- as well as time-dependent reduction in ThT fluorescence could be observed (Fig. 2.25 A). A concentration of 50 µM apomorphine induced a ~2.5-fold decrease in fluorescence after 24 h and a ~5-fold reduction after 48 h. In presence of 100 µM apomorphine a ~5-fold and a ~10-fold reduction in the ThT signal was observed after 24 h and 48 h, respectively.

Next, to investigate a concentration dependency regarding the change in surface hydrophobicity, the ANS assay was performed. Therefore, $H_2O$ supernatant 4 was incubated with 0, 50 or 100 µM apomorphine for 24 h at 37°C. Samples were mixed with 10 µM ANS and a fuorescence emission spectrum from 400 to 600 nm was measured in a Tecan plate reader. ANS fluorescence was dramatically decreased when the indicated concentrations of apomorphine were added to the samples (Fig. 2.25 B). However, no concentration dependent effects could be observed, suggesting

that 50 µM apomorphine is already sufficient to change the surface properties of patient-derived light chain aggregates.

To investigate the formation of SDS-stable structures in a concentration-dependent manner $H_2O$ supernatant 4 was incubated at 37°C in the presence of different apomorphine concentrations (0, 0.5, 5, 12.5, 25 and 50 µM). Samples were taken after 4 h and 24 h and were analyzed using the denaturing FRA[203]. Time-resolved data revealed an increase in the SDS-resistance of patient-derived light chain aggregates when ≥25 µM of the compound was added to reactions for 4 h. A significant effect was also observed when 5 µM of the compound was incubated for 24 h with the samples (Fig. 2.25 C, D).

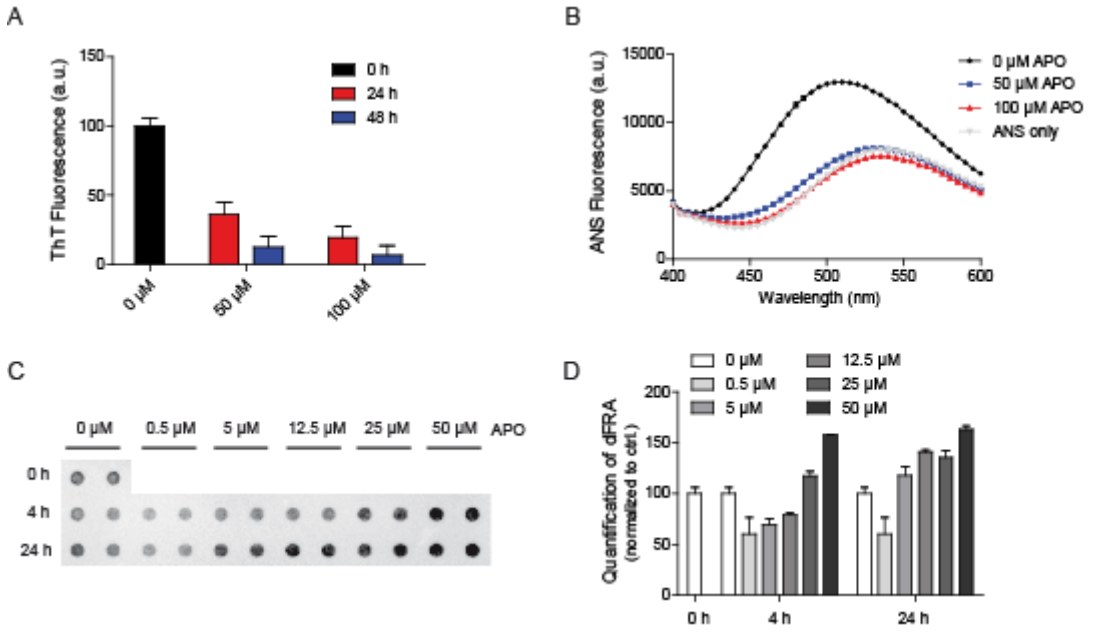


**Fig. 2.25 Analysis of concentration-dependent effects of ampomorphine on patient-derived light chain aggregates.**

**A** Time-resolved ThT binding assays of patient-derived light chain aggregates ($H_2O$ supernatant 4) incubated in the absence and presence of 50 and 100 µM apomorphine for 24 h and 48 h. **B** Concentration-dependent ANS assay of patient-derived light chain aggregates. 0, 50 and 100 µM apomorphine was added to $H_2O$ supernatant 4 and incubated for 24 h at 37°C. **C** Patient-derived light chain aggregates were incubated with different concentrations of apomorphine at 37°C for 4 or 24 h. Then, samples were analyzed using a denaturing FRA. An anti-lambda light chain antibody (A0101, Dako) was used for immunological detection. **D** Quantification of the dots on the filter membrane is shown in C.

### 2.5.6 Effect of apomorphine on the morphology of patient-derived light chain aggregates

As the previously applied biochemical assays do not distinguish between fibrillar and nonfibrillar aggregates, potential morphological changes of patient-derived light chain aggregates were investigated in the presence an absence of apomorphine by using EM. The $H_2O$ supernatant 4 was incubated with 100 µM apomorphine at 300 rpm and 37°C for 24 h. Then, aliquots were spotted onto carbon-coated grids and negatively stained with uranylacetate. Electron micrographs of patient-derived light chain aggregates that were not treated with apomorphine showed fibrillar (Fig. 2.26 A) as well as amorphous structures (Fig. 2.26 C) as previously described (Fig. 2.10). In presence of apomorphine fibrillar structures were not noticeably modified (Fig. 2.26 B). In contrast, amorphous aggregates that were previously present in a dense network of interconnected aggregates with a size of >1 µm appeared to be smaller (~500 nm) in presence of the compound. This suggests that apomorphine does not affect light chain fibrils but instead selectively alters amorphous aggregates.

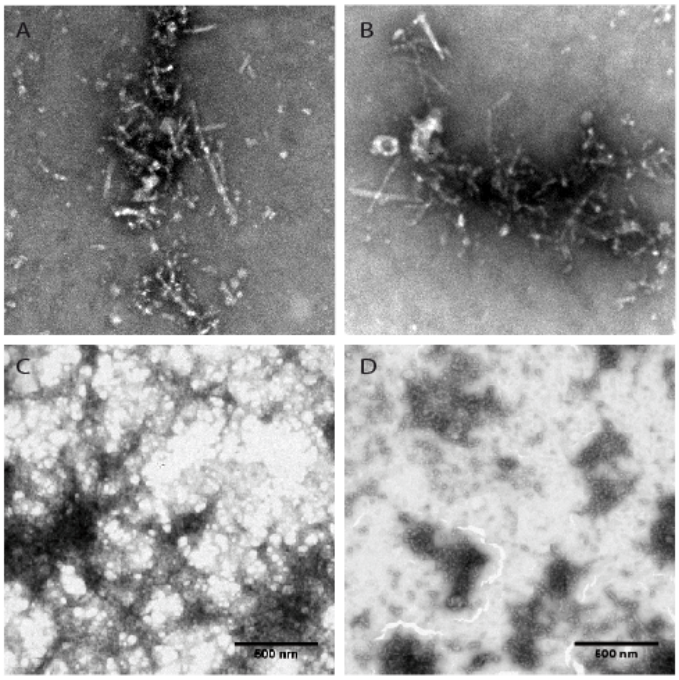


**Fig. 2.26 Morphological analysis of patient-derived light chain aggregates in presence of apomorphine using EM.**

**A, C** Electron micrographs of patient-derived light chain aggregates without apomorphine treatment. A dense network of fibrillar as well as amorphous aggregates was observed. **B, D** Patient-derived light chain aggregates incubated with 100 µM apomorphine at 37°C for 24 h. Scale bar represents 500 nm.

### 2.5.7 Effect of apomorphine on the viability of HeLa cells in presence of patient-dervied light chain aggregates

In order to determine whether apomorphine *per se* is toxic for HeLa cells, they were incubated with 10 and 100 µM apomorphine for 48 h at 37°C. Then, the MTT assay was conducted to measure potential compund toxicity. None of the tested apomorphine concentrations tested caused a reduction in cell viability, compared to untreated control cells. This indicates that the comound *per se* does not induce MTT reduction in HeLa cells under these assay conditions (Fig. 2.27 A).

In order to examine whether apomorphine reduces the toxicity of patient-derived light chain aggregates in HeLa cells (described in section 1.4.1), the MTT assay was conducted. Cells were incubated with $H_2O$ supernatant 4 in the presence or absence of 100 µM apomorphine at 37°C for 48 h. Then, the cells were analyzed using the MTT assay. In the absence of apomorphine patient-derived light chain aggregates reduced the cell viability to ~47% after 48 h (Fig. 2.27 B). In contrast, in the presence of 100 µM apomorphine the cell viability was not decreased compared to untreated control samples, suggesting that apomorphine may have a rescuing effect on mitochondrial dysfunction that was induced by patient-derived light chain aggregates.

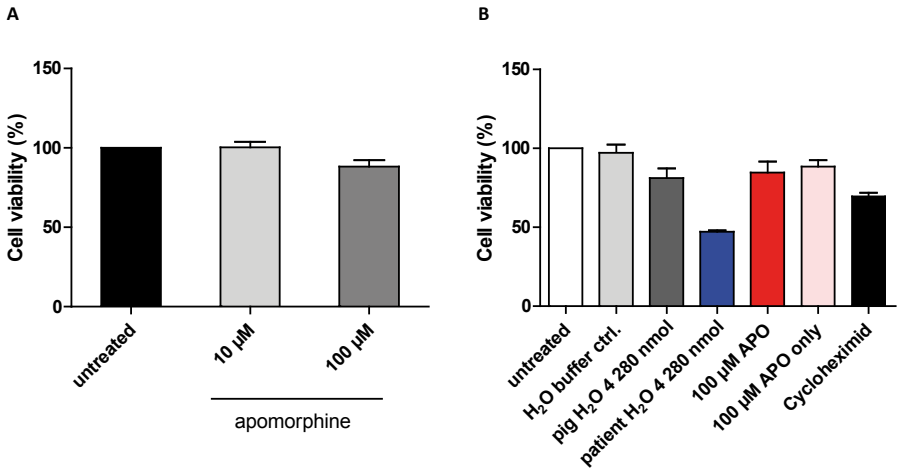


**Fig. 2.27 Apomorphine treated HeLa cells shows increased viability after incubation with patient-derived light chain aggregates.**

**A** HeLa cells were treated with 10 or 100 µM apomorphine at 37°C. After 48 h the toxicity of apomorphine was assessed using the MTT assay as described in the Materials and Methods section 4.2.4.2. No decrease in cell viability was observed in apomorphine treated HeLa cells. **B** HeLa cells were treated with and without apomorphine (100 µM) in the presence of patient-derived light chain aggregates at 37°C. Cell viability was evaluated with the MTT assay after 48 h. Light chain treated cells exhibited ~47% reduced viability when compared to untreated cells or solvent control. In the presence of 100 µM apomorphine cell viability was increased to ~85%.

## 2.6 Investigation of full-length light chain protein aggregation *in vitro*

### 2.6.1 Expression and purification of the full-length light chain protein AL01

In order to study the aggregation of recombinant light chain protein *in vitro*, a full-length light chain protein sequence was obtained from an AL amyloidosis patient with predominant heart involvement. The expression plasmid was a kind gift of Prof. Dr. Vittorio Perfetti's laboratory[224]. Essentially, RNA from bone marrow cells of the AL amyloidosis patient was transcribed into cDNA using RT-PCR (Fig. 2.28). The start codon and two stop codons were introduced through the forward and reverse primer, respectively. The DNA was digested with the *Bsm*BI restriction enzyme and was ligated into the pASK-IBA33plus expression plasmid. The amino acid sequence (217 aa) of the full-length light chain protein AL01 is shown in Fig. 2.28 B.

A

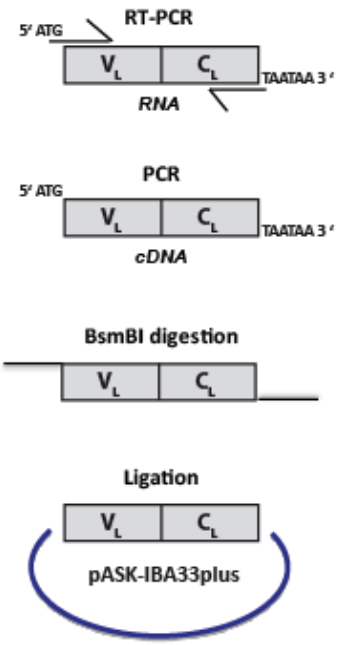


B

MQSVLTQPPSTSGTPGQRVTISCSGSSSNIETNTVNWYQQLPGTAPKLVMHTNNQRPSGVP-
DRFSGSRSGTSASLAIGGLQSEDEADYFCAAWDDNLNGVIFGGGTKLTVLGQPKAAPSVTLFPPSSEELQA
NKATLVCLISDFYPGAVTVAWKADSSPVKAGVETTTPSKQSNNKYAASSYLSLTPEQWKSHKSYSCQVTHE
GSTVEKTVAPTECS

**Fig. 2.28 Schematic representation of the cloning strategy of the cDNA encoding recombinant full-length light chain AL01 protein.**

**A** cDNA encoding the full-length light chain protein was cloned into an expression plasmid as described in Rognoni et al. 2013[224]. Full-length light chain DNA was obtained by RT-PCR of RNA extracted from bone marrow cells from an AL amyloidosis patient with predominant heart involvement. A start codon and two stop codons were introduced at the 5' and 3' end, respectively. After PCR amplification the DNA was digested with the BsmBI restriction enzyme and ligated into the expression plasmid pASK-IBA33plus. $V_L$: Variable domain of the light chain, $C_L$: Constant domain of the light chain. **B** Amino acid sequence of full-length light chain protein AL01.

To produce the full-length light chain protein AL01 *E. coli* BL21 DE3 was transformed with the plasmid pASK-IBA33plus. BL21 DE3 is an expression strain deficient in proteases Lon and OmpT. The expression of the AL01 light chain protein was induced by addition of anhydrotetracycline (AHTC) to the growth medium for 4 h at 37°C. Cells were harvested, lysed and light chain protein AL01 was purified from inclusion bodies (IB). Therefore IBs were solubilized under denaturating conditions using 6 M GndHCl and β-MeEtOH followed by renaturation of the solubilised proteins using a redox shuffling system. To analyze the success of the purification each fraction was subjected to a polyacryamid gel which was stained with Coomassie Brilliant Blue. In contrast to uninduced cells (Fig. 2.29, lane 1,) induced cells (Fig. 2.29, lane 2) show a prominent band migrating at ~25 kDa, indicating the overexpression of the full-length light chain protein AL01. In lanes 3-8 samples from the isolation of proteins from IBs were loaded, (pellet fractions, lane 4, 6 and 8, Fig. 2.29). Solubilized and refolded light chain protein is shown in lane 9 and 10, respectively. Fractions before and after dialysis are shown in lane 11 and 12. The corresponding Western blot is shown in Fig. 2.29 B, in which full-length light chain protein AL01 could be detected with an anti-lambda light chain antibody (A0101, Dako). From one liter of bacterial culture ~34 mg light chain protein AL01 was obtained.

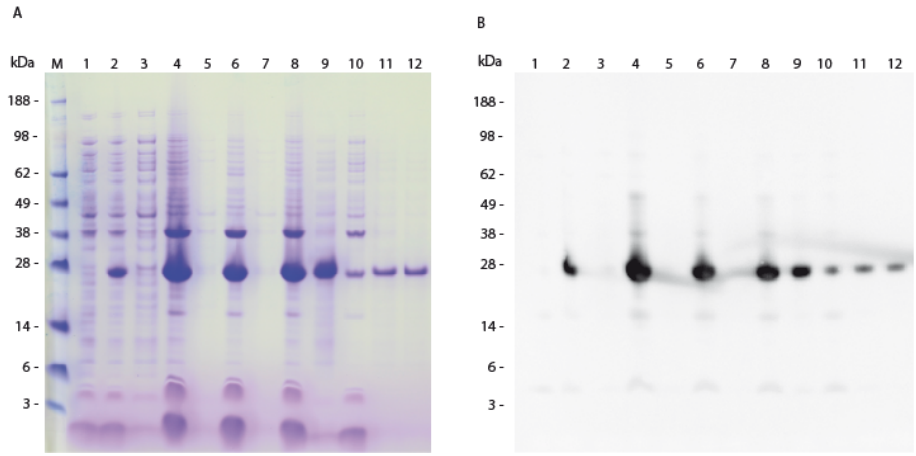


**Fig. 2.29 Analysis of recombinant full-length light chain protein AL01 by SDS-PAGE and Western blotting.**

**A** Coomassie staining of SDS-PAGE which monitors the purification of full-length light chain protein AL01. The protein was expressed in *E. coli* BL21 DE3 and purified from inclusion bodies as described in the Materials and Methods section 4.2.2.12. Samples from each purification step were analyzed on a 4-16% polyacrylamide gel and stained with Coomassie Brilliant Blue. Full-length light chain protein runs at ~25 kDa as expected. M: Seeblue plus2 pre-stained protein standard (Thermo Scientific), **1**: Uninduced cells, **2**: Induced cells, **3**: Supernatant 1, **4**: Pellet 1, **5**: Supernatant 2, **6**: Pellet 2, **7**: Supernatant 3, **8**: Pellet 3, **9**: Solubilized protein, **10**: Refolded protein **11**: Protein before dialysis, **12**: Protein after dialysis. **B**: Proteins from the SDS-gel were transferred to a nitrocellulose membrane by Western blotting. For immunological detection the anti-lambda light chain antibody A0101 (Dako) was used.

### 2.6.2 Establishment of an *in vitro* ThT aggregation assay for the detection of spontaneous light chain protein aggregation

Previous studies have demonstrated that ThT is one of the most commonly used dyes for monitoring the formation of ordered β-sheet rich conformations[73]. ThT binds to protein aggregates thereby enhancing its fluorescence emission which can be measured by a spectrophotometer. In order to monitor full-length light chain AL01 aggregation a time-resolved ThT assay was established. Recombinant full-length light chain protein AL01 (1 mg/ml) was incubated in Tris buffer at 37°C with shaking (400 rpm). Aliquots were taken at indicated time points and were mixed with 10 µM ThT. Then, the fluorescence was measured at an excitation and emission wavelength of 440 nm and 482 nm, respectively. A dramatic increase of ThT fluorescence could be observed over time, indicating the formation of β-sheet-rich aggregates (Fig. 2.30). Fig. 2.30 A illustrates that the aggregation kinetics of full-length light chain protein AL01 immediately started without a detectable lag-phase and reached a plateau after ~18 h. Glutathione-S-Transferase (GST) (30 µM), which is known to be highly soluble was used as a negative control. No increase of ThT fluorescence was observed after 72 h for the control sample (Fig. 2.30 B). By contrast, ThT fluorescence was increased for Aβ (30 µM) after 72 h, which was used as a positive control. These results showed that the ThT assay is suitable for monitoring the aggregation of the full-length light chain protein AL01 *in vitro*.

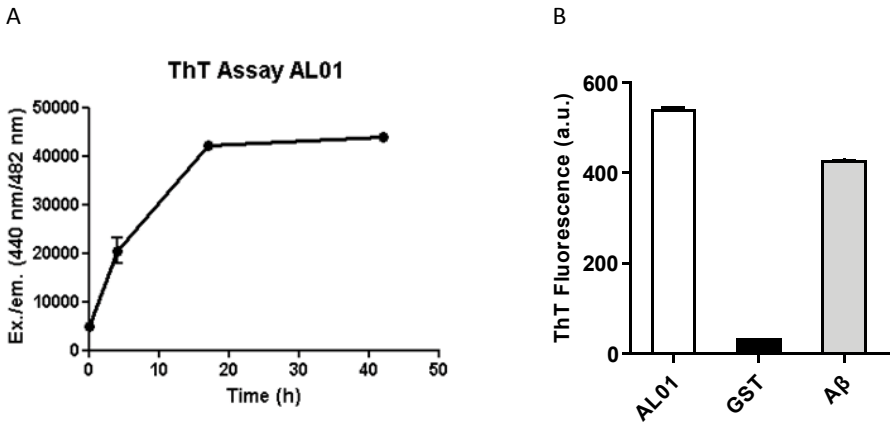


**Fig. 2.30 Establishment of a ThT assay for monitoring the aggregation of recombinant full-length light chain protein AL01.**

**A** 30 µM full-length light chain protein AL01 was incubated at 37°C and 400 rpm and ThT fluorescence was recorded over time in a Tecan plate reader. After 24 h the ThT signal was greatly increased, indicating the formation of β-sheet rich aggregates. **B** GST (30 µM) and Aβ (30 µM) were used as a negative and positive controls, respectively. No increase of the ThT signal was observed for GST throughout the time course.

### 2.6.3 Investigating the effect of DTT on full-length light chain protein AL01 aggregation

Previous studies have demonstrated that aggregation of light chain proteins is induced only in the presence of dithiothreitol (DTT)[225]. DTT is a reducing agent that is frequently used to reduce disulfide

bonds in proteins. To test the influence of DTT on the aggregation of recombinant light chain AL01 protein different concentrations of the light chain protein (0.125, 0.25, 0.5 mg/ml) were incubated in 50 mM NaOAc 150 mM NaCl pH 7 at 37 °C in presence and absence of 1 mM DTT. Aliquots were taken after 2, 4 and 24 h, mixed with 0.05 mM ThT and fluorescence was measured in a Tecan plate reader. In the absence of DTT ThT fluorescenc did not increase after 24 h (Fig. 2.31 A). In contrast, a dramatic increase in ThT fluorescence was observed after 24 h in samples that contain DTT (Fig. 2.31 B). The ThT signal was ~6-fold higher compared to non-reduced samples. This result strongly suggests that full-length light chain AL01 aggregation is promoted in presence of DTT.

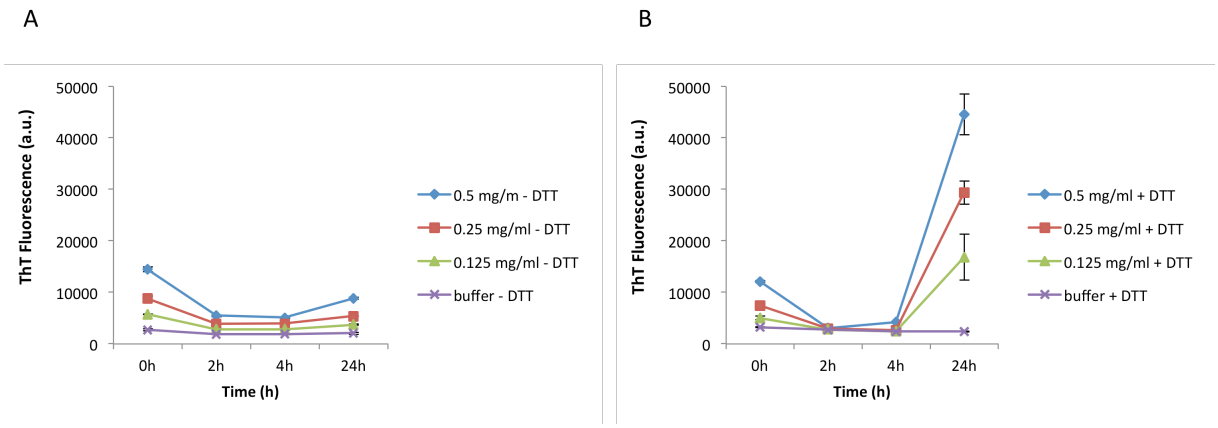


**Fig. 2.31 The influence of DTT on the aggregation of recombinant full-length light chain AL01 monitored by ThT assays.**

**A** Full-length light chain protein AL01 was incubated in 50 mM sodium acetate buffer (pH 7) at indicated concentrations in the absence of DTT at 37°C. ThT fluorescence was measured after 2, 4 and 24 h in a Tecan plate reader. **B** Full-length light chain protein AL01 was incubated as described in A but in the presence of DTT. A dramatic increase of the ThT fluorescence signal was observed in a concentration-dependent manner.

### 2.6.4 Investigating the aggregation of full-length light chain protein AL01 using BN-PAGE and Western blotting

To confirm the results from the ThT assay described in section 2.6.2 samples were analyzed using BN-PAGE followed by Western blotting. 200 ng of each sample was loaded onto a native polyacrylamide gel, separated by electrophoresis and transferred to a PVDF membrane by Western blotting. The samples were immunoprobed with the anti-lambda light chain antibody A0101 (Dako). Before incubation at 37°C a faint band at ~66 kDa and a prominent band at ~250 kDa could be detected in samples incubated without DTT (Fig. 2.32 A). By contrast, only one band with a molecular weight ranging between ~20 and 66 kDa was seen in DTT treated samples (Fig. 2.32 A). After 24 h only samples incubated in the presence of DTT show a high molecular weight protein smear ranging from

~20 to >480 kDa (Fig. 2.32 B, red box). This result confirms the data obtained with the ThT assay, indicating that the aggregation of the AL01 protein is promoted in the presence of DTT.

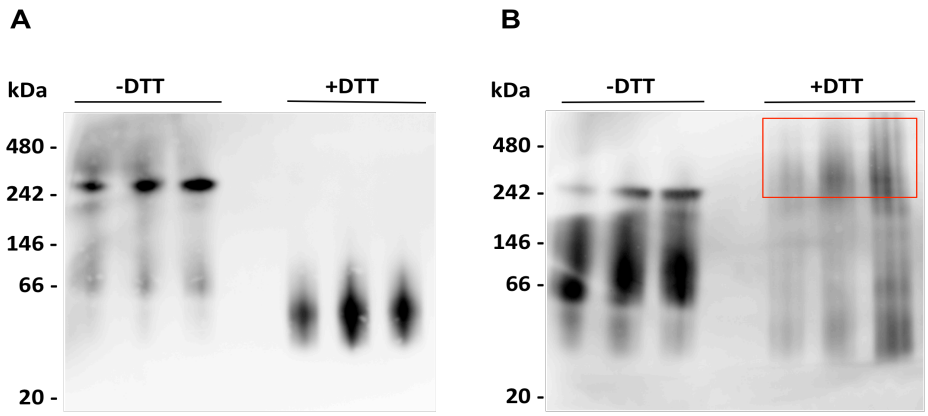


**Fig. 2.32 Analysis of the aggregation of the light chain protein AL01 in the presence of DTT using BN-PAGE followed by Western blotting.**

**A** Full-length light chain protein AL01 at the 0 h time point was analyzed in the presence and absence of DTT by BN-PAGE followed by Western blotting. For immunological detection an anti-lambda light chain antibody (A0101, Dako) was used. In the absence of DTT protein bands with sizes of ~66 and ~250 kDa, respectively, were observed. In contrast, in the presence of DTT only one band migrating between ~20 and 66 kDa was detected. **B** Full-length light chain protein AL01 was analyzed after incubation for 24 h at 37°C in the presence and absence of DTT. Only in presence of DTT a high molecular weight protein smear was observed, indicating that full-length light chain AL01 aggregation is promoted in the presence of DTT.

### 2.6.5 Investigating full-length light chain aggregation at different pH

Extrinsic factors, such as the pH, are known to influence aggregation kinetics[226-229]. In order to evaluate the pH-dependence of AL01 aggregation, recombinant light chain protein was incubated at pH 2 (KCl/HCl), pH 4 (NaOAc), pH 5.5 (100 mM MES), pH 6.6 (100 mM MES) and pH 7.2 (low salt buffer) with 10 µM ThT at 37°C for 24 h in a black 384-well plate. ThT fluorescence was recorded every 10 min at an extinction and emission wavelength of 440 nm and 480 nm, respectively. As illustrated in Fig. 2.33 the aggregation rate shows a strong pH dependence from pH 2 to pH 7.2 with the fastest kinetics at acidic conditions. At pH 2 the plateau is already reached after ~8 h in contrast to the aggregation at pH 4, 5.5, 6.5 and 7.2.

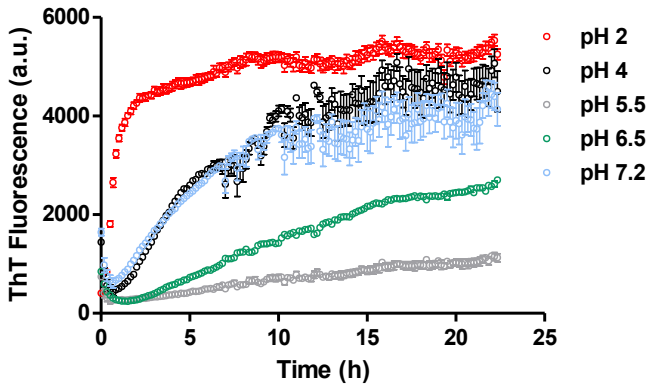


**Fig. 2.33 The effect of the pH on the aggregation of recombinant full-length light chain AL01 protein monitored by ThT assay.**

Recombinant full-length light chain protein AL01 (30 µM) was incubated with ThT (10 µM) at pH 2 (HCl/KCl), pH 4 (NaOAc), pH 5.5 (100 mM MES), pH 6.5 (100 mM MES), pH 7.2 (low salt buffer) at 37°C for 24 h. ThT fluorescence intensity was used to monitor aggregation using a Tecan plate reader.

### 2.6.6 Investigating the aggregation of full-length light chain AL01 protein using a Congo red amyloid-binding assay

To confirm the spontaneous formation of β-sheet-rich AL01 aggregates a CR amyloid-binding assay was performed. CR is a dye that binds to β-sheet rich structures with a concomitant enhancement in its fluorescence[230]. Full-length light chain protein AL01 (30 µM) was incubated at 42°C with agitation (400 rpm) in 1.5 ml LoBind tubes. Aliquots were taken after 24 h and were mixed with a 10 µM CR solution. Fluorescence was measured at an excitation wavelength of 497 nm and an emission spectrum was recorded from 550 nm to 700 nm in a Tecan plate reader. After 24 h the fluorescence was ~2-fold higher compared to the 0 h time point, indicating the spontaneous formation of β-sheet rich structures (Fig. 2.34). The increased CR fluorescence compared to the control at the 0 h time point can be interpreted as the intrinsic β-sheet content of non-aggregated light chain protein.

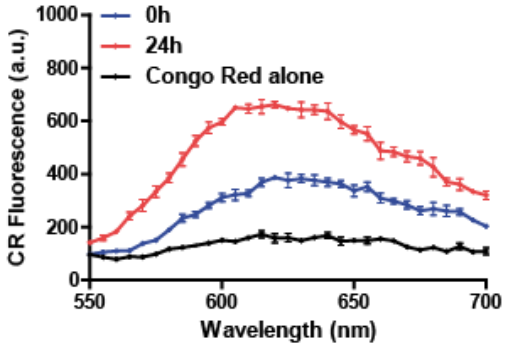


**Fig. 2.34 Monitoring the aggregation of the recombinant full-length light chain protein AL01 using a Congo red assay.**

Recombinant full-length light chain protein AL01 (30 µM) was incubated at 42°C and 400 rpm in a 1.5 ml protein LoBind tube. After 24 h samples were mixed with CR (10 µM) and fluorescence spectra were recorded from 550 to 700 nm at an excitation wavelength of 497 nm in a Tecan plate reader.

### 2.6.7 Establishment of a turbidity assay for monitoring AL01 aggregation *in vitro*

In order to confirm the formation of AL01 aggregates a third independent assay was established using turbidity measurements[231]. As protein aggregation proceeds the solution becomes more turbid and its absorbance increases over time[232]. Recombinant full-length light chain protein AL01 (0.2, 0.4, 0.5 and 0.8 mg/ml) was incubated in Tris buffer at 42°C and the optical density (OD) was measured at 405 nm every 20 min in a Tecan plate reader. Fig. 2.35 A shows a concentration-dependent increase in turbidity over time, indicating the formation of aggregates. The lag-phase was reduced by 1/3 at a ~4-fold higher concentration of full-length light chain protein. As a negative control GST was used at a concentration of 0.3 mg/ml, resulting in no increase of turbidity over time. The difference in the magnitude of the aggregation plateau can be explained by the different initial protein concentrations. In Fig. 2.35 B end-point OD values from the turbidity assay were plotted against the tested protein concentrations. As expected, there is a linear correlation between the protein concentration and the magnitude of the aggregation plateau. Taken together, these studies demonstrate that the aggregation of the recombinant full-length light chain protein AL01 can be monitored by three independent aggregation assays *in vitro*.

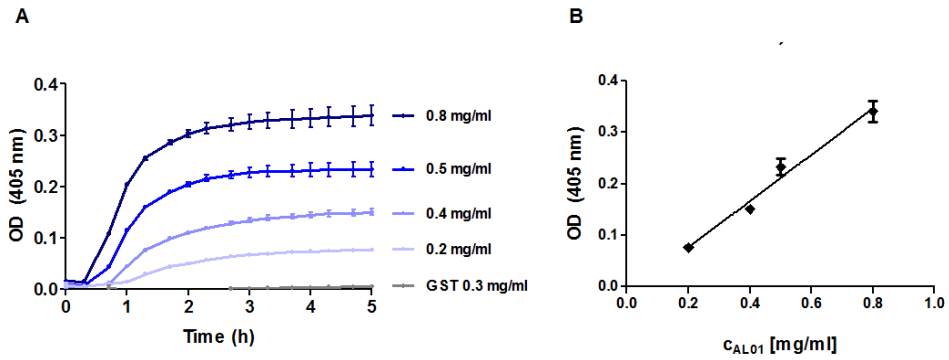


**Fig. 2.35 Concentration-dependent aggregation of light chain protein AL01 monitored by turbidity assays.**

**A** Full-length light chain protein AL01 was incubated at the indicated concentrations at 42°C in a 384-well plate and optical density was measured every 20 min at 405 nm in a Tecan plate reader. The OD increased over time in a concentration-dependent manner. GST at a concentration of 0.3 mg/ml was used as a negative control. **B** End-point $OD_{405}$ values plotted against the protein concentration.

### 2.6.8 Characterization of AL01 light chain aggregates using BN-PAGE and Western blotting

To characterize the spontaneously generated AL01 aggregates in terms of their size BN-PAGE followed by Western blotting was performed. BN-PAGE is a method with which protein assemblies can be separated under native condition[204]. The dye Coomassie Brilliant Blue supplied in the buffer provides the necessary charge in order that protein complexes can be separated electrophoretically in the gel. Recombinant full-length light chain protein AL01 was incubated at different concentrations (0.5, 1, 1.5, 2 and 3 mg/ml) in Tris buffer at 37°C with agitation (300 rpm). After 72 h end-point samples (50 ng) were mixed with 1x native sample buffer and subsequently analyzed by BN-PAGE and Western blotting. The lambda light chain antibody A0101 (Dako) was used for immunological detection. At a protein concentration of 0.5 mg/ml a high molecular weight protein smear ranging from ~66 to ~480 kDa could be detected after 24 h (Fig. 2.36). With higher protein concentration this protein smear gradually shifted up towards the pockets of the native gel, indicating that higher protein concentration correlates with the formation of higher molecular weight protein assemblies. At a protein concentration of 3 mg/ml very large protein aggregates were exclusively observed. These structures were retained in the pockets of the native gels. These results strongly indicate that the formation of full-length light chain protein aggregates is a concentration-dependent process, supporting the results obtained with ThT (Fig. 2.30) and turbidity assays (Fig. 2.35).

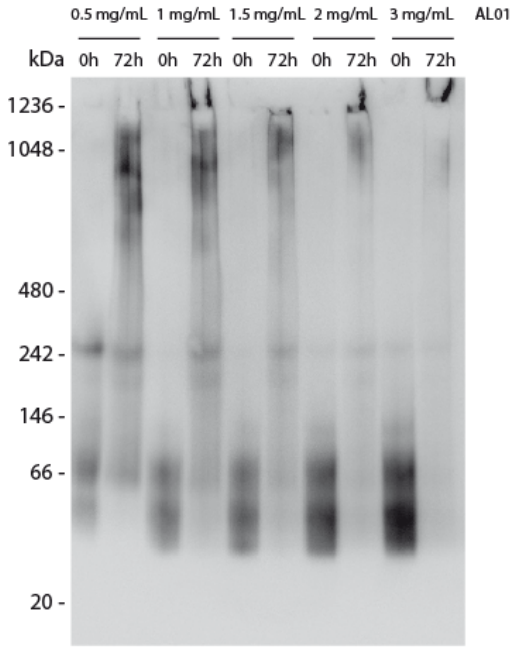


**Fig. 2.36 Characterization of recombinant full-length light chain aggregates using BN-PAGE and Western blotting.**

AL01 was incubated at the indicated concentrations at 37°C for 72 h. 0 h and 72 h time points were analyzed using BN-PAGE followed by Western blotting. Therefore, proteins (50 ng) were mixed with 1x native sample buffer and electrophoretically separated on a 4-16% BN-gel. Then, proteins were transferred on a PVDF membrane by Western blotting and immunoprobed with an anti-lambda light chain antibody (A0101, Dako). At the 0 h time point bands with a molecular size of ~50, ~66 and ~242 kDa were detected. After 72 h a protein smear ranging from ~66 to ≥1236 kDa appeared. With increasing protein concentration this protein smear gradually shifted up and the material was detected in the gel pockets, indicating that the formation of full-length light chain aggregates is a concentration-dependent process.

### 2.6.9 Characterization of AL01 light chain aggregates using a filter retardation assay

Next, FRAs under native, non-reducing conditions were performed to monitor the aggregation of AL01 protein. The protein was incubated in Tris buffer at 37°C with agitation (300 rpm). After 24 h samples were filtered through a cellulose acetate membrane. Aggregates retained on the membrane were detected with the anti-lambda light chain antibody A0101 (Dako). No light chain protein could be detected on the filter membranes when 0 h time point samples were analyzed, suggesting that no light chain aggregates are present in these samples (Fig. 2.37). By contrast, after 24 h light chain protein was detected on the filter membrane, indicating that large aggregates have formed over time.

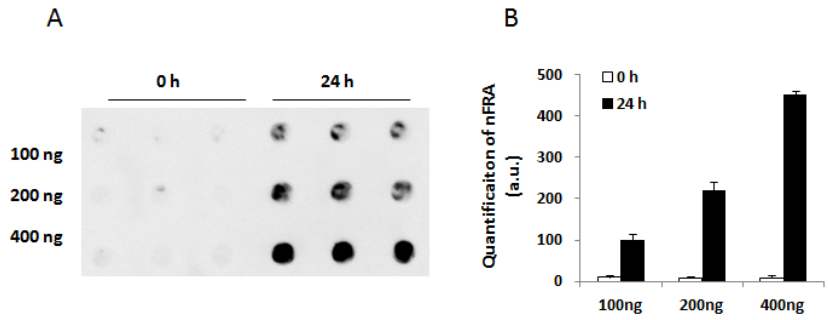


**Fig. 2.37 Aggregation of recombinant AL01 protein can be monitored using a native filter retardation assay.**

**A** Full-length light chain protein AL01 (30 µM) was incubated in Tris buffer at 37°C for 24 h. 0 h and 24 h time point samples (100, 200 and 400 ng) were filtered through a cellulose acetate membrane. The formation of light chain protein aggregates was detected using an anti-lambda light chain antibody (A0101, Dako). In contrast to 0 h time points light chain aggregates could be detected after 24 h on the filter. **B** Quantification of the dots on the filter membrane shown in A using AIDA software.

### 2.6.10 Analysis of spontaneously formed AL01 aggregates using atomic force microscopy

In order to study the morphology of AL01 aggregates they were investigated with atomic force microscopy (AFM). 10 µl of the end-point aggregation reaction samples were spotted onto freshly cleaved mica, incubated for 10 min, washed 3 times with $H_2O$ and air dried overnight. The samples were imaged with a Nano Wizard® II atomic force microscope operating in contact mode. At time point 0 h small spherical particles were visible which might represent full-length light chain monomers or small oligomers (Fig. 2.38 A). In contrast, after incubation of the full-length light chain protein AL01 for 72 h at 37°C multiple amorphous structures with diameters between ~40 and ~200 nm were observed (Fig. 2.38 B). This indicates that AL01 does not form fibrils under the used assay conditions.

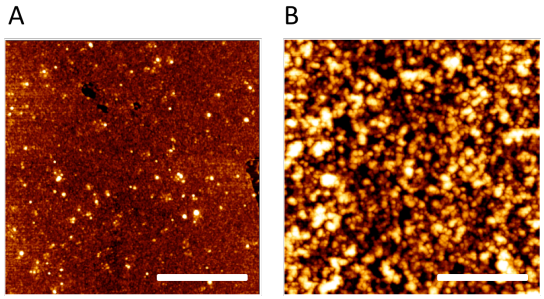


**Fig. 2.38 Analysis of the morphology of full-length light chain AL01 aggregates using AFM.**

**A** Full-length light chain protein AL01 was incubated at 37°C and 300 rpm. After 72 h aliquots were taken and analyzed with AFM. In samples from the 0 h time point small spherical particles were seen most probably corresponding to full-length light chain monomer or small oligomers. **B** After 72 h the full-length light chain protein forms amorphous structures. Scale bars represent 1 µm.

### 2.6.11 Identification of small-molecules that influence spontaneous AL01 aggregation

In order to test small molecules that might influence spontaneous AL01 aggregation eight compounds (Fig. 2.39) were selected. These compounds were previously identified in high throughput screenings (HTS) performed in the laboratory of Prof. Erich E. Wanker and were shown to be effective in Aβ and huntingtin *in vitro* aggregation assays. Thus, they were promising candidates for targeting patient-derived light chain aggregates in cell-free assays. Among these compounds (–)-R-apomorphine, EGCG, epigallocatechin (EGC), (–)-Epicatechin (EC), (–)-Catechin and resveratrol belong to the class of polyphenols[66]. Levodopa and Methyldopa are catecholamines that are derived from the amino acid tyrosine[105,216,217].

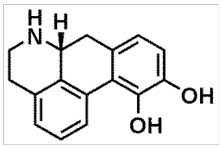

R-(–)-Apomorphine

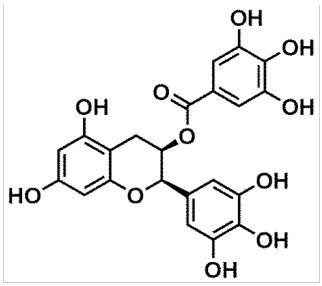

EGCG

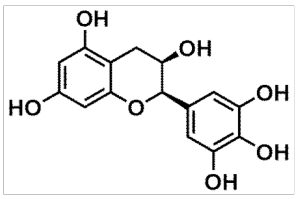

Epigallocatechin (EGC)

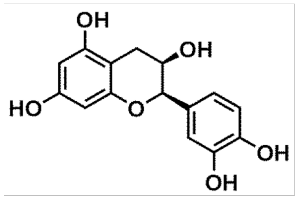

(–)- Epicatechin (EC)

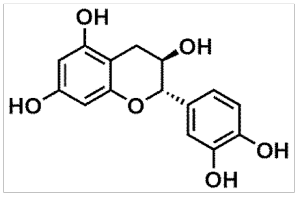

(–)-Catechin

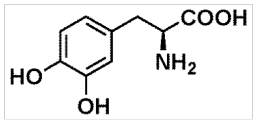

Levodopa

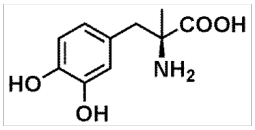

Methyldopa

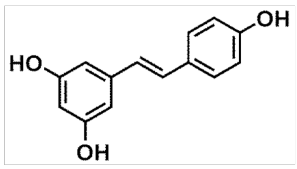

Resveratrol

**Fig. 2.39 Chemical structures of the compounds used in this study.**

The recombinant full-length light chain protein AL01 (30 µM) was incubated with ThT (10 µM), DTT (1 mM) and indicated compounds in a low salt buffer at 37°C in a black 384-well plate and aggregation was monitored over time using the ThT assay. Compounds were tested at a concentration of 10 (Fig. 2.40, blue bar), 50 (Fig. 2.40, red bar) and 100 µM (Fig. 2.40, green bar). ThT fluorescence was recorded every 20 min with 5 s of orbital shaking at an excitation wavelength of 440 nm and an emission wavelength of 485 nm for 72 h in a Tecan plate reader. In the absence of compounds the ThT fluorescence increased after 72 h (Fig. 2.40, black bar). In contrast, the ThT fluorescence was decreased in presence of apomorphine, EGCG and EGC in a concentration-dependent manner, suggesting that these compounds may influence the formation of light chain aggregates.

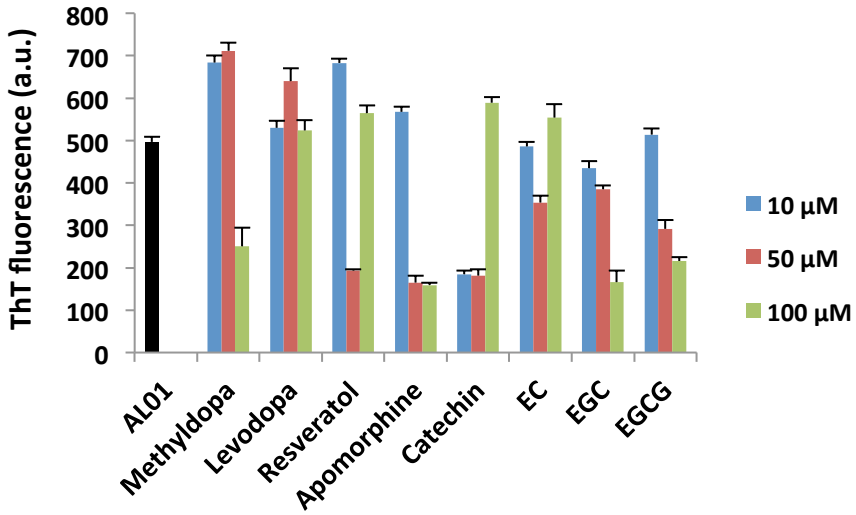


**Fig. 2.40 Identification of small molecules affecting recombinant full-length light chain AL01 aggregation using a ThT assay.**

Full-length light chain protein AL01 (30 µM) was incubated at 37°C in the absence and presence of the indicated compounds at a concentration of 10 (blue bar), 50 (red bar) and 100 µM (green bar) which corresponds to a molar ration of AL01 to compound of 1:1.5, 1:2 and 1:4. ThT fluorescence reading was recorded at 20 min intervals prior to 5 s of orbital shaking.

To confirm that the compounds apomorphine, EGCG and EGC have indeed an effect on AL01 aggregation they were additionally tested in three independent experiments using the ThT assay as described above. In these experiments, 100 µM of each compound were incubated with 30 µM AL01 protein at 37°C for 72 h. In the presence of apomorphine, EGCG and EGC the ThT fluorescence was significantly reduced to ~20, ~44 and ~46%, respectively, compared to the untreated control (Fig. 2.41). This may indicate that the β-sheet content is reduced in presence of these compounds.

However, it could also imply that compounds competitively bind to the fibrils thereby replacing ThT molecules. This observation supports the results obtained from the experiments with patient-derived light chain aggregates which also showed that apomorphine reduced the ThT fluorescence most effectively (Fig. 2.22).

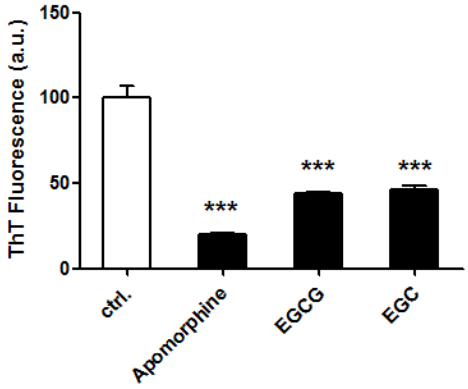


**Fig. 2.41 Effects of the compounds apomorphine, EGCG and EGC on full-length light chain AL01 aggregation analyzed by ThT assay.**

The full-length light chain protein AL01 (30 µM) was incubated at 37°C for 72 h in the presence and absence of 100 µM apomorphine, EGCG or EGC. ThT fluorescence was recorded every 20 min with 10 s shaking prior measurement in a plate reader. Asterisks indicate a significant reduction of the ThT fluorescence in the presence of the indicated compounds compared to the untreated control. Statistical significance was calculated using 1way ANOVA and GraphPad Prism (*** p <0.0001).

### 2.6.12 Analysis of AL01 aggregation in the presence and absence of chemical compounds using SDS-PAGE and Western blotting

To analyze the compound effects on AL01 aggregation SDS-PAGE followed by Western blotting was performed using the anti-lambda light chain antibody A0101 (Dako). 200 ng of protein was boiled in 1x LDS sample buffer at 95°C for 5 min, separated by electrophoresis and transferred to a nitrocellulose membrane by Western blotting. The 0 h time point sample shows a prominent band at a molecular weight of ~28 kDa corresponding to light chain monomers (Fig. 2.42). After 3 days at 37°C no high molecular species >45 kDa could be detected in the absence of compounds, suggesting that the spontaneously formed ThT-reactive light chain aggregates (Fig. 2.30) are unstable structures that dissolve into monomers when treated with SDS and heat. By contrast, in the presence of apomorphine, EGCG and EGC SDS-stable high molecular species ranging from ~50-198 kDa were detected. These results indicate that the chemical compounds promote the formation of SDS-stable light chain aggregates *in vitro*. Most of the protein, however, had a size of light chain monomers,

suggesting that only a minor fraction of the light chain protein was converted into SDS-stable high molecular weight structures in the presence of these compounds.

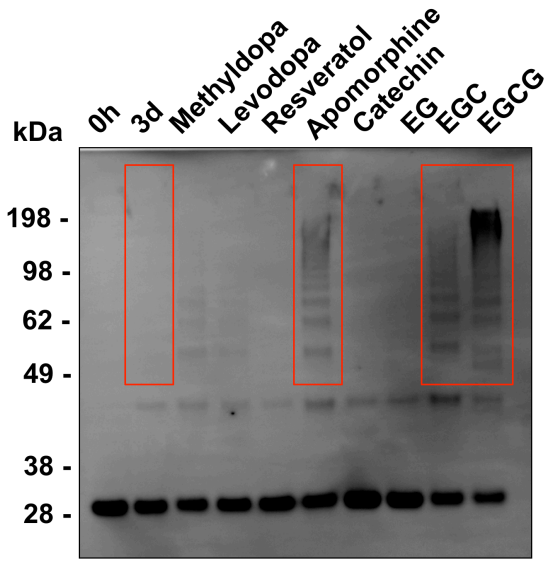


**Fig. 2.42 Analysis of spontaneous AL01 aggregation in the presence of chemical compounds using SDS-PAGE and Western blotting.**

The light chain protein AL01 (30 µM) was incubated at 37°C for 3 d in the presence and absence of the indicated compounds and was analyzed by SDS-PAGE followed by Western blotting using the anti-lambda light chain antibody A0101 (Dako). No SDS-stable light chain aggregates could be detected in the absence of compounds or in the presence of resveratrol, catechin and EG. By contrast, in the presence of apomorphine, EGCG and EGC SDS-stable high molecular weight species up to ~200 kDa were detected.

### 2.6.13 Analysis of AL01 aggregation in the presence of chemical compounds using BN-PAGE and Western blotting

The effects of the tested compounds were further analyzed under native condition using BN-PAGE followed by Western blotting. Therefore, 200 ng of each sample were subjected to native polyacrylamid gels and transferred to PVDF membranes by Western blotting. For immunological detection the anti-lambda light chain antibody A0101 (Dako) was used. The 0 h time point sample shows a major band between 20 and 66 kDa that corresponds to the size of a dimer (Fig. 2.43). After 3 d of incubation at 37°C a high molecular weight protein smear ranging from ~60-1048 kDa was observed with the most prominent band at ~242 kDa corresponding to the size of a decamer. This pattern was comparable to the pattern obtained in the presence of all tested compounds, except for EGCG, indicating that the compounds do not dramatically influence the size of the light chain aggregates under native conditions.

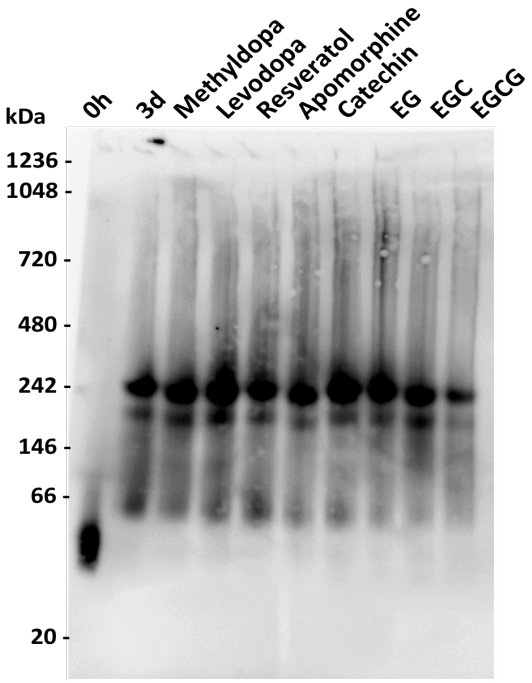


**Fig. 2.43 Investigation of the compound effect on full-length light chain AL01 aggregation using BN-PAGE and Western blotting.**

Recombinant full-length light chain protein AL01 (30 µM) was incubated at 37°C for 3 d in the presence and absence of the indicated compounds. After 3 d each sample was mixed with 1x native buffer and loaded onto a 4-16% Bis-Tris native polyacrylamide gel and separated by electrophoresis. Proteins were then transferred to a PVDF membrane by Western blotting and immunoprobed with the anti-lambda light chain antibody A0101 (Dako). The 0 h time point sample shows one major band between ~20 and ~66 kDa. After 3 d a high molecular weight protein smear could be detected with a prominent band migrating at ~242 kDa. In the presence of the indicated compounds the pattern of the protein smear is comparable to the sample in the absence of the compounds.

### 2.6.14 Analysis of the morphology of AL01 protein aggregates in the presence of chemical compounds using AFM

The morphology of AL01 protein aggregates was analyzed using AFM. AFM images were acquired after 3 d. Therefore, samples (10 µl) were spotted onto freshly cleaved mica, incubated for 10 min, washed three times with $H_2O$ and air-dried overnight. All micrographs were taken as 3 x 3 µm images and recorded in triplicate. In the absence of the compounds recombinant light chain aggregates displayed an amorphous morphology as previously described in section 2.6.10. Aggregates were round with a size of <1 µm and were connected in a net-like fashion (Fig. 2.44 A, E). In the presence of apomorphine (Fig. 2.44 B, F) the aggregates were also amorphous but did not form a net-like structure. EGCG- (Fig. 2.44 C, G) and EGC-treated (Fig. 2.44 D, H) samples displayed morphologies similar to apomorphine-treated samples. These results indicate that the structures of AL01 aggregates may potentially be altered in the presence of apomorphine, EGCG and EGC.

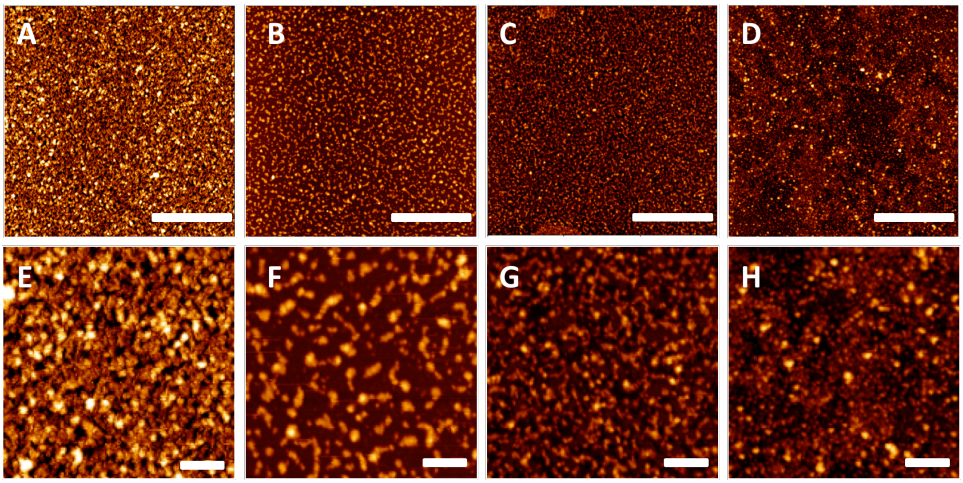


**Fig. 2.44 Analysis of morphologies of compound-treated light chain AL01 aggregates using AFM.**

**A, E** Recombinant full-length light chain protein AL01 (30 µM) incubated at 37°C for 3 d forms interconnected amorphous aggregates. **B, F** In the presence of apomorphine smaller, amorphous aggregates were observed that were not interconnected. **C, G** In the presence of EGC amorphous structures were observed that were not interconnected. **D, H** EGCG-treated samples exhibited morphologies similar to those observed in G. **E-H** Expanded regions of images shown in A-D. Scale bar represents 1 µm for A-D and 200 nm for E-H.

### 2.6.15 Influence of small molecules on the kinetics of AL01 aggregation

In order to explore the influence of small molecules on the kinetics of light chain aggregation recombinant full-length AL01 protein (25 µM) was incubated in the absence and presence of ThT (10 µM) and indicated compounds (100 µM) at 37°C in a Tecan plate reader. ThT fluorescence was recorded ever 20 min over a time course of ~65 h. Fig.2.45 shows the ThT-based AL01 aggregation profiles in the presence of apomorphine, EGCG, EGC, EC, methyldopa, levodopa or resveratrol. Compounds without full-length light chain protein were used as controls (Fig.2.45, grey line). Aβ (Fig.2.45 H, green line) and GST (Fig.2.45 H, blue line) were used as positive and negative controls, respectively (Fig.2.45 H). As previously reported, the initial decrease in ThT fluorescence emission during the first 90 min of incubation in the plate reader is due to the warming up of the plate to the incubation temperature of 37°C[233]. ThT fluorescence of full-length light chain AL01 alone increased over time and reached a plateau after ~65 h (Fig.2.45, black line), which is an indication of the formation of β-sheet rich aggregates. In contrast, in the presence of apomorphine ThT fluorescence dropped after 45 h close to buffer values (Fig.2.45 A). EGCG promoted also a marked reduction of ThT fluorescence after 50 h to ~23% (Fig.2.45 B). When AL01 was incubated with EGC the plateau was already reached after ~20 h and the end point ThT value is reduced to approximately the half (Fig.2.45 C). The decrease of ThT fluorescence in the presence of apomorphine, EGCG and EGC occurred when the aggregation process was already in the exponential phase or almost at the plateau phase. This suggests that these compounds likely target larger protein assemblies and alter

their structure or influence their ThT binding capability. No marked change in fluorescence was observed in the presence of EGC (Fig.2.45 F), methyldopa (Fig.2.45 E), levodopa (Fig.2.45 F) or resveratrol (Fig.2.45 G), suggesting that these comounds do not significantly influence the aggregation process. When compounds were incubated in the absence of protein, there was no change in ThT fluorescence over the course of the incubation period, indicating that these compounds do not form β-sheet rich structures (Fig.2.45, grey line). Only in samples containing EC an increase of ThT fluorescence could be observed after 42 h, indicating that EC forms structures that induce ThT fluorescence over time (Fig.2.45 F). Taken together, apomorphine has the most dramatic effect on light chain AL01 aggregation.

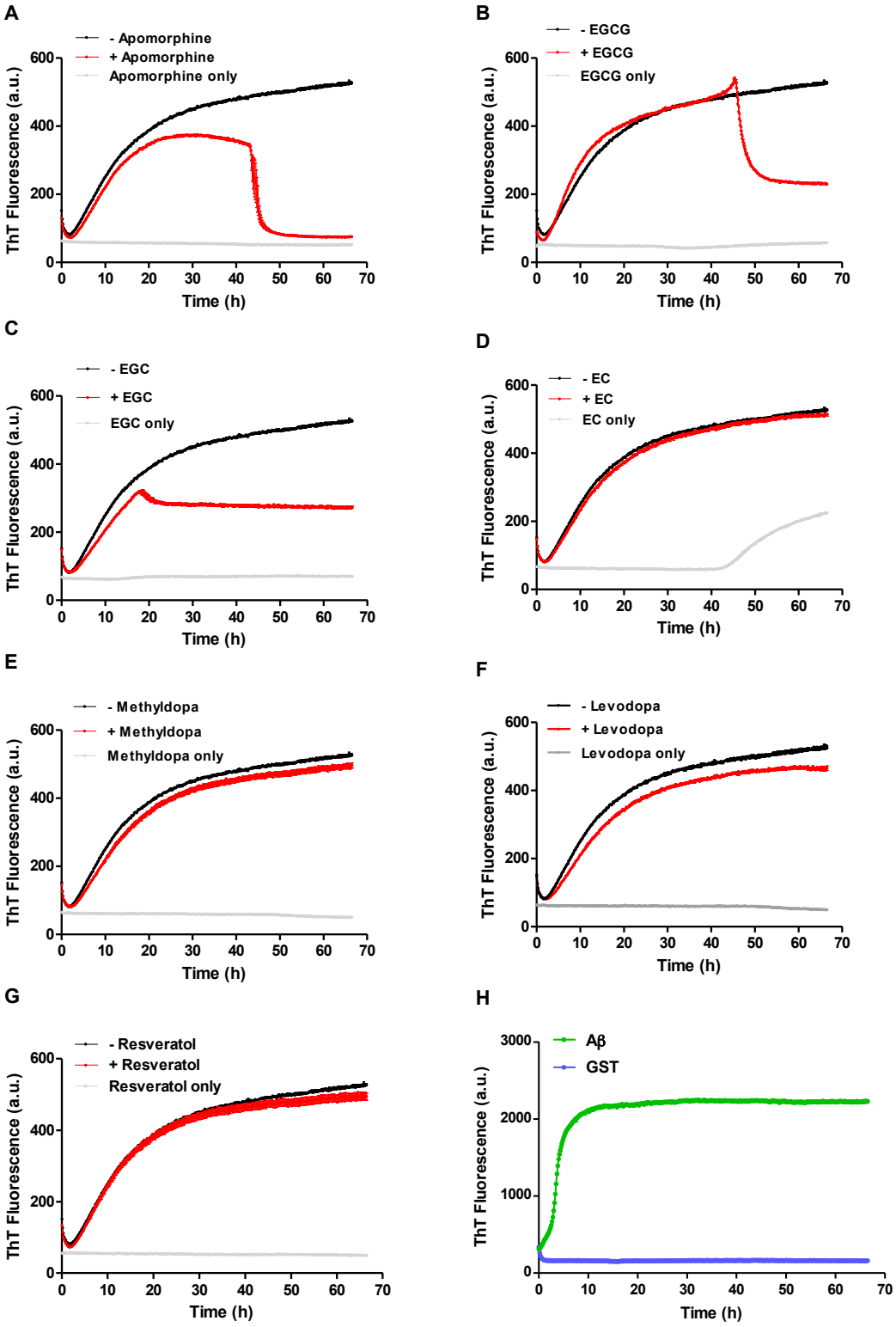


**Fig.2.45 The effects of small molecules on spontaneous AL01 aggregation monitored by the ThT assay.**

**A-G** Full-length light chain protein AL01 (30 µM) was incubated in the absence (black line) and the presence (red line) of the indicated compounds (100 µM) at 37°C in a black 384-well plate. The ThT fluorescence was measured every 10 min for 65 h in a Tecan plate reader. Compound only control samples are also shown (grey line). **H** Aβ (green line) and GST (blue line) were used as positive and negative controls, respectively.

### 2.6.16 Concentration-dependent effects of apomorphine, EGCG and EGC on spontaneous AL01 aggregation

In order to monitor potential concentration-dependent effects of the compounds apomorphine, EGCG, EGC or resveratrol on light chain aggregation, the protein AL01 (25 µM) was incubated with 10, 50 and 100 µM of each compound at 37°C and ThT fluorescence was measured every 10 min with 5 s shaking prior measurement for a time course of 65 h. Aggregation of the AL01 protein is shown as a black line in Fig. 2.46 A-D. The effects of the compounds (10, 50 and 100 µM) on AL01 aggregation are indicated in green, turquoise and blue, respectively. Compound controls are shown in grey. In the presence of 10 µM apomorphine (green line, Fig. 2.46 A) no significant compound effect compared to the control sample could be observed. At a concentration of 50 µM (turquoise line, Fig. 2.46 A), however, a reduction of ThT fluorescence after ~45 h could be detected which occurred already after ~40 h at a concentration of 100 µM (Fig. 2.46 A, blue line), suggesting a concentration-dependent decrease of ThT-reactive structures. In the presence of 10 µM EGCG the magnitude of the plateau was slightly reduced. Interestingly, the addition of 50 and 100 µM EGCG promoted a reduction of ThT fluorescence after ~45 h and ~28 h, respectively (Fig. 2.46 B). However, I observed that the final ThT value in the presence of 50 µM EGCG was lower than the value obtained with 100 µM EGCG. This indicates that 50 µM is sufficient to be effective. For EGC a concentration-dependent reduction in the final ThT value could also be observed (Fig. 2.46 C) but is not as dramatic as compared to the effect in the presence of apomorphine and EGCG. Resveratrol did not change ThT kinetics at any tested concentration (Fig. 2.46 D). Taken together, these kinetic studies suggest that the compounds apomorphine, EGCG and EGC do not inhibit spontaneous AL01 aggregation, but rather remodel aggregates when they are already formed, leading to a rapid decrease in ThT fluorescence.

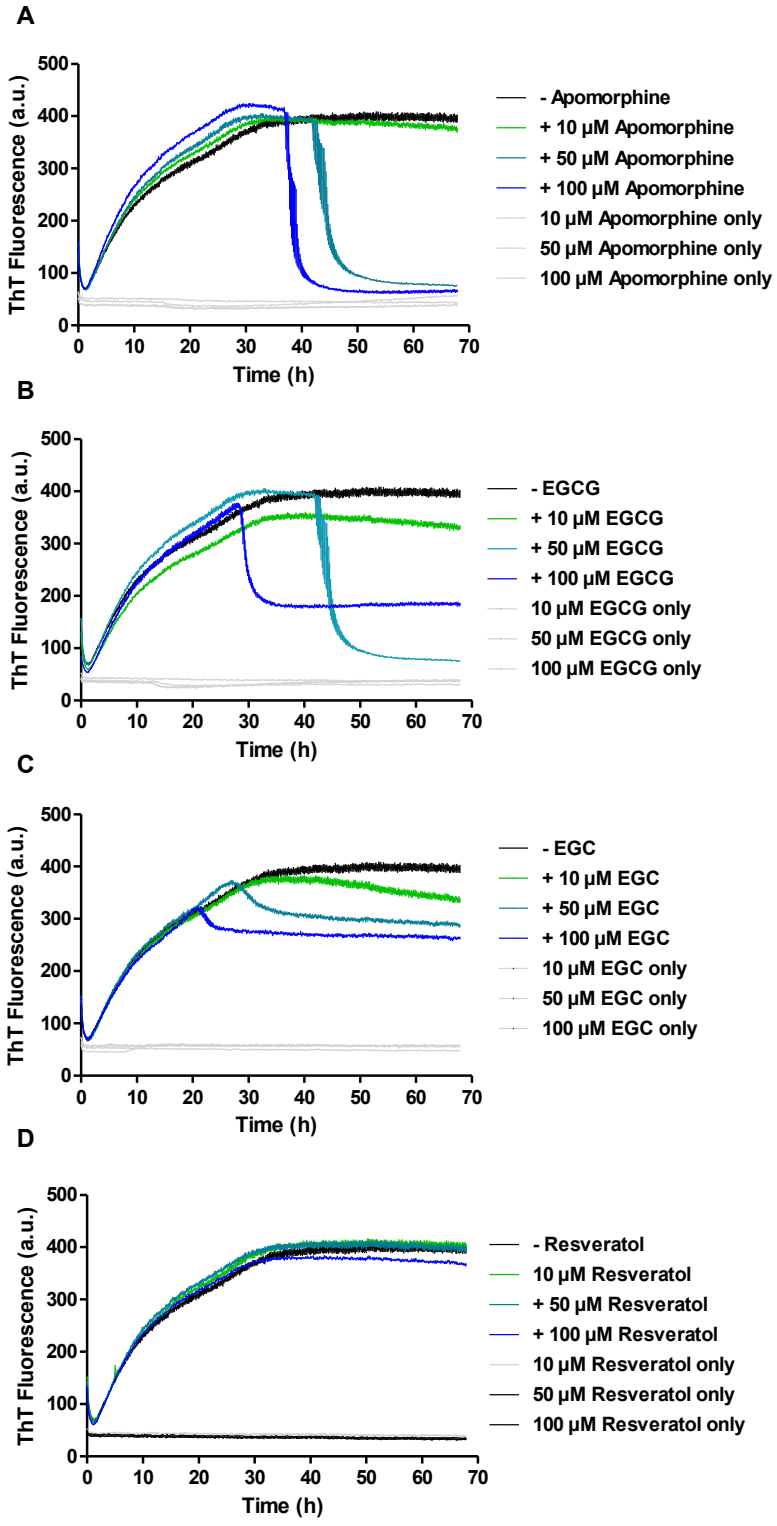


**Fig. 2.46 Investigation of concentration-dependent effects of small molecules on AL01 aggregation monitored by quantification of the ThT fluorescence.**

Recombinant full-length light chain protein AL01 (30 µM) was incubated with ThT (10 µM) in the absence (black line) and in the presence of 10 µM (green line), 50 µM (turquoise line) and 100 µM (blue line) apomorphine, EGCG, EGC or resveratrol at 37°C for 65 h. ThT fluorescence was measured every 10 min with 5 s orbital shaking prior measurement. Compound only control samples are illustrated in grey.

## 2.7 The effects of apomorphine on preformed full-length light chain aggregates

The analysis of spontaneous AL01 aggregation reactions (Fig.2.45, Fig. 2.46) suggests that apomorphine directly targets light chain aggregates rather than spontaneously interacting with monomers. Therefore, preformed light chain aggregates were investigated in the presence of apomorphine using the ThT assay. Recombinant AL01 protein was incubated at 37°C for 24 h. Preformed high molecular weight (Fig. 2.36, Fig. 2.37) light chain aggregates were further incubated with a concentration series of apomorphine (1, 5, 10, 25, 50, 75 µM) for additional 24 h at 37°C and 300 rpm in a 1.5 ml LoBind tube. Aliquots were taken and ThT fluorescence was measured. Fig. 2.47 shows that ThT fluorescence was decreased when increasing concentrations of apomorphine were added to the samples. This indicates that apomorphine may reduce the β-sheet content of preformed recombinant full-length light chain AL01 aggregates in a concentration-dependant manner. However, it can not be excluded that the binding affinity of ThT to the aggregates is reduced in the presence of the compound. This result is in excellent agreement with the ThT kinetics (Fig. 2.46) as well as with studies conducted with patient-derived light chain aggregates (Fig. 2.25).

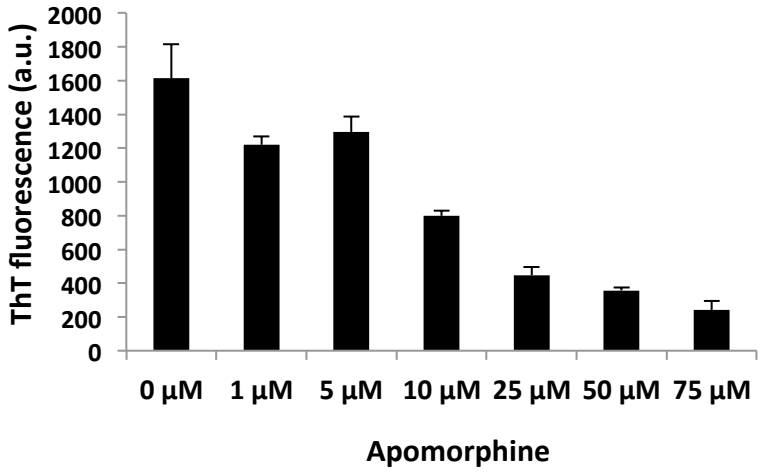


**Fig. 2.47 The effects of apomorphine on preformed light chain aggregates monitored by quantification of ThT fluorescence.**

Recombinant full-length light chain protein AL01 (30 µM) was incubated at 37°C and 300 rpm for 24 h. Apomorphine was then added at the indicated concentrations and samples were further incubated for 24 h at 37°C and 300 rpm. Aliquots were taken in triplicate and ThT was added to a final concentration of 10 µM. ThT fluorescence was measured in a Tecan plate reader at an excitation and emission wavelength of 440 nm and 485 nm, respectively.

### 2.7.1 The effects of apomorphine on preformed light chain aggregates analyzed by SDS-PAGE and Western blotting

To monitor the effects on apomorphine on preformed light chain aggregates samples were subjected to SDS-PAGE followed by Western blotting using the anti-lambda light chain antibody A0101 (Dako). In the absence of apomorphine a major band migrating at ~35 kDa and a thin band at ~55 kDa were detected on immunoblots (Fig. 2.48). With increasing concentrations of apomorphine multiple higher molecular weight bands (~100, ~130 and ~250 kDa) appeared. Furthermore, at a concentration of 75 µM apomorphine a protein smear ranging to the pockets of the gel was detectable, indicating that the compound promotes the formation of SDS-stable high molecular weight light chain aggregates.

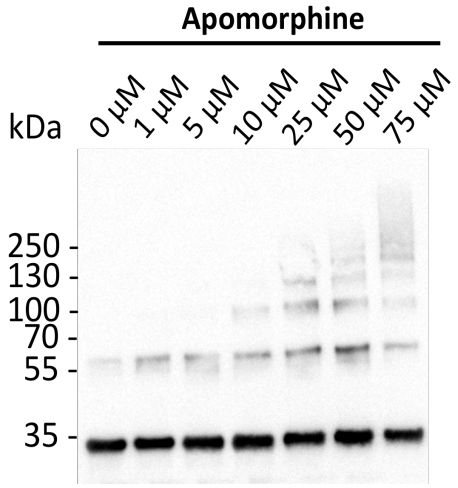


**Fig. 2.48 The effect of apomorphine on preformed light chain aggregates monitored by SDS-PAGE and Western blotting.**

Recombinant full-length light chain protein AL01 was incubated at 37°C for 24 h. Apomorphine was then added at the indicated concentrations and samples were further incubated for 24 h at 37°C. Samples were subjected to SDS-PAGE and Western blotting. An anti-lambda light chain antibody (A0101, Dako) was used for immunological detection. Through the addition of apomorphine to AL01 aggregates a concentration-dependent increase of higher molecular weight SDS-stable structures was detectable.

# 3. DISCUSSION

Many studies are conducted with the aim of inhibiting the process of amyloid formation by targeting or stabilizing the soluble precursor protein with small molecules or peptides. In case of AL amyloidosis, however, most patients were diagnosed at a very late stage after disease onset due to diffuse symptoms. Thus, massive deposition of light chain aggregates already occurred at the time of diagnosis. Current treatments for AL amyloidosis aim to destroy the underlying clonal plasma cells that are responsible for the overproduction of immunoglobulin light chain proteins. This strategy, however, is very aggressive to the patients. An alternative approach to treat AL amyloidosis would be to develop new therapeutic strategies that directly target light chain aggregates with small molecules. This might either lead to a remodeling or disassembly of the pathogenic aggregates. Commonly, recombinant proteins produced by bacterial systems, such as *E. coli*, are used for the screening of small molecules. However, recombinant proteins produced in bacteria are certainly distinct from human proteins synthesized in patients. Proteins synthesized in humans undergo posttranslational modification such as glycosylation, resulting in a completely different glycosylation pattern. Thus, targeting light chain aggregates with small molecules that were isolated from AL amyloidosis patients might be a very interesting strategy. Accordingly, the first part of this study focuses on the preparation and characterization of light chain aggregates from the heart of an AL amyloidosis patient in order to utilize this material for systematic compound testing.

## 3.1 Isolation and characterization of light chain aggregates from the heart of an AL amyloidosis patient

For the first time, light chain aggregates were successfully isolated from the heart tissue of a patient with AL amyloidosis and systematically characterized using biochemical and biophysical methods. For the preparation the water-extraction protocol previously described by Pras and colleagues[40] was used. They extracted the amyloids from the spleen of an AL amyloidosis patient and analyzed the ultrastructure, the sedimentation properties, the electrophoretical mobility and the amino acid composition. In my studies I analyzed the size, the stability, the β-sheet content, the morphology and the toxicity of the isolated light chain aggregates. To the best of my knowledge aggregates isolated from patients with systemic diseases have never been characterized as I did it for this thesis. The added value to the original work by Pras et al. is that patient-derived light chain aggregates are not

stable under denaturing conditions, are β-sheet-rich structures and induce reduced metabolic activity in HeLa cells.

The morphology of patient-derived light chain aggregates that are present in $H_2O$ supernatant 4 was determined by EM. EM studies of $H_2O$ supernatant 4 revealed typical amyloid morphology characterized by long, straight and unbranched fibrils with diameters ranging between 5 and 10 nm and an average length of 100 nm (Fig. 2.10). These structures closely resemble amyloid fibrils isolated from patients with primary and secondary amyloidosis previously described in the literature[39,40]. Pras and colleagues showed that amyloid fibrils isolated from the spleen of an AL amyloidosis patient ranged from 8-20 nm in width, the majority measuring roughly 10 nm and from 4-7.5 nm in diameter[40]. Shirahama and Cohen characterized amyloid fibrils isolated from spleens and livers of patients with secondary amyloidosis with a width ranging from 5-30 nm and a length from 30-1 µm[39]. Thus, my results are similar to previous ultrastructural observations obtained from other infiltrated organs. Moreover, immunogold labeling of the $H_2O$ supernatant 4 confirmed that aggregated material indeed contained lambda light chain protein. In addition to fibrils $H_2O$ supernatant 4 contained amorphous structures (Fig. 2.10 C). The existence of two aggregate species, fibrillar and amorphous, was also reported for *in vitro* aggregation studies with full-length light chain protein AL09[234]. The authors reported a mixture of clustered amyloid fibrils together with amorphous aggregates, suggesting that amorphous aggregation may be a prerequisite for amyloid formation or the result of an off-pathway aggregation process. Thus, it is reasonable to speculate that amorphous structures represent early stage aggregates that might convert to fibrils over time. Why both types of aggregates were formed remains to be elucidated.

In order to analyze whether lambda light chain containing $H_2O$ supernatants are resistant to the treatment with SDS, samples were analyzed under reducing conditions using SDS-PAGE followed by Western blotting. Surprisingly, $H_2O$ supernatants showed no aggregates in the pockets of the stacking gel (Fig. 2.6). Instead, a prominent band at a molecular weight consistent with a full-length light chain monomer (~25 kDa) appeared. Thus, the data suggests that $H_2O$ supernatants contain lambda light chain aggregates that are not resistant to SDS denaturation. Most studies were conducted with free light chains purified from the urine of AL amyloidosis patients which do not contain aggregates. Hence, a comparative analysis of the SDS-stability of light chain aggregates is difficult. Sikkink and Ramirez-Alvarado showed that urine of AL amyloidosis patients contains light chain proteins with a molecular weight of ~26 kDa in SDS-gels[235]. This is in good accordance with the SDS-PAGE analysis from this study.

Another finding from Western blot analysis is that multiple other bands above and below the major band at ~25 kDa appeared, indicating that patient-derived light chain aggregates are composed of

full-length light chains as well as oligomers and fragments. This is in good agreement with previous studies reporting that amyloids contain light chain proteins of two or more molecular weights within a single organ[130,236-243]. Kiyama et al., for instance, investigated amyloid deposits in the liver of an AL amyloidosis patient. Using Western blotting they identified a major band migrating at ~27 kDa and minor bands at 20, 15, 14 and <10 kDa[240]. It is assumed that the AL fibril can consist of the variable region of the light chain, the variable region plus part of the constant region, the intact light chain, or a combination of various molecular forms[239,244]. The latter seems to be the case in this patient, as indicated by Western blotting (Fig. 2.6). Picken et al. reported that the bone marrow cells of a patient synthezied an excess of intact lambda light chains, which were assembled into dimers and tetramers, and an additional fragment of ~10-12 kDa[239]. They suggest that aberrant synthesis and/or proteolytic degradation may play a pathogenic role in the process of amyloidogenesis[239]. Interestingly, Röcken and colleagues reported that amyloid undergoes proteolysis after deposition, resulting in different immunostaining patterns and different sized bands on Western blots[238].

The Coomassie staining of SDS-gels showed that $H_2O$ supernatant 4 contained a lot of other proteins besides light chains (Fig. 2.8). This could implicate either that these proteins were contaminants or they could be associated with light chain aggregates. Several studies identified coaggregated proteins, such as SAP or ApoE, in AA and AL amyloidosis biopsie specimens and are described to be involved in fibrillogenesis[245-248]. In order to examine whether SAP and ApoE are present in $H_2O$ supernatants, they were analyzed with antibodies against SAP and ApoE. Immunoblot analysis showed the presence of SAP and ApoE in $H_2O$ supernatant 4 (Fig. 2.8 B). Thus, these results are in excellent agreement to recent findings resulted from mass spectrometry (MS) analysis of microdissected tissue sections of renal amyloidosis biopsies[245-248]. The identification of amyloid-associated proteins may play an important role in the pathogenic process of amyloid formation. Recently, Lavatelli et al. studied the interaction of amyloidogenic cardiotoxic light chains with cellular proteins[249]. They identified novel mitochondrial protein interactors of light chains which possibly sequestering them or perturbing their function[250].

Hitherto, the toxicity of patient-derived light chain aggregates has not been demonstrated in a cell-based assay. There is only one publication in which the effects of amyloid fibrils produced from recombinant light chain variable domains were studied in human cardiomyocytes[114]. Previously reported results indicate that recombinant light chain fibrils severely impair cardiomyocyte metabolism in a dose-dependent manner stressing the need to include strategies for removing potentially toxic amyloid fibrils. In order to determine whether patient-derived light chain aggregates are cytotoxic in mammalian cells, a cell-based toxicity assay, the MTT assay, was conducted with HeLa cells. This assay measures cytosolic and intracellular membrane NAD(P)H oxidoreductase

activity, as an indicator of metabolic dysfunction[214]. HeLa cells treated with $H_2O$ supernatant 4 showed a dose-dependent decrease in cell viability monitored by a reduction in the MTT signal (Fig. 2.17). The data showed that undiluted patient-derived light chain aggregates lead to a significant decrease (~50%) in MTT reduction compared to the control $H_2O$ supernatant from a pig heart preparation and the vehicle control (Fig. 2.19 E). This decrease in MTT reduction suggests that patient-derived light chain aggregates induces metabolic dysfunction via inhibition of NAD(P)H oxidoreductase activity.

Growing body of evidence emerges showing that soluble light chain proteins were also cytotoxic independent of fibril deposition[117,118,196,119,251,252]. The toxicity exerted by soluble light chains has been confirmed in *in vitro* and *in vivo* experiments conducted by Liao and coworkers[117-119]. They investigated the effect of free light chains isolated from the urine of AL amyloidosis patients in isolated cardiomyocytes, in mice and in human heart tissue[117,118,196]. They showed that infusion of cardiac light chains resulted in a marked impairment of ventricular relaxation with preservation of the contractile function[119]. Another study by Liao and colleagues demonstrated that patient-derived light chain proteins alter the cellular redox state in isolated cardiomyocytes, marked by an increase in intracellular reactive oxygen species (ROS). Furthermore, they measured an upregulation of the redox-sensitve protein heme oxygenase-1 (HO-1). The resulting oxidative stress resulted in direct impairment of cardiomyocyte contractility and relaxation, associated with alteration in intracellular calcium handling[119]. Moreover, recent studies showed that the activation of the stress-induced mitogen-acivated protein kinase (MAPK) lead to redox stress, cellular dysfunction and apoptosis in a rat cardiomyocyte model[118]. Using immunoblot analysis they determind the phosphorylation levels of p38, c-Jun N-terminal kinase (JNK) and extracellular signal-regulated kinase (ERK) in light chain treated and untreated cardiomyocytes. They also showed that the contractility of cardiomyocytes was impaired upon light chain exposure. Terminal deoxynuceleotidyl transferase dUTP nick end labeling (TUNEL) assays showed an increase in apoptosis in cardiomyocytes incubated with light chains. *In vivo* experiments with mice suggest that light chain-induced apoptosis occurs after short-term exposure to circulating light chains and is mediated by a p38 MAPK-dependent mechanism. They claim that the infiltration of the heart alone did not correlate with the degree of heart failure or survival and hypothesized that circulating monoclonal light chains may directly impair cardiac function, in addition to any mechanical effects of amyloid deposition[119,251,252]. Taken together, it is conceivable that soluble as well as aggregated light chain proteins induce toxicity in mammalian cells.

Until now, three *in vivo* models of AL amyloidosis were published. Shi et al. provided evidence that injection of light chain proteins purified from the urine of AL amyloidosis patients induced apoptosis in mice[118]. Furthermore, Mishra and colleagues demonstrated impaired cardiac function and increased cell death resulting from injecting free light chain protein isolated from the urine of AL

patients in the circulation of zebra fish[197]. According to these findings light chain precursor proteins trigger a direct cytotoxic response independent of fibril formation. Guan and coworkers demonstrated in isolated cardiomyocytes and in a zebrafish model that disruption of the autophagic flux is the underlying mechanism critical for the induction of mitochondrial dysfunction and development of AL amyloid cardiomyopathy[196]. Recently, Diomede et al. observed that the pharyngeal pumping of *C. elegans* was significantly and selectively reduced by light chains obtained from the urine and from serum of AL amyloidosis patients suffering from cardiomyopathy[198]. Investigating the toxicity of patient-derived light chain aggregates isolated from the heart of an AL amyloidosis patient in an animal model, such as *D. rerio* or *C. elegans,* is of paramount importance in order to develop novel therapeutic strategies. It would be interesting to expose such animals to patient-derived light chain aggregates in order to explore whether they induce a toxic effect *in vivo*. Taken together, there is emerging evidence that AL amyloidosis is associated with rapidly progressive and fatal cardiomyopathy resulting from direct cardiotoxic effects of circulating light chain proteins as well as from indirect effects of light chain fibril infiltration.

## 3.2 The need of new treatments for AL amyloidosis

### 3.2.1 Small molecule intervention

The accumulating mass of light chain aggregates is known as one of the hallmarks in the pathogenesis of AL amyloidosis[253]. Consequently, drugs with the potential to lower the amyloid load by remodeling or even promoting the disassembly or clearance of these protein assemblies may lead to new therapies to control or even cure the disease. In this context, patient-derived light chain aggregates isolated from heart tissue were subjected to small molecule targeting to investigate whether they have the potential to remodel or even dissolve heart-derived light chain aggregates. The results presented in this work show for the first time that the polyphenol apomorphine potentially remodels light chain aggregates isolated from the heart tissue of an AL amyloidosis patient *in vitro*.

### 3.2.2 Identification of apomorphine as a potential remodeling agent of patient-derived light chain aggregates using a ThT-based assay

In order to identify compounds that influence patient-derived light chain aggregates a ThT assay was developed. The assay was established in a 384-well plate format to minimize the sample volume. ThT is very commonly used to monitor the effects of compounds on amyloid fibril aggregation reactions

and complex biosamples[71-73,254,255]. However, it should be noted that this fluorescence-based assay can be biased by the presence of exogenous compounds as described by Carver and co-workers[233]. They investigated the fibril formation of $A\beta_{42}$ in the presence of three polyphenols (curcumin, quercetin and resveratrol) and showed that such compounds can significantly bias fibril-associated ThT fluorescence in both *in situ* real-time ThT assays and single time-point dilution ThT assays. It was suggested that these compounds led to a concentration-dependent quenching of the ThT fluorescence intensity by interacting directly with ThT or competitively binding to the fibrils and displacing ThT[233]. To exclude a possible quenching effect of apomorphine on the ThT fluorescence different concentrations of the compound were incubated with a fixed concentration of $H_2O$ supernatant 4. As no concentration-dependent loss of the ThT signal was observed in the presence of the tested compound concentrations (Fig. 2.22), the observed reduction of ThT intensity is unlikely to be attributable to a quenching effect. Rather, the results suggest that either apomorphine competitively binds with ThT for β-sheet-rich sites along the length of fibrils and is able to displace ThT from these sites, or it remodels the fibrils in a way that ThT binding is reduced. In order to assess these possibilities other methods should also be used to assess fibril remodeling.

## 3.3 The effect of apomorphine on patient-derived light chain aggregates

### 3.3.1 Apomorphine reduces the surface hydrophobicity of patient-derived light chain aggregates monitored by ANS assay

Exposed hydrophobic surfaces in proteins have been found to be critical in triggering amyloidogenesis[256-258]. In exploring the effects of apomorphine on potential conformational changes in terms of exposed hydrophobic surface in patient-derived light chain aggregates, an ANS fluorescence study was performed. ANS is a dye that preferentially bind to such hydrophobic patches thereby enhancing its fluorescence accompanied by a blue shift of the spectral maximum[259]. Several lines of evidence have demonstrated that ANS is a useful tool to monitor changes in surface hydrophobicity in the presence of compounds[80]. In these studies, ANS fluorescence was markedly reduced after compound treatment. Sarkar et al., for example, studied the effect of rottlerin on the surface hydrophobicity of preformed hen egg white lysozme (HEWL) fibils using the ANS fluorescence assay[258]. They showed that rottlerin attenuated the ANS fluorescence and promoted a red shift in $\lambda_{max}$ by 25 nm, suggesting that disaggregation of HEWL fibrils is achieved by reducing their surface hydrophobicity. To monitor whether apomorphine influences the surface hydrophobicity of patient-derived light chain aggregates, they were analyzed in an ANS assay. Addition of apomorphine to patient-derived light chain aggregates resulted in decreased ANS fluorescence and a red shift in $\lambda_{max}$

(Fig. 2.24, Fig. 2.25 B), suggesting that hydrophobic regions present in untreated samples may no longer be surface exposed when treated with apomorphine. However, it cannot be excluded that apomorphine affects ANS fluorescence or that apomorphine and ANS bind competitively to the same sites on the aggregates.

### 3.3.2 Apomorphine converts patient-derived light chain aggregates into SDS-stable conformers

To characterize the effect of apomorphine on the stability of patient-derived light chain aggregates to SDS denaturation filter retardation assays under native as well as under denaturing conditions were performed. Under native, non-reducing conditions the antibody signal was slightly reduced in the presence of apomorphine (Fig. 2.23 A). This result can have different reasons. The reduced signal can be a result of a conversion of patient-derived light chain aggregates into smaller species which are not retained but instead filtered through the pores of the membrane, resulting in a decreased antibody signal. Another explanation could be that patient-derived light chain aggregates undergo a conformational change in the presence of the compound so that the antibody is not able to recognize the epitope on the surface of the aggregates. To address this question, it would be helpful to have conformation-specific antibodies able to distinguish between oligomers and larger aggregates.

To further characterize the effect of apomorphine on patient-derived light chain aggregates, a filter retardation assay was also performed under denaturing conditions. Surprisingly, in presence of apomorphine light chain aggregates became increasingly resistant to SDS over time, indicating that the compound remodels the aggregates into SDS-resistant species (Fig. 2.23 B, Fig. 2.25). Strikingly, this result is reminiscent of the effect of EGCG, a polyphenol present in green tea, on Aβ and α-synuclein aggregates, described in Bieschke et al.[185]. In this study an equimolar concentration of EGCG converts SDS-unstable into SDS-stable α-synuclein and amyloid-β aggregates after an incubation period of 2-6 h. Hence, the authors suggested that EGCG converts mature Aβ and α-synuclein fibrils into off-pathway aggregates. Recently, they investigated the effect of EGCG on light chains purified from the urine of AL amyloidosis patients. Strikingly, they described that EGCG induced the formation of SDS-stable aggregates whereas light chain aggregates formed in the absence of the compound dissocciated by boiling in SDS[260]. As apomorphine is also a phenolic compound, it may remodel patient-derived light chain aggregates by a mechanism similar to that of EGCG.

### 3.3.3 Apomorphine increased cell viability of HeLa cells treated with patient-derived light chain aggregates

In order to monitor the effects of apomorphine on the toxicity induced by patient-derived light chain aggregates, a cell-based MTT assay was conducted. This assay measures cytosolic and intracellular membrane NAD(P)H oxidoreductase activity, as an indicator of metabolic dysfunction[214]. Cells were treated with patient-derived light chain aggregates and with the compound which was simultaneously added to the growth medium. HeLa cells treated with patient-derived light chain aggregates showed a dose-dependent decrease in cell viability monitored by a reduction in the MTT signal (Fig. 2.18). However, when cells were treated with apomorphine an increase in cell viability to ~85% was observed after 48 h, suggesting a protective effect of apomorphine against patient-derived light chain aggregates induced toxicity (Fig. 2.27 B). Considering the results obtained from EM analysis which showed morphologically different aggregates, a critical question would be whether amorphous, fibrillar or both species are responsible for the observed toxicity. Interestingly, a similar effect of EGCG-treated α-syn and Aβ aggregates on PC12 cells was observed by Bieschke et al.[185]. They observed that untreated α-syn and Aβ fibrils caused a significant inhibition of MTT reduction, while this effect was diminished when fibils were treated with EGCG.

### 3.3.4 Structure and physicochemical properties of apomorphine

It was shown by Landsbury and colleagues that apomorphine inhibits α-synuclein aggregation, an amyloidogenic protein that was found to be accumulated in Lewy bodies in the brain of Parkinson's disease patients[192]. Apomorphine was later reported by Callaway and coworkers to inhibit β-amyloid aggregation that is considered to be one of the major pathological hallmarks of Alzheimer's disease[66,82]. In order to determine structural principles of the inhibition, these authors tested several derivatives of apomorphine. The data suggested that the two hydroxyl groups on the D-aromatic ring are crucial for the inhibition as the methylation of the latter reduced the inhibitory effect of apomorphine. Moreover, they claim a significant importance for the additional ring structure that distinguishes apomorphine from naturally occurring catechols, such as dopamine and epinephrine, which shows relative low inhibitory effectiveness. A more hydrophobic molecule could increase its affinity for binding with hydrophobic amyloids. Moreover, they suggested that autoxidation of apomorphine is required for inhibiting Aβ aggregation[82]. They showed that blocking autoxidation either through modification of the hydroxyl groups or by the addition of antioxidants, such as sodium metabisulfite, results in the loss of the inhibitory effect. Strikingly, the authors suggested that it

might be possible that apomorphine has the same effect on fibrils that are produced from other amyloidogenic proteins. The results presented in this work support this assumption. It is conceivable that the oxidation product of apomorphine is responsible for the observed remodeling of patient-derived light chain aggregates. Its protective role as a potent antioxidant that protects lipids and proteins from radical damage further underpins this hypothesis[261]. However, further studies are necessary to verify whether autoxidation is the mechanism of action by which apomorphine remodels patient-derived light chain aggregates.

Palhano and coworkers recently demonstrated that the remodeling activity of EGCG is also dependent on autoxidation. They showed that a decrease in oxidation of EGCG was accompanied by a decrease in its amyloid remodeling activity on $A\beta_{1-40}$, $IAPP_{8-24}$ and $Sup35NM_{Ac7-16}$ fibrils[189]. The data strongly demonstrated that EGCG does not disaggregate amyloid structures but instead alter their conformation[189]. However, how EGCG oxidation drives remodeling remains unclear. With this in mind it seems reasonable to hypothesize that apomorphine remodels patient-derived light chain aggregates via autoxidation similar to the described studies for EGCG. However, the exact mechanism by which apomorphine reverts aggregation remains elusive.

## 3.4 The aggregation behavior of full-length light chain protein AL01

The formation of insoluble protein aggregates is a characteristic hallmark in the development of AL amyloidosis and other protein deposition diseases[262-265]. Consequently, studying the aggregation process of light chain proteins increases our understanding of the molecular mechanism by which amyloid aggregates are formed. *In vitro* aggregation studies have long been focused primarily on the variable domain of light chain proteins[11,50,74,75,266]. This was supported by early reports that stated that amyloid deposits from AL amyloidosis patients consist mainly of the variable domain and small regions of the constant domain[50]. However, a growing body of evidence indicates that the full-length protein is also involved in the pathogenesis of AL amyloidosis. Proteomic studies conducted with amyloid fat aspirates identified full-length light chain proteins as part of the deposits[243]. Another study using biopsy samples from affected tissues also reported the existence of full-length protein[130]. Strikingly, the present study supports the view that the full-length light chain protein is mainly aggregated in the affected heart (Fig. 2.6). For this reason, a full-length light chain protein was chosen for studying spontaneous light chain aggregation as well as for investigating the effects of small molecules on aggregation.

In the present study, the aggregation of the full-length lambda light chain protein AL01 described by Rognoni et al. was analyzed[224]. The sequence of this light chain protein is obtained from a patient

with predominant cardiac AL amyloidosis. Light chain protein AL01 was produced in *E. coli* and purified from inclusion bodies. The formation of aggregates was monitored by different biochemical and biophysical techniques. The data showed that recombinant full-length light chain protein AL01 forms β-sheet-rich, high molecular weight aggregates *in vitro* that are predominantly amorphous in structure.

## 3.5 Characterization of full-length light chain AL01 aggregation

### 3.5.1 Full length light chain AL01 forms high molecular weight aggregates *in vitro*

The formation of AL01 aggregates was monitored by ThT and CR assays. ThT binding studies indicated that full-length light chain protein AL01 converts into β-sheet-rich structures over time (Fig. 2.30). ThT results were confirmed by CR binding assays in which an increase in CR fluorescence also indicated the formation of β-sheet-rich structures (Fig. 2.34). Turbidity of a solution is known to be an indicator for the formation of aggregates[232]. The results from the turbidity assay showed that the OD at 405 nm increased, indicating the formation of aggregates (Fig. 2.35). End-point analysis of full-length light chain aggregation using BN-PAGE followed by Western blotting using a lambda light chain specific antibody revealed lambda light chain aggregates with a molecular weight >1048 kDa, which retained in the pockets of the native gel (Fig. 2.36). Using a filter retardation assay lambda light chain aggregates were detected under non-reducing conditions on the cellulose acetate membrane, indicating the formation of lambda light chain aggregates (Fig. 2.37). Full-length light chain aggregates were not SDS-resistant because no light chain aggregates could be detected on the membrane when they were analyzed under denaturing conditions (Fig. 2.42). Light chain aggregation could be monitored as a concentration-dependent process in ThT, CR and turbidity assays. Although the generated light chain aggregates are ThT- and CR-positive structures, they do not exhibit a typical fibrillar morphology (Fig. 2.38). Thus, they are more similar to “amorphous” p53 aggregates that were previously described by Fersht and colleagues[267]. Numerous studies have demonstrated that light chain proteins form fibrillar structures only under acidic conditions and reported a key role of the pH in aggregate formation[11]. Khurana and colleagues observed fibrils of a recombinant amyloidogenic light chain variable domain (SMA) at pH 2 after 24 h. By contrast, amorphous aggregates were formed at pH 5 and pH 7[11]. Therefore, full-length light chain AL01 was incubated at different pH ranging from pH 2 to pH 7. ThT kinetics were accelerated at pH 2 as the plateau phase is reached faster than at higher pH (Fig. 2.33). One explanation for this observation could be that partially unfolded proteins are obtained at low pH which might favor the formation of aggregates as it is described by Khurana et al.[11]. However, full-length light chain protein AL01 never formed fibrils

even under acidic condition. One explanation for this observation could be that the full-length light chain protein AL01 tends to dimerize in a fashion similar to the association of light and heavy chains in intact immunoglobulins. From the work of Eisenberg and coworker it is known that the monomers are the critical species for the formation of fibrils and dimers that are the naturally occurring species have to dissociate into monomers prior to forming amyloid fibrils[86,223,241]. One possibility that explains the observed formation of amorphous AL01 aggregates is that the aggregation process is not initiated by monomeric light chain proteins. BN-PAGE analysis of 0 h time point samples showed the formation of two light chain protein species that runs at ~50 kDa and ~75 kDa (Fig. 2.36). These molecular weights correspond to dimers and trimers, respectively. AFM studies further confirmed the presence of oligomeric structures at time point 0 h (Fig. 2.38). Furthermore, the absence of a lag-phase is in excellent agreement with the detection of early oligomers. They might serve as nuclei or seeds forcing a rapid formation of amorphous aggregates. The formation of oligomers at a very early time point might also explain the fact that aggregation reaches a plateau already after ~40 h which is relatively rapid compared to other light chain protein aggregation kinetics with lag times of ~100 h at pH 7[223]. Furthermore, no sigmoidal growth curve was observed which is commonly observed for fibrillation[268,269]. These observations support the view that aggregation was not induced by monomers, resulting in the formation of amorphous aggregates. However, it might be possible that both types of aggregate species are formed (fibrillar and amorphous). Other findings that support this hypothesis are the EM images of heart-derived light chain aggregates from the AL amyloidosis patient. In this case fibrils as well as amorphous structures were found (Fig. 2.10). These findings are also in good agreement to published studies from the laboratory of Marina Ramirez-Alvarado where the amyloid formation properties of the full-length light chain protein AL09 were analyzed[234]. EM images of *in vitro* AL09 aggregation studies revealed the presence of “fibrillar-like structures” in addition to amorphous aggregates that were tightly attached to the fibrillary bundles. Furthermore, Qin et al. reported that the light chain variable domain SMA, an amyloidogenic light chain extracted from lymph node of an AL amyloidosis patient, tend to form amorphous aggregates, while more unfolded intermediate formed fibrils most rapidly[40,223]. Based on this study it seems reasonable to assume that the light chain protein AL01 is a native-like protein at pH 7 that spontaneously form amorphous aggregates over time. The molecular mechanisms underlying the formation of light chain aggregates, in particular, why some light chains form fibrils and others form amorphous deposits remains to be elucidated.

## *3.6* Investigating the effects of small molecules on light chain aggregation *in vitro*

### 3.6.1 State of the art: Small molecules affecting light chain aggregation

Until now, there have been only few studies that focused their efforts on the identification of small molecules which affect light chain fibril formation. Only recently, two studies were published dealing with this issue. Pelaez-Aguilar and coworkers demonstrated that EGCG inhibits light chain fibrillogenesis using ThT fluorescence and EM[193]. At a 1:1 stoichiometry nonfibrillar aggregates were observed instead of long well-structured fibers, suggesting that EGCG promotes a different aggregation pathway. Few months later, Brumshtein et al., 2015 screened 27 compounds to identify those that stabilize the dimer form of the $V_L$ protein[86]. The authors showed previously that monomeric light chains are the amyloid-prone species and represent the starting point for fibrillation[86]. Among the tested compounds sulfasalazine and methylene blue showed inhibitory effects on the formation of amyloid fibrils.

### 3.6.2 Apomorphine, EGCG and EGC modify full-length light chain aggregation

Intervention into the aggregation process with small molecules is emerging as a potential therapeutic strategy in AL amyloidosis[86]. Compounds, such as apomorphine or EGCG, are able to inhibit amyloid formation of many amyloidogenic proteins including Aβ and α-Syn[82,174,185]. To this end, the effects of eight compounds were assessed on recombinant full-length light chain AL01 aggregation. Selected compounds were previously identified in high throuput screenings against Aβ and Htt and were therefore promising candidate drugs. By employing a ThT fluorescence based assay apomorphine, EGCG and EGC were identified to influence the aggregation process. Strikingly, kinetic ThT data showed that these compounds remodel AL01 aggregation at a later stage when larger aggregate species have already be formed (Fig.2.45, Fig. 2.46). The effect of apomorphine on preformed recombinant light chain aggregates strongly supports this result (Fig. 2.47). EC, methyldopa, levodopa and resveratrol, in contrast, did not change spontaneous aggregate formation. Concentration-dependent analysis showed that ~50 µM which corresponds to a 2-fold molar excess of the compound over light chain protein exerts a marked reduction of ThT fluorescence, suggesting that 50 µM is sufficient to modify aggregation. Furthermore, analysis of samples by SDS-PAGE followed by Western blotting revealed that apomorphine, EGCG and EGC convert SDS-soluble AL01 aggregates into SDS-resistant structures (Fig. 2.42). These results are in excellent agreement with the effect of apomorphine on patient-derived light chain aggregates isolated from the heart of an AL amyloidosis patient (Fig. 2.23, Fig. 2.25 C, D). Morphological analysis using AFM showed that the compounds did

not inhibit or revert AL01 aggregation (Fig. 2.44). Several studies reported that small molecules and peptides can redirect the aggregation cascade instead of inhibiting it[177,270-273]. This seems also be the case when apomorphine is added to light chain aggregates. However, further studies will be required in order to define the mechanism by which apomorphine remodels light chain aggregates *in vitro*.

## 3.7 Concluding remarks and future directions

Purification and characterization of light chain aggregates from the heart of an AL amyloidosis patient are essential for the understanding of their contribution to the pathogenesis of AL amyloidosis. It also raises other important questions starting from my new findings. The role of amorphous aggregates is one example. Do they represent early-stage structures that will convert into fibrils, or do they represent second aggregate species that coexists with fibrils *in vivo*? Which of these aggregates are the toxic species or is one type more toxic than the other? Does apomorphine bind to amorphous, fibrillar or both structures? Another question to be answered is the importance of sequestered proteins in the fibrils.

Although considerable progress has been made in the elucidation of AL amyloidosis, current therapeutic strategies fail to effectively manage the disease. Hence, there is an urgent need for novel therapies that ameliorate amyloid deposition. In general, there are different therapeutic strategies. One desired therapeutic option is to decrease the amyloid deposition with small molecules in order to reduce the load of aggregates in affected organs. To address this issue, heart-derived light chain aggregates isolated from an AL amyloidosis patient were targeted by small molecules *in vitro*. The studies described in this thesis revealed a small molecule, the polyphenol apomorphine that may have a potential to be effective in AL amyloidosis. The results suggest that the compound remodels patient-derived light chain aggregates. However, I did not obtain clear evidence that the polyphenol indeed disrupts light chain fibrils. It would be interesting to test whether combinatorial strategies that simultaneously include several compounds promote aggregate disruption. For example, apomorphine could be tested together with other compounds, such as EGCG, in form of drug cocktails that may finally result in a disassembly of patient-derived light chain aggregates.

One future goal is to gain mechanistic insights about the mode of action of apomorphine. To confirm apomorphine-mediated remodeling of patient-derived light chain aggregates further investigations are needed. For example, a comprehensive EM analysis should elucidate whether apomorphine indeed preferentially targets amorphous structures and if so, it should be examined which

consequences result from this selective binding. To gain insight into the exact mechanism by which apomorphine interferes with light chain aggregates, studies with different derivatives of apomorphine are essential. Studies with apomorphine derivatives revealed that the hydroxyl groups on the D-ring are required for the inhibition of amyloid aggregates. The modification of -OH groups attached to the phenyl ring is also known to have an effect in EGCG studies. Several reports indicate that the potency of certain polyphenolic compounds to inhibit or disaggregate α-synuclein oligomers correlates with the number of vicinal -OH groups present on a single phenyl ring[274]. To determine whether these structural properties are also important for the potency of apomorphine further studies involving different derivatives are necessary.

It would be also interesting to examine the precise binding site as well as the binding stoichiometry of apomorphine to patient-derived aggregates using methods, such as nuclear magnatic resonance (NMR) spectroscopy or X-ray crystallography and surface plasmon resonance (SPR) or analytical ultracentrifugation (AUC), respectively[275].

Certainly, *in vivo* studies will be required to demonstrate the pharmaceutical efficacy of apomorphine in valid animal models. Therefore, a *C. elegans*-based assay or the zebra fish model that have been recently established are valuable tools to address this issue. This will open new routes to better treatment options for AL amyloidosis.

The here described findings are based on a single heart, as AL amyloidosis belongs to the group of rare diseases and human hearts in general are not often available for research. A comparative study with different patient hearts is desired in order to adequately interpret the data. In addition, a comparison to a gender- and age-matched healthy human control heart is needed to increase the impact of the findings. Clearly, it will be necessary to analyze more samples from different hearts, including a control human heart.

# 4. MATERIALS AND METHODS

## 4.1 Materials

### 4.1.1 Chemicals and consumables

| | |
|---|---|
| 3-(4,5-dimethylthiazol-2-yl)-2,5-diphenyltetrazolium bromide (MTT) | Promega |
| 8-Anilinonaphthalene-1-sulfonic acid (ANS) | Roth |
| Agarose | Biozym |
| Albumin (BSA) | Roth |
| Amicon™ centrifugal filter units, cutoff 10 kDa | Millipore |
| Amicon™ Ultra-15 centrifugal filter units | MIllipore |
| Ampicillin | Sigma-Aldrich |
| Anhydrotetracycline | Sigma-Aldrich |
| R-Apomorphine | |
| Bacto peptone | Becton Dickinson |
| Bacto tryptone | Becton Dickinson |
| Bacto yeast | Becton Dickinson |
| β-Mercaptoethanol | Roth |
| Cell culture dishes | BD Falcon |
| Cell scrapers | TPP |
| Cellulose acetate membrane 0.2µm | Schleicher and Schuell |
| Complete™ protease inhibitor cocktail | Roche |
| Congo red | Roth |
| Coomassie brilliant blue G-250 | Serva |
| Dialysis membrane, 10.000 kDa cutoff | Roth |
| Deoxyribonucleotides (dNTPs) | Fermentas |
| Dithiothreitol (DTT) | Serva |
| Dimethylsulfoxide (DMSO) | Sigma-Aldrich |
| (-)-Epigallocatechin gallate | Sigma-Aldrich |
| Ethidium bromide solution 10mg/ml | Sigma-Aldrich |
| Ethylenediamine tetraacetic acid (EDTA) | Merck Eurolab GmbH |
| Ethanol | Roth |
| Fetal calf serum (FCS) | Gibco |
| Filter paper GB005 | Schleicher and Schuell |
| Glutathione oxidized | Sigma-Aldrich |
| Glutathione reduced | Sigma-Aldrich |
| Glycerol | Sigma-Aldrich |
| Hoechst 33342 | Invitrogen |
| Isopropyl β-D-1 thiogalactopyranoside (IPTG) | Apply Chem |
| Lysozyme | Sigma-Aldrich |
| Microtiter plates 96-well, 384-well | Greiner |

| | |
|---|---|
| Needles | Braun |
| Nitrocellulose membrane 0.2µm | Schleicher and Schuell |
| NP-40 (IGEPAL CA 630) | Sigma-Aldrich |
| Pasteru pipettes | Roth |
| Phusion High Fidelity Polymerase | Thermofisher Scientific |
| p-t-Octylphenyl-polyoxyethylen (Triton X-100) | Sigma-Aldrich |
| Polypropylene columns 5 ml | Qiagen |
| Ponceau S-solution, 0.1% | Sigma-Aldrich |
| Polypropylene columns 5 ml | Qiagen |
| Protein LoBind tubes 0.5 ml, 1.5 mL, 2 mL | Eppendorf |
| Ready-Load 1 Kb Plus DNA ladder | Invitrogen |
| Thioflavin T | Merck |
| Tris(hydroxymethyl)aminomethane | Merck |
| Tubes 15 mL, 50 mL | BD Falcon |

### 4.1.2 Enzymes, proteins and markers

| | |
|---|---|
| Benchmark pre-stained protein ladder | Invitrogen |
| Benzonase purity grade II | Merck |
| BSA 10 mg/ml | NEB |
| Complete™ protease inhibitor | Roche |
| Ready-Load™ 1 Kb Plus DNA ladder | Invitrogen |
| Restriction enzymes | NEB, Thermofisher Scientific |
| T4 DNA Ligase | Fermentas |
| NativeMark™ Unstained Protein Standard | Invitrogen |
| SeeBlue Plus2 Pre-stained Protein Standard | Thermo Scientific |

### 4.1.3 Kits

| | |
|---|---|
| BCA Protein assay reagent | Pierce |
| Cell Proliferation Assay (MTT) | Promega |
| Gel filtration calibration kit LMW | GE Healthcare |
| Gel filtration calibration kit HMW | GE Healthcare |
| NativePAGE Novex Bis-Tris gel system | Invitrogen |
| NuPAGE MES SDS running buffer | Invitrogen |
| Qiaprep spin miniprep kit | Qiagen |
| Qiagen gel extraction kit | Qiagen |
| WesternBright Chemiluminescence | Biozym |

### 4.1.4 Laboratory Equipment

| | |
|---|---|
| Atomic force microscope (AFM) | JPK |
| Äkta purifier | GE Healthcare |
| ArrayScan VTI (Cellomics) | Thermo Scientific |
| Centrifuge Evolution RC | Sorval |
| DNA electroporesis chamer | BioRad |
| Electron Microscope | Zeiss |
| Electrophoresis Power Supply EPS 601 | Amersham |
| Gene Genius UV imager | Bio Imaging Systems |
| Homogenizer | Virtis |
| Infinite M200 microplate reader | Tecan |
| Infinite M1000 microplate reader | Tecan |
| Innova 4430 incubator shaker | New Brunswick Scientific |
| Magnetic stirrer MR3001 | Heidolph |
| Micro 22R centrifuge | Hettich |
| Microwave | Privileg |
| Multichannel pipettes | Eppendorf |
| Nanodrop | Eppendorf |
| LAS-3000 photo imager | Fujifilm |
| Optima TLX ultracentrifuge | Beckman Coulter |
| Photometer | Eppendorf |
| Pipettes | Gilson |
| PCT200 Thermal Cycler | MJ Research |
| Scanjet 2400 | HP |
| Shaking incubator | Infors Unitron |
| Ultrasonic bath Sonorex TK52 | Bandelin |
| SpeedVac | Eppendorf |
| Thermomixer | Eppendorf |
| Trans-blot semi-dry transfer cell | BioRad |
| Vortex-Genie 2 | Scientific industries |
| Waterbath TW8 | Julabo |

### 4.1.5 Software

| | |
|---|---|
| AIDA | Free ware by Erik Hom |
| EndNote | Thomson Reuters |
| Illustrator | Adobe |
| GraphPad Prism 6 | GraphPad software |
| ImageJ | Wayne Rasband |
| JPK Data Processing | JPK Instruments AG |
| Microsoft office 2007 | Microsoft |
| Photoshop | Adobe |
| ProtParam | http://au.expasy.org/tools/protparam.html |

| | |
|---|---|
| Serial Cloner 2.5 | Serial Basics |
| Unicorn 5.11 | Amersham Biosciences |

### 4.1.6 Buffers

| | |
|---|---|
| Blocking buffer | 3% mild powder in PBS-T |
| Coomassie staining solution | 45% ethanol, 10% acetic acid, 0.05% Coomassie brilliant blue |
| Coomassie destaining solution | 45% ethanol, 10% acetic acid |
| 4x DNA sample buffer | 0.25% bromophenol blue, 0.25% xylene cyanole FF, 40%glycerol |
| Homogenization buffer 1 | 0.15 M NaCl |
| Homogenization buffer 2 | ddH2O |
| Kathode buffer | |
| LB medium | 1% (w/v) Bacto Pepton, 0.5% (w/v) yeast-extract, 1% (w/v)NaCl |
| 4x LDS sample buffer | |
| MTT-stop buffer | 47.75% DMF, 20% SDS, 2% acetic acid, 25 mM HCl |
| 10x PBS | 1.37 M NaCl, 27 mM KCl, 100 mM Na2HPO4, 17.6 mM KH2PO4 |
| PBS-T | 0.05% v/v Tween in PBS |
| 4x SDS loading buffer | 200 mM Tris pH 6.8, 400 mM DTT, 8% SDS, 40% glycerol,bromophenol blue |
| S.O.C. medium | 2% (w/v) Tryptone, 0.5% (w/v) yeast extract,10 mM NaCl, 2.5mM KCl, 10 mM MgCl2, 10 mM MgSO4, 20 mM Glucose |
| 1x TAE buffer | 40 mM Tris-Acetate, 1 mM EDTA, pH 8 |
| 1x TBE buffer | 45 mM Tris-Borate, 1 mM EDTA, pH 8.0 |
| 1x TBS buffer | 20 mM Tris-HCl pH 7.5, 150 mM NaCl |
| 1x TBS-T buffer | 20 mM Tris-HCl pH 7.5, 150 mM NaCl, 0.05% Triton X-100 |
| 10x WB transfer buffer | 250 mM Tris, 2 M Glycin |
| 1x WB buffer | 1 x WB-buffer, 10% Ethanol |

### 4.1.7 Media

#### 4.1.7.1 Media for bacterial culture

| | |
|---|---|
| LB medium | 1% (w/v) Bacto Pepton, 0.5% (w/v) yeast-extract, 1% (w/v) NaCl |
| S.O.C mdium | 2% (w/v) Tryptone, 0.5% (w/v) yeast extract,10 mM NaCl, 2.5 mM KCl, 10 mM MgCl2, 10 mM MgSO4, 20 mM Glucose |

#### 4.1.7.2 Media and supplements for cell culture

| | |
|---|---|
| Dulbecco's modified Eagle medium (DMEM) | Gibco |
| Dulbecco's phosphate buffered saline (D-PBS) | Gibco |
| Fetal calf serum (FCS) | Gibco |
| 0.5% Trypsin | Gibco |

### 4.1.8 Antibodies

| Primary antibodies | Species | Dilution | Supplier |
|---|---|---|---|
| anti-human kappa light chain | rabbit | 1:5000 | Dako Cytometrics |
| anti-human lambda light chain | rabbit | 1:5000 | Dako Cytometrics |

| Secondary antibodies | Conjugate | Dilution | Supplier |
|---|---|---|---|
| anti-rabbit | Peroxidase | 1:8000 | Sigma |
| anti-goat | Peroxidase | 1:8000 | Sigma |
| anti-rabbit | Gold | 1:30 | Dianova |

### 4.1.9 *E. coli* strains and mammalian cell lines

| | |
|---|---|
| BL21 (DE3) | F– ompT gal dcm lon hsdSB(rB- mB-) λ(DE3 [lacI lacUV5-T7 gene 1 ind1 sam7 nin5]) |
| Mach1 | ΔrecA1398 endA1 tonA Φ80ΔlacM15 ΔlacX74 hsdR($r_K^-$ $m_K^+$) |

HEK293 generated by transformation of human embryonic kidney cells with sheared adenovirus 5 DNA (Graham et al., 1977), origin is not clarified but neuronal background has been suggested; grow inadherent monolayers

## 4.2 Methods

### 4.2.1 Human heart tissue

Human heart used in this study was obtained from Dr. Ute Hegenbart and Dr. Stefan Schönland from Heidelberg University Hospital. The heart was a transplant from a 50 year-old female AL amyloidosis patient with extensive cardiac involvement. After transplantation the amyloid heart was sectioned and immediately stored at -80°C until used for extraction.

### 4.2.2 Biochemical methods

#### 4.2.2.1 Aggregate extraction procedure

Extraction of the amyloid was performed as described by Pras et al.[40] with minor modifications. Briefly, heart samples of approximately 4 g were first sectioned in thin slices using a scalpel. Heart slices were then homogenized in 20 volumes of ice-cold saline using an electric homogenizer. After centrifugation (Sorvall Evolution, Thermo Scientific) at 11,800 x g for 30 min at 4°C, the supernatant was decanted and the resulting pellet was homogenized in 20 volumes of saline using a glass homogenizer (vwr). This step was repeated 5 times. The resulting pellet was homogenized in distilled water and centrifuged at 50,000 x g for 1h at 4°C. This step was repeated 4 times with progressively smaller volumes (5, 5 and 1.5 volumes) of distilled water. The first 3 steps were centrifugated at 50,000 x g for 1 h and the last centrifugation at 11,800 x g for 3 h. All supernatants were then subjected to lyophylization. NaCl supernatants were concentrated to 1/10 of the initial volume and water-extracted lyophylizates were resuspended in 1 ml water. Samples were immediately snap frozen in liquid nitrogen and stored at -80°C until use. Protein concentration was determined with BCA assay (Thermo Scientific).

#### 4.2.2.2 Dot blot assay

Protein samples were spotted onto a nitrocellulose membrane and filtered using a vacuum device. Anti-lambda light chain antibody A0101 (1:2000) was used for immunological detection.

#### 4.2.2.3 SDS-PAGE

Protein samples were electrophoretically separated using NuPAGE™ Novex™ 4-12% Bis-Tris protein gels according to the manufacturer's protocol. For SDS-PAGE samples were boiled in 1x LDS loading buffer and 150 mM DTT (for reducing condition) for 5 min at 95°C. Prestained protein ladder (Invitrogen) was used for molecular weight determination.

#### 4.2.2.4 Blue-Native PAGE

Blue-Native PAGE was performed according to the manufacturer's guidelines using Invitrogen's NativePAGE™ Novex™ 4-16% Bis-Tris system. 20x Running Buffer and 20x Cathode Buffer were purchased. 1x Native sample buffer were added to the protein samples and gel were run for 2 h at 150 V. After separation gels were stained with Coomassie Brilliant Blue or were transferred onto PVDF membranes. The proteins on membranes were fixed for 15 min in 8% acetic acid prior immunodetection.

#### 4.2.2.5 Coomassie staining of SDS-PAGE

After SDS-PAGE gels were boiled in Coomassie staining solution using a microwave and were incubated for 1 h on a horizontal shaker at room temperature. Coomassie staining solution was removed and gels were then incubated in destain solution until distinct protein bands were visible. Gels were documented using a scanner.

#### 4.2.2.6 Western blotting

SDS or native gels were blotted to a nitrocellulose membrane or PVDF membrane, respectively, for 1 h at 20 V in a semi-dry apparatus. Membranes were blocked in 3% milk for 1 h at room termperature. Primary antibodies were diluted 1:5000 in blocking buffer and incubated with the membrane at least 2 h at room temperature or overnight at 4°C. After washing the membrane in 1x TBST secondary POD-conjugated anti-rabbit antibody (1:8000, Sigma) was incubated for 1 h at room temperature. Blots were developed with WesternBright (Biozym) and analyzed with a CCD camera (Fuji).

#### 4.2.2.7 Filter retardation assay

Samples were filtered through a 0.2 µm cellulose acetate membrane filter using a 96-well vacuum apparatus. If samples were analyzed under native conditions pure samples without additives were spotted onto the membrane. Under denaturing conditions 0.2% SDS was added followed by boiling for 5 min at 95°C. Membrane was washed 3x with 0.2% SDS-containing wash buffer. Immunological detection was performed using the anti-lambda A0101 (1:5000, Dako) and anti-rabbit POD conjugate

(1:8000, Sigma) as the primary and secondary antibody, respectively. Membranes were developed with WesternBright (Biozym) and images were taken using Fuji Imager. Filters were quantified using AIDA image analyzer software.

#### 4.2.2.8 ThT assay

ThT (10 µM) were added to all examined supernatants and the fluorescence was then measured with an Infinite M200 or M1000 spectrometer (Tecan) with an excitation and emission wavelength of 440 nm and 485 nm, respectively. Measurements were performed in triplicates at room temperature in black 96- or 384-well plates (Falcon).

#### 4.2.2.9 CR assay

For CR binding assays CR was added to samples to a final concentration of 10 µM and the absorption spectrum was recorded from 500 nm to 700 nm using an Infinite M200 spectrometer (Tecan). The wavelength of maximum absorption was determined to measure the fluorescence emission of CR.

#### 4.2.2.10 ANS binding assay

ANS were added to samples to a final concentration of 10 µM in a black 384-well plate. ANS fluorescence was performed by exciting samples at 350 nm and emission spectrum was recorded from 400 to 600 nm using an Infinite M200 spectrometer (Tecan).

#### 4.2.2.11 Ultracentrifugation experiments

Samples were centrifugated at 55,000 rpm (TLA rotor) and 4°C for 40 min. Supernatant was transferred to a fresh tube and the pellet was resuspended in 150 µL $H_2O$.

### 4.2.2.12 Expression and purification of full-length light chain protein AL01 in *E. coli*

For expression of light chain protein a single colony of *E. coli* BL21 DE3 containing the expression plasmid were inoculated in 100 ml LB/Amp. The culture was incubated over night at 37°C with shaking. The next day 2 liter of LB containing ampicilin were inoculated with overnight culture to OD 0.1. Culture was grown until OD has reached 0.6 and was induced with 0.2 µg/ml AHTC. After incubation for 4 h at 37°C and 120 rpm shaking culture were centrifuged at 4000 g for 15 min at 4°C. Pellets were stored at -20°C until use.

For protein purification pellet was resuspended in 70 ml ice-cold buffer A (50 mM Tris-HCl pH 8.0; 1 mM EDTA, Roche Inhibitor Cocktail Tablet). The lysate was sonicated for 3x 10 s and centrifuged at 30,000 g for 15 min at 4°C. The supernatant was decanted and pellet was resuspended in 30 ml buffer A. This step was repeated 3 times. The resulting pellet containing inclusion bodies were solublized in 15 ml ice-bold buffer A containing 6 M GndHCl and 5 mM β-MeEtOH. After 5 h incubation at 4°C with stirring solubilized protein solution were centrifugated 30,000 g for 15 min at 4°C. The supernatant were diluted 1:20 in ice-cold buffer A containing 5 mM GSH and 0.5 mM GSSG. Refolding was carried out overnight at 4°C with stirring. The next day protein solution was centrifugated at 30,000 g for 15 min at 4°C. The supernatant was dialyzed against 50 mM Tris-HCl pH 8.0 overnight at 4°C.

### 4.2.2.13 Size exclusion chromatography (SEC)

Samples (200 µL) were loaded onto a Superdex75 or Superose6 column that was equilibrated with water. Chromatography were performed at flow rate of 0.2ml/min. 400 µl fractions were collected. Calibration was performed with molecular mass standard proteins (GE Healthcare): Blue Dextran 200 000 kDa, Aldolase 158 000 kDa.

### 4.2.2.14 BCA assay

20 µl sample (1:30 dilution) was incubatd with 200 µl BCA solution at 37°C for 30 min. Protein concentration was determined spectrophotometrically by measuring the absorption at 280 nm using a Tecan plate reader. Corresponding extinction coefficients were calculated according to the respective amino acid sequence using ExPASY-ProtParam tool.

### 4.2.3 Biophysical methods

#### 4.2.3.1 Transmission electron microscopy

10 µl of the sample (10 µg/ml) were absorbed onto 300-mesh carbon-coated grids, negatively stained with 5% uranyl acetate and viewed on a Philips CM100 transmission electron microscope. For immunogold-labeling samples were first incubated with primary antibody (1:2200) for 15 min at room temperature. After washing, the samples were incubated with the secondary antibody (1:30, Dianova) conjugated with 10 nm diameter gold particles. After extensive washing, samples were stained with 5% uranyle acetate.

#### 4.2.3.2 Atomic force microscopy

10 µl aliquots were spotted on freshly cleaved mica, incubated for 10 min and washed four times with 40 µl distilled water. Samples were air dry overnight in a petri dish to prevent contamination. Images were taken with a digital multimode Nano Wizard® II atomic force microscope operating in intermitted contact mode. Final images were analyzed with JPK Data Processing software.

### 4.2.4 Cell biology

#### 4.2.4.1 Cultivation of mammalian cells

HeLa cells were cultivated in DMEM. Adherent mammalian cells were split twice a week. Cells were washed once with PBS and trypsin was added at a concentration of 0.5% supplemented with 1 mM EDTA to detach the cells. These were resuspended in fresh medium and one-tenth of the suspension was transferred to a new flask with 10 ml (75$cm^2$ flak) or 20 ml (125$cm^2$ flask) of new medium.

#### 4.2.4.2 MTT assay

HeLa cells were cultured in DMEM, 10% FCS, 1% PenStrep. Cells were plated at a densitiy of 20,000 cells per well on 96-well plates in 90 µL fresh medium. After 24 h, 10 µl samples were added to the microtiter plate, and the cells were further incubated for 48h at 37°C. Cytotoxicity was measured using a MTT assay kit (Promega). Absorbance values of formazan were determined at 590 nm with an Infinite M200 spectrometer (Tecan).

# 5. REFERENCES


1 Bruce Alberts, A. J., Julian Lewis, Martin Raff, Keith Roberts, and Peter Walter. Molecular Biology of the Cell, 4th edition. *Garland Science* (2002).

2 Berg JM, T. J., Stryer L. Biochemistry. 5th edition. *W H Freeman* (2002).

3 Hurle, M. R., Helms, L. R., Li, L., Chan, W. & Wetzel, R. A role for destabilizing amino acid replacements in light-chain amyloidosis. *Proceedings of the National Academy of Sciences of the United States of America* **91**, 5446-5450 (1994).

4 McCutchen, S. L., Lai, Z., Miroy, G. J., Kelly, J. W. & Colon, W. Comparison of lethal and nonlethal transthyretin variants and their relationship to amyloid disease. *Biochemistry* **34**, 13527-13536 (1995).

5 Booth, D. R. *et al.* Instability, unfolding and aggregation of human lysozyme variants underlying amyloid fibrillogenesis. *Nature* **385**, 787-793, doi:10.1038/385787a0 (1997).

6 Chiti, F. *et al.* Mutational analysis of the propensity for amyloid formation by a globular protein. *The EMBO journal* **19**, 1441-1449, doi:10.1093/emboj/19.7.1441 (2000).

7 Krebs, M. R. *et al.* Formation and seeding of amyloid fibrils from wild-type hen lysozyme and a peptide fragment from the beta-domain. *Journal of molecular biology* **300**, 541-549, doi:10.1006/jmbi.2000.3862 (2000).

8 Moraitakis, G. & Goodfellow, J. M. Simulations of human lysozyme: probing the conformations triggering amyloidosis. *Biophysical journal* **84**, 2149-2158, doi:10.1016/S0006-3495(03)75021-8 (2003).

9 De Felice, F. G. *et al.* Formation of amyloid aggregates from human lysozyme and its disease-associated variants using hydrostatic pressure. *FASEB journal : official publication of the Federation of American Societies for Experimental Biology* **18**, 1099-1101, doi:10.1096/fj.03-1072fje (2004).

10 Ferrao-Gonzales, A. D., Souto, S. O., Silva, J. L. & Foguel, D. The preaggregated state of an amyloidogenic protein: hydrostatic pressure converts native transthyretin into the amyloidogenic state. *Proceedings of the National Academy of Sciences of the United States of America* **97**, 6445-6450 (2000).

11 Khurana, R. *et al.* Partially folded intermediates as critical precursors of light chain amyloid fibrils and amorphous aggregates. *Biochemistry* **40**, 3525-3535 (2001).

12 Zurdo, J., Guijarro, J. I., Jimenez, J. L., Saibil, H. R. & Dobson, C. M. Dependence on solution conditions of aggregation and amyloid formation by an SH3 domain. *Journal of molecular biology* **311**, 325-340, doi:10.1006/jmbi.2001.4858 (2001).

13 Stefani, M. & Dobson, C. M. Protein aggregation and aggregate toxicity: new insights into protein folding, misfolding diseases and biological evolution. *Journal of molecular medicine* **81**, 678-699, doi:10.1007/s00109-003-0464-5 (2003).

14 Yoshimura, Y. *et al.* Distinguishing crystal-like amyloid fibrils and glass-like amorphous aggregates from their kinetics of formation. *Proceedings of the National Academy of Sciences of the United States of America* **109**, 14446-14451, doi:10.1073/pnas.1208228109 (2012).

15 Sunde, M. & Blake, C. C. From the globular to the fibrous state: protein structure and structural conversion in amyloid formation. *Quarterly reviews of biophysics* **31**, 1-39 (1998).

16 Surmacz-Chwedoruk, W., Malka, I., Bozycki, L., Nieznanska, H. & Dzwolak, W. On the heat stability of amyloid-based biological activity: insights from thermal degradation of insulin fibrils. *PloS one* **9**, e86320, doi:10.1371/journal.pone.0086320 (2014).

17 Kumar, P. N. *et al.* Light chain deposition disease presenting as cholestatic jaundice: a case report. *Oman medical journal* **27**, 56-59, doi:10.5001/omj.2012.12 (2012).

18 Ardalan, M. R. Light chain deposition disease; there are reasons for confusion. *Journal of renal injury prevention* **2**, 127-128, doi:10.12861/jrip.2013.41 (2013).

19 Truscott, R. J. Age-related nuclear cataract-oxidation is the key. *Experimental eye research* **80**, 709-725, doi:10.1016/j.exer.2004.12.007 (2005).

20 Hartl, F. U., Bracher, A. & Hayer-Hartl, M. Molecular chaperones in protein folding and proteostasis. *Nature* **475**, 324-332, doi:10.1038/nature10317 (2011).

21 Zimmerman, S. B. & Trach, S. O. Estimation of macromolecule concentrations and excluded volume effects for the cytoplasm of Escherichia coli. *Journal of molecular biology* **222**, 599-620 (1991).

22 Ellis, R. J. & Minton, A. P. Cell biology: join the crowd. *Nature* **425**, 27-28, doi:10.1038/425027a (2003).

23 Chen, B., Retzlaff, M., Roos, T. & Frydman, J. Cellular strategies of protein quality control. *Cold Spring Harbor perspectives in biology* **3**, a004374, doi:10.1101/cshperspect.a004374 (2011).

24 Wong, E. & Cuervo, A. M. Integration of clearance mechanisms: the proteasome and autophagy. *Cold Spring Harbor perspectives in biology* **2**, a006734, doi:10.1101/cshperspect.a006734 (2010).

25 Haas, A. L. & Siepmann, T. J. Pathways of ubiquitin conjugation. *FASEB journal : official publication of the Federation of American Societies for Experimental Biology* **11**, 1257-1268 (1997).

26 Kraft, C., Peter, M. & Hofmann, K. Selective autophagy: ubiquitin-mediated recognition and beyond. *Nature cell biology* **12**, 836-841, doi:10.1038/ncb0910-836 (2010).

27 Knowles, T. P., Vendruscolo, M. & Dobson, C. M. The amyloid state and its association with protein misfolding diseases. *Nature reviews. Molecular cell biology* **15**, 384-396, doi:10.1038/nrm3810 (2014).

28 Dobson, C. M. Protein folding and misfolding. *Nature* **426**, 884-890, doi:10.1038/nature02261 (2003).

29 Selkoe, D. J. Folding proteins in fatal ways. *Nature* **426**, 900-904, doi:10.1038/nature02264 (2003).

30 Stefani, M. Protein misfolding and aggregation: new examples in medicine and biology of the dark side of the protein world. *Biochimica et biophysica acta* **1739**, 5-25, doi:10.1016/j.bbadis.2004.08.004 (2004).

31 Westermark, P. *et al.* Amyloid fibril protein nomenclature -- 2002. *Amyloid : the international journal of experimental and clinical investigation : the official journal of the International Society of Amyloidosis* **9**, 197-200 (2002).

32 Blancas-Mejia, L. M. & Ramirez-Alvarado, M. Systemic amyloidoses. *Annual review of biochemistry* **82**, 745-774, doi:10.1146/annurev-biochem-072611-130030 (2013).

33 Sanchorawala, V. Light-chain (AL) amyloidosis: diagnosis and treatment. *Clinical journal of the American Society of Nephrology : CJASN* **1**, 1331-1341, doi:10.2215/CJN.02740806 (2006).

34 Sipe, J. D. *et al.* Amyloid fibril protein nomenclature: 2010 recommendations from the nomenclature committee of the International Society of Amyloidosis. *Amyloid : the international journal of experimental and clinical investigation : the official journal of the International Society of Amyloidosis* **17**, 101-104, doi:10.3109/13506129.2010.526812 (2010).

35 Rokitansky, K. Im Handbuch der Pathologischen Anatomie. *Braunmuller & Siedel* **3** (1842).

36 Sipe, J. D. & Cohen, A. S. Review: history of the amyloid fibril. *Journal of structural biology* **130**, 88-98, doi:10.1006/jsbi.2000.4221 (2000).

37 Kaplan, B., Shtrasburg, S. & Pras, M. Micropurification techniques in the analysis of amyloid proteins. *Journal of clinical pathology* **56**, 86-90 (2003).

38 Cohen, A. S. & Calkins, E. The Isolation of Amyloid Fibrils and a Study of the Effect of Collagenase and Hyaluronidase. *The Journal of cell biology* **21**, 481-486 (1964).

39 Shirahama, T. & Cohen, A. S. High-resolution electron microscopic analysis of the amyloid fibril. *The Journal of cell biology* **33**, 679-708 (1967).

40 Pras, M. The characterization of soluble amyloid prepared in water. *The Journal of clinical investigation* **47** (1968).

41 Roher, A., Wolfe, D., Palutke, M. & KuKuruga, D. Purification, ultrastructure, and chemical analysis of Alzheimer disease amyloid plaque core protein. *Proceedings of the National Academy of Sciences of the United States of America* **83**, 2662-2666 (1986).

42 Rostagno, A. & Ghiso, J. Isolation and biochemical characterization of amyloid plaques and paired helical filaments. *Current protocols in cell biology / editorial board, Juan S. Bonifacino ... [et al.]* **Chapter 3**, Unit 3 33 33 33 31-33, doi:10.1002/0471143030.cb0333s44 (2009).

43 Diaz-Hernandez, M. *et al.* Biochemical, ultrastructural, and reversibility studies on huntingtin filaments isolated from mouse and human brain. *The Journal of neuroscience : the official journal of the Society for Neuroscience* **24**, 9361-9371, doi:10.1523/JNEUROSCI.2365-04.2004 (2004).

44 Prusiner, S. B. & DeArmond, S. J. Prion diseases of the central nervous system. *Monographs in pathology*, 86-122 (1990).

45 Batia Kaplan, S. Y., Asok Kurna, Nordechai Pras & Gloria Gallo. Immunochemical characterization of amyloid in diagnostic biopys tissues. *Amyloid - The Journal of Protein Folding Disorders* **4**, 80-86 (1997).

46 Nelson, S. R., Lyon, M., Gallagher, J. T., Johnson, E. A. & Pepys, M. B. Isolation and characterization of the integral glycosaminoglycan constituents of human amyloid A and monoclonal light-chain amyloid fibrils. *The Biochemical journal* **275 ( Pt 1)**, 67-73 (1991).

47 Magnus, J. H., Husby, G. & Kolset, S. O. Presence of glycosaminoglycans in purified AA type amyloid fibrils associated with juvenile rheumatoid arthritis. *Annals of the rheumatic diseases* **48**, 215-219 (1989).

48 Westermark, P., Westermark, G. T., Suhr, O. B. & Berg, S. Transthyretin-derived amyloidosis: probably a common cause of lumbar spinal stenosis. *Upsala journal of medical sciences* **119**, 223-228, doi:10.3109/03009734.2014.895786 (2014).

49 Pras, M., Zucker-Franklin, D., Rimon, A. & Franklin, E. C. Physical, chemical, and ultrastructural studies of water-soluble human amyloid fibrils. Comparative analyses of nine amyloid preparations. *The Journal of experimental medicine* **130**, 777-796 (1969).

50 Glenner, G. G., Cuatrecasas, P., Isersky, C., Bladen, H. A. & Eanes, E. D. Physical and chemical properties of amyloid fibers. II. Isolation of a unique protein constituting the major component from human splenic amyloid fibril concentrates. *The journal of histochemistry and cytochemistry : official journal of the Histochemistry Society* **17**, 769-780 (1969).

51 Relini, A. *et al.* Ultrastructural organization of ex vivo amyloid fibrils formed by the apolipoprotein A-I Leu174Ser variant: an atomic force microscopy study. *Biochimica et biophysica acta* **1690**, 33-41, doi:10.1016/j.bbadis.2004.04.007 (2004).

52 Chamberlain, A. K. *et al.* Ultrastructural organization of amyloid fibrils by atomic force microscopy. *Biophysical journal* **79**, 3282-3293, doi:10.1016/S0006-3495(00)76560-X (2000).

53 Fitzpatrick, A. W. *et al.* Atomic structure and hierarchical assembly of a cross-beta amyloid fibril. *Proceedings of the National Academy of Sciences of the United States of America* **110**, 5468-5473, doi:10.1073/pnas.1219476110 (2013).

54 Toyama, B. H. & Weissman, J. S. Amyloid structure: conformational diversity and consequences. *Annual review of biochemistry* **80**, 557-585, doi:10.1146/annurev-biochem-090908-120656 (2011).

55 Xue, W. F., Homans, S. W. & Radford, S. E. Amyloid fibril length distribution quantified by atomic force microscopy single-particle image analysis. *Protein engineering, design & selection : PEDS* **22**, 489-496, doi:10.1093/protein/gzp026 (2009).

56 Sunde, M. *et al.* Common core structure of amyloid fibrils by synchrotron X-ray diffraction. *Journal of molecular biology* **273**, 729-739, doi:10.1006/jmbi.1997.1348 (1997).

57 Serpell, L. C. *et al.* The protofilament substructure of amyloid fibrils. *Journal of molecular biology* **300**, 1033-1039, doi:10.1006/jmbi.2000.3908 (2000).

58 Bodin, K. *et al.* Antibodies to human serum amyloid P component eliminate visceral amyloid deposits. *Nature* **468**, 93-97, doi:10.1038/nature09494 (2010).

59 Kisilevsky, R. The relation of proteoglycans, serum amyloid P and apo E to amyloidosis current status, 2000. *Amyloid : the international journal of experimental and clinical investigation : the official journal of the International Society of Amyloidosis* **7**, 23-25 (2000).

60 Westermark, G. T., Norling, B. & Westermark, P. Fibronectin and basement membrane components in renal amyloid deposits in patients with primary and secondary amyloidosis. *Clinical and experimental immunology* **86**, 150-156 (1991).

61 Eisenberg, D. & Jucker, M. The amyloid state of proteins in human diseases. *Cell* **148**, 1188-1203, doi:10.1016/j.cell.2012.02.022 (2012).

62 Howie, A. J. & Brewer, D. B. Optical properties of amyloid stained by Congo red: history and mechanisms. *Micron* **40**, 285-301, doi:10.1016/j.micron.2008.10.002 (2009).

63 Klunk, W. E., Pettegrew, J. W. & Abraham, D. J. Quantitative evaluation of congo red binding to amyloid-like proteins with a beta-pleated sheet conformation. *The journal of histochemistry and cytochemistry : official journal of the Histochemistry Society* **37**, 1273-1281 (1989).

64 Klunk, W. E., Jacob, R. F. & Mason, R. P. Quantifying amyloid by congo red spectral shift assay. *Methods in enzymology* **309**, 285-305 (1999).

65 Klunk, W. E., Jacob, R. F. & Mason, R. P. Quantifying amyloid beta-peptide (Abeta) aggregation using the Congo red-Abeta (CR-abeta) spectrophotometric assay. *Analytical biochemistry* **266**, 66-76, doi:10.1006/abio.1998.2933 (1999).

66 Porat, Y., Abramowitz, A. & Gazit, E. Inhibition of amyloid fibril formation by polyphenols: structural similarity and aromatic interactions as a common inhibition mechanism. *Chemical biology & drug design* **67**, 27-37, doi:10.1111/j.1747-0285.2005.00318.x (2006).

67 Turnell, W. G. & Finch, J. T. Binding of the dye congo red to the amyloid protein pig insulin reveals a novel homology amongst amyloid-forming peptide sequences. *Journal of molecular biology* **227**, 1205-1223 (1992).

68 Kim, Y. S., Randolph, T. W., Manning, M. C., Stevens, F. J. & Carpenter, J. F. Congo red populates partially unfolded states of an amyloidogenic protein to enhance aggregation and amyloid fibril formation. *The Journal of biological chemistry* **278**, 10842-10850, doi:10.1074/jbc.M212540200 (2003).

69 Caughey, B., Ernst, D. & Race, R. E. Congo red inhibition of scrapie agent replication. *Journal of virology* **67**, 6270-6272 (1993).

70 Groenning, M. Binding mode of Thioflavin T and other molecular probes in the context of amyloid fibrils-current status. *Journal of chemical biology* **3**, 1-18, doi:10.1007/s12154-009-0027-5 (2010).

71 Naiki, H., Higuchi, K., Hosokawa, M. & Takeda, T. Fluorometric determination of amyloid fibrils in vitro using the fluorescent dye, thioflavin T1. *Analytical biochemistry* **177**, 244-249 (1989).

72 Naiki, H., Higuchi, K., Nakakuki, K. & Takeda, T. Kinetic analysis of amyloid fibril polymerization in vitro. *Laboratory investigation; a journal of technical methods and pathology* **65**, 104-110 (1991).

73 LeVine, H., 3rd. Thioflavine T interaction with synthetic Alzheimer's disease beta-amyloid peptides: detection of amyloid aggregation in solution. *Protein science : a publication of the Protein Society* **2**, 404-410, doi:10.1002/pro.5560020312 (1993).

74 Souillac, P. O. *et al.* Effect of association state and conformational stability on the kinetics of immunoglobulin light chain amyloid fibril formation at physiological pH. *The Journal of biological chemistry* **277**, 12657-12665, doi:10.1074/jbc.M109230200 (2002).

75 Souillac, P. O. *et al.* Elucidation of the molecular mechanism during the early events in immunoglobulin light chain amyloid fibrillation. Evidence for an off-pathway oligomer at acidic pH. *The Journal of biological chemistry* **277**, 12666-12679, doi:10.1074/jbc.M109229200 (2002).

76 Bourhim, M., Kruzel, M., Srikrishnan, T. & Nicotera, T. Linear quantitation of Abeta aggregation using Thioflavin T: reduction in fibril formation by colostrinin. *Journal of neuroscience methods* **160**, 264-268, doi:10.1016/j.jneumeth.2006.09.013 (2007).

77 Ban, T., Hamada, D., Hasegawa, K., Naiki, H. & Goto, Y. Direct observation of amyloid fibril growth monitored by thioflavin T fluorescence. *The Journal of biological chemistry* **278**, 16462-16465, doi:10.1074/jbc.C300049200 (2003).

78 Zhu, M. *et al.* The flavonoid baicalein inhibits fibrillation of alpha-synuclein and disaggregates existing fibrils. *The Journal of biological chemistry* **279**, 26846-26857, doi:10.1074/jbc.M403129200 (2004).

79 Yang, S. G. *et al.* alpha-Tocopherol quinone inhibits beta-amyloid aggregation and cytotoxicity, disaggregates preformed fibrils and decreases the production of reactive oxygen species, NO and inflammatory cytokines. *Neurochemistry international* **57**, 914-922, doi:10.1016/j.neuint.2010.09.011 (2010).

80 Wang, S. S., Liu, K. N. & Lee, W. H. Effect of curcumin on the amyloid fibrillogenesis of hen egg-white lysozyme. *Biophysical chemistry* **144**, 78-87, doi:10.1016/j.bpc.2009.06.010 (2009).

81 Thapa, A., Jett, S. D. & Chi, E. Y. Curcumin Attenuates Amyloid-beta Aggregate Toxicity and Modulates Amyloid-beta Aggregation Pathway. *ACS chemical neuroscience* **7**, 56-68, doi:10.1021/acschemneuro.5b00214 (2016).

82 Lashuel, H. A. *et al.* New class of inhibitors of amyloid-beta fibril formation. Implications for the mechanism of pathogenesis in Alzheimer's disease. *The Journal of biological chemistry* **277**, 42881-42890, doi:10.1074/jbc.M206593200 (2002).

83 Guo, C. *et al.* Inhibitory effects of magnolol and honokiol on human calcitonin aggregation. *Scientific reports* **5**, 13556, doi:10.1038/srep13556 (2015).

84 Giorgetti, S. *et al.* Effect of tetracyclines on the dynamics of formation and destructuration of beta2-microglobulin amyloid fibrils. *The Journal of biological chemistry* **286**, 2121-2131, doi:10.1074/jbc.M110.178376 (2011).

85 Cheruvara, H., Allen-Baume, V. L., Kad, N. M. & Mason, J. M. Intracellular screening of a peptide library to derive a potent peptide inhibitor of alpha-synuclein aggregation. *The Journal of biological chemistry* **290**, 7426-7435, doi:10.1074/jbc.M114.620484 (2015).

86 Brumshtein, B. *et al.* Inhibition by small-molecule ligands of formation of amyloid fibrils of an immunoglobulin light chain variable domain. *eLife* **4**, e10935, doi:10.7554/eLife.10935 (2015).

87 Biancalana, M. & Koide, S. Molecular mechanism of Thioflavin-T binding to amyloid fibrils. *Biochimica et biophysica acta* **1804**, 1405-1412, doi:10.1016/j.bbapap.2010.04.001 (2010).

88 Arosio, P. *et al.* Kinetic analysis reveals the diversity of microscopic mechanisms through which molecular chaperones suppress amyloid formation. *Nature communications* **7**, 10948, doi:10.1038/ncomms10948 (2016).

89 Naiki, H. & Gejyo, F. Kinetic analysis of amyloid fibril formation. *Methods in enzymology* **309**, 305-318 (1999).

90 Jarrett, J. T. & Lansbury, P. T., Jr. Seeding "one-dimensional crystallization" of amyloid: a pathogenic mechanism in Alzheimer's disease and scrapie? *Cell* **73**, 1055-1058 (1993).

91 Cohen, S. I., Vendruscolo, M., Dobson, C. M. & Knowles, T. P. From macroscopic measurements to microscopic mechanisms of protein aggregation. *Journal of molecular biology* **421**, 160-171, doi:10.1016/j.jmb.2012.02.031 (2012).

92 Knowles, T. P. *et al.* An analytical solution to the kinetics of breakable filament assembly. *Science* **326**, 1533-1537, doi:10.1126/science.1178250 (2009).

93 Kumar, S. & Walter, J. Phosphorylation of amyloid beta (Abeta) peptides - a trigger for formation of toxic aggregates in Alzheimer's disease. *Aging* **3**, 803-812, doi:10.18632/aging.100362 (2011).

94 Merlini, G. & Palladini, G. Amyloidosis: is a cure possible? *Annals of oncology : official journal of the European Society for Medical Oncology / ESMO* **19 Suppl 4**, iv63-66, doi:10.1093/annonc/mdn200 (2008).

95 Gertz, M. A. & Kyle, R. A. Prognostic value of urinary protein in primary systemic amyloidosis (AL). *American journal of clinical pathology* **94**, 313-317 (1990).

96 Kyle, R. A. & Gertz, M. A. Primary systemic amyloidosis: clinical and laboratory features in 474 cases. *Seminars in hematology* **32**, 45-59 (1995).

97 Gertz, M. A. & Kyle, R. A. Hepatic amyloidosis: clinical appraisal in 77 patients. *Hepatology* **25**, 118-121, doi:10.1002/hep.510250122 (1997).

98 Sezer, O., Eucker, J., Schmid, P. & Possinger, K. New therapeutic approaches in primary systemic AL amyloidosis. *Annals of hematology* **79**, 1-6 (2000).

99 Herczenik, E. & Gebbink, M. F. Molecular and cellular aspects of protein misfolding and disease. *FASEB journal : official publication of the Federation of American Societies for Experimental Biology* **22**, 2115-2133, doi:10.1096/fj.07-099671 (2008).

100 Pinney, J. H. & Hawkins, P. N. Amyloidosis. *Annals of clinical biochemistry* **49**, 229-241, doi:10.1258/acb.2011.011225 (2012).

101 Kumar, S. K. *et al.* Recent improvements in survival in primary systemic amyloidosis and the importance of an early mortality risk score. *Mayo Clinic proceedings. Mayo Clinic* **86**, 12-18, doi:10.4065/mcp.2010.0480 (2011).

102 Banypersad, S. M., Moon, J. C., Whelan, C., Hawkins, P. N. & Wechalekar, A. D. Updates in cardiac amyloidosis: a review. *Journal of the American Heart Association* **1**, e000364, doi:10.1161/JAHA.111.000364 (2012).

103 Falk, R. H. Diagnosis and management of the cardiac amyloidoses. *Circulation* **112**, 2047-2060, doi:10.1161/CIRCULATIONAHA.104.489187 (2005).

104 Quarta, C. C., Kruger, J. L. & Falk, R. H. Cardiac amyloidosis. *Circulation* **126**, e178-182, doi:10.1161/CIRCULATIONAHA.111.069195 (2012).

105 (!!! INVALID CITATION !!!).

106 Janeway C.A., T. P., Walport M., Shlomchik M.J. Immunobiology, 5th edition. *Garland Science* (2001).

107 Harris, L. J., Skaletsky, E. & McPherson, A. Crystallographic structure of an intact IgG1 monoclonal antibody. *Journal of molecular biology* **275**, 861-872, doi:10.1006/jmbi.1997.1508 (1998).

108 Karlsson, F. A., Peterson, P. A. & Berggard, I. A structural feature of human immunoglobulin light chains. Two compact domains connected by a small switch region. *The Journal of biological chemistry* **247**, 1065-1073 (1972).

109 Cruse J.M., L. R. E. Illustrated Dictionary of Immunology, Thrid Edition. (2009).

110 Tiller, T. *et al.* Efficient generation of monoclonal antibodies from single human B cells by single cell RT-PCR and expression vector cloning. *Journal of immunological methods* **329**, 112-124, doi:10.1016/j.jim.2007.09.017 (2008).

111 Abraham, R. S. *et al.* Immunoglobulin light chain variable (V) region genes influence clinical presentation and outcome in light chain-associated amyloidosis (AL). *Blood* **101**, 3801-3808, doi:10.1182/blood-2002-09-2707 (2003).

112 Janeway, C. A., Jr. How the immune system works to protect the host from infection: a personal view. *Proceedings of the National Academy of Sciences of the United States of America* **98**, 7461-7468, doi:10.1073/pnas.131202998 (2001).

113 Butterfield, S., Hejjaoui, M., Fauvet, B., Awad, L. & Lashuel, H. A. Chemical strategies for controlling protein folding and elucidating the molecular mechanisms of amyloid formation and toxicity. *Journal of molecular biology* **421**, 204-236, doi:10.1016/j.jmb.2012.01.051 (2012).

114 McWilliams-Koeppen, H. P. *et al.* Light Chain Amyloid Fibrils Cause Metabolic Dysfunction in Human Cardiomyocytes. *PloS one* **10**, e0137716, doi:10.1371/journal.pone.0137716 (2015).

115 Haass, C. & Selkoe, D. J. Soluble protein oligomers in neurodegeneration: lessons from the Alzheimer's amyloid beta-peptide. *Nature reviews. Molecular cell biology* **8**, 101-112, doi:10.1038/nrm2101 (2007).

116 Reixach, N., Deechongkit, S., Jiang, X., Kelly, J. W. & Buxbaum, J. N. Tissue damage in the amyloidoses: Transthyretin monomers and nonnative oligomers are the major cytotoxic species in tissue culture. *Proceedings of the National Academy of Sciences of the United States of America* **101**, 2817-2822, doi:10.1073/pnas.0400062101 (2004).

117 Brenner, D. A. *et al.* Human amyloidogenic light chains directly impair cardiomyocyte function through an increase in cellular oxidant stress. *Circulation research* **94**, 1008-1010, doi:10.1161/01.RES.0000126569.75419.74 (2004).

118 Shi, J. *et al.* Amyloidogenic light chains induce cardiomyocyte contractile dysfunction and apoptosis via a non-canonical p38alpha MAPK pathway. *Proceedings of the National Academy of Sciences of the United States of America* **107**, 4188-4193, doi:10.1073/pnas.0912263107 (2010).

119 Liao, R. *et al.* Infusion of light chains from patients with cardiac amyloidosis causes diastolic dysfunction in isolated mouse hearts. *Circulation* **104**, 1594-1597 (2001).

120 Schutz, A. K. *et al.* The amyloid-Congo red interface at atomic resolution. *Angewandte Chemie* **50**, 5956-5960, doi:10.1002/anie.201008276 (2011).

121 Westermark, P. & Stenkvist, B. A new method for the diagnosis of systemic amyloidosis. *Archives of internal medicine* **132**, 522-523 (1973).

122 Gertz, M. A., Li, C. Y., Shirahama, T. & Kyle, R. A. Utility of subcutaneous fat aspiration for the diagnosis of systemic amyloidosis (immunoglobulin light chain). *Archives of internal medicine* **148**, 929-933 (1988).

123 Duston, M. A., Skinner, M., Meenan, R. F. & Cohen, A. S. Sensitivity, specificity, and predictive value of abdominal fat aspiration for the diagnosis of amyloidosis. *Arthritis and rheumatism* **32**, 82-85 (1989).

124 van, G., II, Hazenberg, B. P., Bijzet, J. & van Rijswijk, M. H. Diagnostic accuracy of subcutaneous abdominal fat tissue aspiration for detecting systemic amyloidosis and its utility in clinical practice. *Arthritis and rheumatism* **54**, 2015-2021, doi:10.1002/art.21902 (2006).

125 Ladewig, P. & Eser, S. Malignant tubular adenoma in a horseshoe kidney; its significance with regard to general cancer pathology. *The Journal of pathology and bacteriology* **57**, 405-411 (1945).

126 Romhanyi, G. Selective differentiation between amyloid and connective tissue structures based on the collagen specific topo-optical staining reaction with congo red. *Virchows Archiv. A, Pathology. Pathologische Anatomie* **354**, 209-222 (1971).

127 Schonland, S. O. *et al.* Immunohistochemistry in the classification of systemic forms of amyloidosis: a systematic investigation of 117 patients. *Blood* **119**, 488-493, doi:10.1182/blood-2011-06-358507 (2012).

128 Lavatelli F., d. F. A., Palladini G., Merlini G. Systemic amyloidoses and proteomics: The state of the art. *EuPA Open Proteomics* **11**, 4-10 (2016).

129 Picken, M. M. Proteomics and mass spectrometry in the diagnosis of renal amyloidosis. *Clinical kidney journal* **8**, 665-672, doi:10.1093/ckj/sfv087 (2015).

130 Vrana, J. A. *et al.* Classification of amyloidosis by laser microdissection and mass spectrometry-based proteomic analysis in clinical biopsy specimens. *Blood* **114**, 4957-4959, doi:10.1182/blood-2009-07-230722 (2009).

131 Vrana, J. A. *et al.* Clinical diagnosis and typing of systemic amyloidosis in subcutaneous fat aspirates by mass spectrometry-based proteomics. *Haematologica* **99**, 1239-1247, doi:10.3324/haematol.2013.102764 (2014).

132 Vila-Rico, M. *et al.* Quantitative analysis of post-translational modifications in human serum transthyretin associated with familial amyloidotic polyneuropathy by targeted LC-MS and intact protein MS. *Journal of proteomics* **127**, 234-246, doi:10.1016/j.jprot.2015.04.016 (2015).

133 Ankarcrona, M. *et al.* Current and future treatment of amyloid diseases. *Journal of internal medicine* **280**, 177-202, doi:10.1111/joim.12506 (2016).

134 Dember, L. M. Emerging treatment approaches for the systemic amyloidoses. *Kidney international* **68**, 1377-1390, doi:10.1111/j.1523-1755.2005.00535.x (2005).

135 Wechalekar, A. D., Gillmore, J. D. & Hawkins, P. N. Systemic amyloidosis. *Lancet* **387**, 2641-2654, doi:10.1016/S0140-6736(15)01274-X (2016).

136 Colon, W. & Kelly, J. W. Partial denaturation of transthyretin is sufficient for amyloid fibril formation in vitro. *Biochemistry* **31**, 8654-8660 (1992).

137 Rochet, J. C. Novel therapeutic strategies for the treatment of protein-misfolding diseases. *Expert reviews in molecular medicine* **9**, 1-34, doi:10.1017/S1462399407000385 (2007).

138 Miller, S. R., Sekijima, Y. & Kelly, J. W. Native state stabilization by NSAIDs inhibits transthyretin amyloidogenesis from the most common familial disease variants. *Laboratory investigation; a journal of technical methods and pathology* **84**, 545-552, doi:10.1038/labinvest.3700059 (2004).

139 Bartalena, L. & Robbins, J. Thyroid hormone transport proteins. *Clinics in laboratory medicine* **13**, 583-598 (1993).

140 Bulawa, C. E. *et al.* Tafamidis, a potent and selective transthyretin kinetic stabilizer that inhibits the amyloid cascade. *Proceedings of the National Academy of Sciences of the United States of America* **109**, 9629-9634, doi:10.1073/pnas.1121005109 (2012).

141 Pepys, M. B. *et al.* Human serum amyloid P component is an invariant constituent of amyloid deposits and has a uniquely homogeneous glycostructure. *Proceedings of the National Academy of Sciences of the United States of America* **91**, 5602-5606 (1994).

142 Botto, M. *et al.* Amyloid deposition is delayed in mice with targeted deletion of the serum amyloid P component gene. *Nature medicine* **3**, 855-859 (1997).

143 Pepys, M. B. *et al.* Targeted pharmacological depletion of serum amyloid P component for treatment of human amyloidosis. *Nature* **417**, 254-259, doi:10.1038/417254a (2002).

144 Denny, R. A., Gavrin, L. K. & Saiah, E. Recent developments in targeting protein misfolding diseases. *Bioorganic & medicinal chemistry letters* **23**, 1935-1944, doi:10.1016/j.bmcl.2013.01.089 (2013).

145 Kolstoe, S. E. *et al.* Interaction of serum amyloid P component with hexanoyl bis(D-proline) (CPHPC). *Acta crystallographica. Section D, Biological crystallography* **70**, 2232-2240, doi:10.1107/S1399004714013455 (2014).

146 Hirschfield, G. M. & Hawkins, P. N. Amyloidosis: new strategies for treatment. *The international journal of biochemistry & cell biology* **35**, 1608-1613 (2003).

147 Kolstoe, S. E. *et al.* Molecular dissection of Alzheimer's disease neuropathology by depletion of serum amyloid P component. *Proceedings of the National Academy of Sciences of the United States of America* **106**, 7619-7623, doi:10.1073/pnas.0902640106 (2009).

148 Meersman, F. & Dobson, C. M. Probing the pressure-temperature stability of amyloid fibrils provides new insights into their molecular properties. *Biochimica et biophysica acta* **1764**, 452-460, doi:10.1016/j.bbapap.2005.10.021 (2006).

149 Cohen, F. E. & Kelly, J. W. Therapeutic approaches to protein-misfolding diseases. *Nature* **426**, 905-909, doi:10.1038/nature02265 (2003).

150 Hrncic, R. *et al.* Antibody-mediated resolution of light chain-associated amyloid deposits. *Am J Pathol* **157**, 1239-1246, doi:10.1016/S0002-9440(10)64639-1 (2000).

151 Wall, J. S. *et al.* AL amyloid imaging and therapy with a monoclonal antibody to a cryptic epitope on amyloid fibrils. *PloS one* **7**, e52686, doi:10.1371/journal.pone.0052686 (2012).

152 Gertz, M. A. *et al.* First-in-Human Phase I/II Study of NEOD001 in Patients With Light Chain Amyloidosis and Persistent Organ Dysfunction. *Journal of clinical oncology : official journal of the American Society of Clinical Oncology* **34**, 1097-1103, doi:10.1200/JCO.2015.63.6530 (2016).

153 Richards, D. B. *et al.* Therapeutic Clearance of Amyloid by Antibodies to Serum Amyloid P Component. *The New England journal of medicine* **373**, 1106-1114, doi:10.1056/NEJMoa1504942 (2015).

154 Zhang, S. *et al.* A novel strategy for MALDI-TOF MS analysis of small molecules. *Journal of the American Society for Mass Spectrometry* **21**, 154-160, doi:10.1016/j.jasms.2009.09.024 (2010).

155 Ganellin C. R., J. R., Roberts S.M. Introduction to biological and small molecule drug research and development. *Academic Press*, 187 (2013).

156 Lorenzo, A. & Yankner, B. A. Beta-amyloid neurotoxicity requires fibril formation and is inhibited by congo red. *Proceedings of the National Academy of Sciences of the United States of America* **91**, 12243-12247 (1994).

157 Lee, V. M. Amyloid binding ligands as Alzheimer's disease therapies. *Neurobiology of aging* **23**, 1039-1042 (2002).

158 Poli, G. *et al.* In vitro evaluation of the anti-prionic activity of newly synthesized congo red derivatives. *Arzneimittel-Forschung* **53**, 875-888, doi:10.1055/s-0031-1299845 (2003).

159 Roberts, B. E. *et al.* A synergistic small-molecule combination directly eradicates diverse prion strain structures. *Nature chemical biology* **5**, 936-946, doi:10.1038/nchembio.246 (2009).

160 Roberts, B. E. & Shorter, J. Escaping amyloid fate. *Nature structural & molecular biology* **15**, 544-546, doi:10.1038/nsmb0608-544 (2008).

161 Wells, J. A. & McClendon, C. L. Reaching for high-hanging fruit in drug discovery at protein-protein interfaces. *Nature* **450**, 1001-1009, doi:10.1038/nature06526 (2007).

162 Jones, S. & Thornton, J. M. Principles of protein-protein interactions. *Proceedings of the National Academy of Sciences of the United States of America* **93**, 13-20 (1996).

163 Lo Conte, L., Chothia, C. & Janin, J. The atomic structure of protein-protein recognition sites. *Journal of molecular biology* **285**, 2177-2198 (1999).

164 Cheng, A. C. *et al.* Structure-based maximal affinity model predicts small-molecule druggability. *Nature biotechnology* **25**, 71-75, doi:10.1038/nbt1273 (2007).

165 Smith, R. D. *et al.* Exploring protein-ligand recognition with Binding MOAD. *Journal of molecular graphics & modelling* **24**, 414-425, doi:10.1016/j.jmgm.2005.08.002 (2006).

166 Chene, P. Drugs targeting protein-protein interactions. *ChemMedChem* **1**, 400-411, doi:10.1002/cmdc.200600004 (2006).

167 Hopkins, A. L. & Groom, C. R. The druggable genome. *Nature reviews. Drug discovery* **1**, 727-730, doi:10.1038/nrd892 (2002).

168 Nelson, R. & Eisenberg, D. Structural models of amyloid-like fibrils. *Advances in protein chemistry* **73**, 235-282, doi:10.1016/S0065-3233(06)73008-X (2006).

169 Bhak, G., Choe, Y. J. & Paik, S. R. Mechanism of amyloidogenesis: nucleation-dependent fibrillation versus double-concerted fibrillation. *BMB reports* **42**, 541-551 (2009).

170 Kodali, R. & Wetzel, R. Polymorphism in the intermediates and products of amyloid assembly. *Current opinion in structural biology* **17**, 48-57, doi:10.1016/j.sbi.2007.01.007 (2007).

171 Wetzel, R., Shivaprasad, S. & Williams, A. D. Plasticity of amyloid fibrils. *Biochemistry* **46**, 1-10, doi:10.1021/bi0620959 (2007).

172 Gosal, W. S. *et al.* Competing pathways determine fibril morphology in the self-assembly of beta2-microglobulin into amyloid. *Journal of molecular biology* **351**, 850-864, doi:10.1016/j.jmb.2005.06.040 (2005).

173 Ehrnhoefer, D. E. *et al.* Green tea (-)-epigallocatechin-gallate modulates early events in huntingtin misfolding and reduces toxicity in Huntington's disease models. *Human molecular genetics* **15**, 2743-2751, doi:10.1093/hmg/ddl210 (2006).

174 Ehrnhoefer, D. E. Redirecting aggregation pathways: small molecule-mediated conversion of amyloidogenic polypeptides in unstructured, off-pathway oligomers. *Nat. Struct. Mol. Biol.* **15**, 558-566 (2008).

175 Gestwicki, J. E., Crabtree, G. R. & Graef, I. A. Harnessing chaperones to generate small-molecule inhibitors of amyloid beta aggregation. *Science* **306**, 865-869, doi:10.1126/science.1101262 (2004).

176 Li, J., Zhu, M., Rajamani, S., Uversky, V. N. & Fink, A. L. Rifampicin inhibits alpha-synuclein fibrillation and disaggregates fibrils. *Chemistry & biology* **11**, 1513-1521, doi:10.1016/j.chembiol.2004.08.025 (2004).

177 Wang, H. *et al.* Direct and selective elimination of specific prions and amyloids by 4,5-dianilinophthalimide and analogs. *Proceedings of the National Academy of Sciences of the United States of America* **105**, 7159-7164, doi:10.1073/pnas.0801934105 (2008).

178 Yang, C. S., Maliakal, P. & Meng, X. Inhibition of carcinogenesis by tea. *Annual review of pharmacology and toxicology* **42**, 25-54, doi:10.1146/annurev.pharmtox.42.082101.154309 (2002).

179 Nance, C. L. & Shearer, W. T. Is green tea good for HIV-1 infection? *The Journal of allergy and clinical immunology* **112**, 851-853, doi:10.1016/j.jaci.2003.08.048 (2003).

180 Cabrera, C., Artacho, R. & Gimenez, R. Beneficial effects of green tea--a review. *Journal of the American College of Nutrition* **25**, 79-99 (2006).

181 Hauber, I., Hohenberg, H., Holstermann, B., Hunstein, W. & Hauber, J. The main green tea polyphenol epigallocatechin-3-gallate counteracts semen-mediated enhancement of HIV infection. *Proceedings of the National Academy of Sciences of the United States of America* **106**, 9033-9038, doi:10.1073/pnas.0811827106 (2009).

182 Ehrnhoefer, D. E. *et al.* EGCG redirects amyloidogenic polypeptides into unstructured, off-pathway oligomers. *Nature structural & molecular biology* **15**, 558-566, doi:10.1038/nsmb.1437 (2008).

183 Meng, F., Abedini, A., Plesner, A., Verchere, C. B. & Raleigh, D. P. The flavanol (-)-epigallocatechin 3-gallate inhibits amyloid formation by islet amyloid polypeptide, disaggregates amyloid fibrils, and protects cultured cells against IAPP-induced toxicity. *Biochemistry* **49**, 8127-8133, doi:10.1021/bi100939a (2010).

184 Miyata, M. *et al.* The crystal structure of the green tea polyphenol (-)-epigallocatechin gallate-transthyretin complex reveals a novel binding site distinct from the thyroxine binding site. *Biochemistry* **49**, 6104-6114, doi:10.1021/bi1004409 (2010).

185 Bieschke, J. *et al.* EGCG remodels mature alpha-synuclein and amyloid-beta fibrils and reduces cellular toxicity. *Proceedings of the National Academy of Sciences of the United States of America* **107**, 7710-7715, doi:10.1073/pnas.0910723107 (2010).

186 Chandrashekaran, I. R., Adda, C. G., Macraild, C. A., Anders, R. F. & Norton, R. S. EGCG disaggregates amyloid-like fibrils formed by Plasmodium falciparum merozoite surface protein 2. *Archives of biochemistry and biophysics* **513**, 153-157, doi:10.1016/j.abb.2011.07.008 (2011).

187 Stenvang, M., Christiansen, G. & Otzen, D. E. Epigallocatechin Gallate Remodels Fibrils of Lattice Corneal Dystrophy Protein, Facilitating Proteolytic Degradation and Preventing Formation of Membrane-Permeabilizing Species. *Biochemistry* **55**, 2344-2357, doi:10.1021/acs.biochem.6b00063 (2016).

188 Cao, P. & Raleigh, D. P. Analysis of the inhibition and remodeling of islet amyloid polypeptide amyloid fibers by flavanols. *Biochemistry* **51**, 2670-2683, doi:10.1021/bi2015162 (2012).

189 Palhano, F. L., Lee, J., Grimster, N. P. & Kelly, J. W. Toward the molecular mechanism(s) by which EGCG treatment remodels mature amyloid fibrils. *Journal of the American Chemical Society* **135**, 7503-7510, doi:10.1021/ja3115696 (2013).

190 Mereles, D., Wanker, E. E. & Katus, H. A. Therapy effects of green tea in a patient with systemic light-chain amyloidosis. *Clinical research in cardiology : official journal of the German Cardiac Society* **97**, 341-344, doi:10.1007/s00392-008-0649-6 (2008).

191 Yang, F. *et al.* Curcumin inhibits formation of amyloid beta oligomers and fibrils, binds plaques, and reduces amyloid in vivo. *The Journal of biological chemistry* **280**, 5892-5901, doi:10.1074/jbc.M404751200 (2005).

192 Conway, K. A., Rochet, J. C., Bieganski, R. M. & Lansbury, P. T., Jr. Kinetic stabilization of the alpha-synuclein protofibril by a dopamine-alpha-synuclein adduct. *Science* **294**, 1346-1349, doi:10.1126/science.1063522 (2001).

193 Pelaez-Aguilar, A. E. *et al.* Inhibition of Light Chain 6aJL2-R24G Amyloid Fiber Formation Associated with Light Chain Amyloidosis. *Biochemistry* **54**, 4978-4986, doi:10.1021/acs.biochem.5b00288 (2015).

194 Trinkaus-Randall, V. *et al.* Cellular Response of Cardiac Fibroblasts to Amyloidogenic Light Chains. *The American Journal of Pathology* **166**, 197-208, doi:http://dx.doi.org/10.1016/S0002-9440(10)62244-4 (2005).

195 Sikkink, L. A. & Ramirez-Alvarado, M. Cytotoxicity of amyloidogenic immunoglobulin light chains in cell culture. *Cell death & disease* **1**, e98, doi:10.1038/cddis.2010.75 (2010).

196 Guan, J. *et al.* Lysosomal dysfunction and impaired autophagy underlie the pathogenesis of amyloidogenic light chain-mediated cardiotoxicity. *EMBO molecular medicine* **6**, 1493-1507, doi:10.15252/emmm.201404190 (2014).

197 Mishra, S. *et al.* Human amyloidogenic light chain proteins result in cardiac dysfunction, cell death, and early mortality in zebrafish. *American journal of physiology. Heart and circulatory physiology* **305**, H95-103, doi:10.1152/ajpheart.00186.2013 (2013).

198 Diomede, L. *et al.* A Caenorhabditis elegans-based assay recognizes immunoglobulin light chains causing heart amyloidosis. *Blood* **123**, 3543-3552, doi:10.1182/blood-2013-10-525634 (2014).

199 Migrino, R. Q. *et al.* Systemic and microvascular oxidative stress induced by light chain amyloidosis. *International journal of cardiology* **145**, 67-68, doi:10.1016/j.ijcard.2009.04.044 (2010).

200 Migrino, R. Q. *et al.* Human microvascular dysfunction and apoptotic injury induced by AL amyloidosis light chain proteins. *American journal of physiology. Heart and circulatory physiology* **301**, H2305-2312, doi:10.1152/ajpheart.00503.2011 (2011).

201 Puchtler, H. & Sweat, F. Congo red as a stain for fluorescence microscopy of amyloid. *The journal of histochemistry and cytochemistry : official journal of the Histochemistry Society* **13**, 693-694 (1965).

202 Smith, P. K. *et al.* Measurement of protein using bicinchoninic acid. *Analytical biochemistry* **150**, 76-85 (1985).

203 Wanker, E. E. *et al.* Membrane filter assay for detection of amyloid-like polyglutamine-containing protein aggregates. *Methods in enzymology* **309**, 375-386 (1999).

204 Schagger, H. & von Jagow, G. Blue native electrophoresis for isolation of membrane protein complexes in enzymatically active form. *Analytical biochemistry* **199**, 223-231 (1991).

205 Towbin, H., Staehelin, T. & Gordon, J. Electrophoretic transfer of proteins from polyacrylamide gels to nitrocellulose sheets: procedure and some applications. *Proceedings of the National Academy of Sciences of the United States of America* **76**, 4350-4354 (1979).

206 Laemmli, U. K. Cleavage of structural proteins during the assembly of the head of bacteriophage T4. *Nature* **227**, 680-685 (1970).

207 Fazekas de St Groth, S., Webster, R. G. & Datyner, A. Two new staining procedures for quantitative estimation of proteins on electrophoretic strips. *Biochimica et biophysica acta* **71**, 377-391 (1963).

208 Gallo, G., Wisniewski, T., Choi-Miura, N. H., Ghiso, J. & Frangione, B. Potential role of apolipoprotein-E in fibrillogenesis. *Am J Pathol* **145**, 526-530 (1994).

209 Bolder, S. G., Sagis, L. M., Venema, P. & van der Linden, E. Effect of stirring and seeding on whey protein fibril formation. *Journal of agricultural and food chemistry* **55**, 5661-5669, doi:10.1021/jf063351r (2007).

210 Hawe, A., Sutter, M. & Jiskoot, W. Extrinsic fluorescent dyes as tools for protein characterization. *Pharmaceutical research* **25**, 1487-1499, doi:10.1007/s11095-007-9516-9 (2008).

211 Lodish H, B. A., Zipursky SL,. Molecular Cell Biology. 4th edition. (2000).

212 Aguilar, M. HPCL of peptides and proteins. **251** (2004).

213 Kastner, M. Protein Liquid Chromatography. *Elsevier Science* **61** (1999).

214 Mosmann, T. Rapid colorimetric assay for cellular growth and survival: application to proliferation and cytotoxicity assays. *Journal of immunological methods* **65**, 55-63 (1983).

215 Siegel, M. R. & Sisler, H. D. Inhibition of Protein Synthesis in Vitro by Cycloheximide. *Nature* **200**, 675-676 (1963).

216 Rashad, M. A. Pharmacological enhancement of treatment for amblyopia. *Clinical ophthalmology* **6**, 409-416, doi:10.2147/OPTH.S29941 (2012).

217 Kovacic, P. & Thurn, L. A. Cardiovascular toxicity from the perspective of oxidative stress, electron transfer, and prevention by antioxidants. *Current vascular pharmacology* **3**, 107-117 (2005).

218 Conroy, E. A., Liranzo, M. O., McMahon, J., Steck, W. D. & Tuthill, R. J. Quinidine-induced pigmentation. *Cutis* **57**, 425-427 (1996).

219 Neef, C. & van Laar, T. Pharmacokinetic-pharmacodynamic relationships of apomorphine in patients with Parkinson's disease. *Clinical pharmacokinetics* **37**, 257-271, doi:10.2165/00003088-199937030-00004 (1999).

220 Deleu, D., Hanssens, Y. & Northway, M. G. Subcutaneous apomorphine : an evidence-based review of its use in Parkinson's disease. *Drugs & aging* **21**, 687-709 (2004).

221 Alexandrov, P. N., Pogue, A., Bhattacharjee, S. & Lukiw, W. J. Retinal amyloid peptides and complement factor H in transgenic models of Alzheimer's disease. *Neuroreport* **22**, 623-627, doi:10.1097/WNR.0b013e3283497334 (2011).

222 Bolognesi, B. *et al.* ANS binding reveals common features of cytotoxic amyloid species. *ACS chemical biology* **5**, 735-740, doi:10.1021/cb1001203 (2010).

223 Qin, Z. Structural characterization of the partially folded intermediates of an immunoglobulin light chain leading to amyloid fibrillation an damorphous aggregation. *Biochemistry* **46**, 3521 - 3531 (2007).

224 Rognoni, P. A strategy for synthesis of pathogenic human immunoglobulin free light chains in *E. coli*. *PloS one* **8** (2013).

225 Kim, Y. S., Randolph, T. W., Stevens, F. J. & Carpenter, J. F. Kinetics and energetics of assembly, nucleation, and growth of aggregates and fibrils for an amyloidogenic protein. Insights into transition states from pressure, temperature, and co-solute studies. *The Journal of biological chemistry* **277**, 27240-27246, doi:10.1074/jbc.M202492200 (2002).

226 Martsev, S. P. *et al.* Amyloid fibril formation of the mouse V(L) domain at acidic pH. *Biochemistry* **41**, 3389-3395 (2002).

227 Martin, D. J. & Ramirez-Alvarado, M. Comparison of amyloid fibril formation by two closely related immunoglobulin light chain variable domains. *Amyloid : the international journal of experimental and clinical investigation : the official journal of the International Society of Amyloidosis* **17**, 129-136, doi:10.3109/13506129.2010.530081 (2010).

228 Chiti, F. *et al.* Solution conditions can promote formation of either amyloid protofilaments or mature fibrils from the HypF N-terminal domain. *Protein science : a publication of the Protein Society* **10**, 2541-2547, doi:10.1110/ps.10201 (2001).

229 Sasahara, K., Yagi, H., Sakai, M., Naiki, H. & Goto, Y. Amyloid nucleation triggered by agitation of beta2-microglobulin under acidic and neutral pH conditions. *Biochemistry* **47**, 2650-2660, doi:10.1021/bi701968g (2008).

230 LeVine, H., 3rd. Mechanism of A beta(1-40) fibril-induced fluorescence of (trans,trans)-1-bromo-2,5-bis(4-hydroxystyryl)benzene (K114). *Biochemistry* **44**, 15937-15943, doi:10.1021/bi051252l (2005).

231 Jarrett, J. T. & Lansbury, P. T., Jr. Amyloid fibril formation requires a chemically discriminating nucleation event: studies of an amyloidogenic sequence from the bacterial protein OsmB. *Biochemistry* **31**, 12345-12352 (1992).

232 Jarrett, J. T., Berger, E. P. & Lansbury, P. T., Jr. The carboxy terminus of the beta amyloid protein is critical for the seeding of amyloid formation: implications for the pathogenesis of Alzheimer's disease. *Biochemistry* **32**, 4693-4697 (1993).

233 Hudson, S. A., Ecroyd, H., Kee, T. W. & Carver, J. A. The thioflavin T fluorescence assay for amyloid fibril detection can be biased by the presence of exogenous compounds. *The FEBS journal* **276**, 5960-5972, doi:10.1111/j.1742-4658.2009.07307.x (2009).

234 Blancas-Mejia, L. M. *et al.* Thermodynamic and fibril formation studies of full length immunoglobulin light chain AL-09 and its germline protein using scan rate dependent thermal unfolding. *Biophysical chemistry* **207**, 13-20, doi:10.1016/j.bpc.2015.07.005 (2015).

235 Sikkink, L. A. & Ramirez-Alvarado, M. Biochemical and aggregation analysis of Bence Jones proteins from different light chain diseases. *Amyloid : the international journal of experimental and clinical investigation : the official journal of the International Society of Amyloidosis* **15**, 29-39, doi:10.1080/13506120701815324 (2008).

236 Kaplan, B., Martin, B. M., Livneh, A., Pras, M. & Gallo, G. R. Biochemical subtyping of amyloid in formalin-fixed tissue samples confirms and supplements immunohistologic data. *American journal of clinical pathology* **121**, 794-800, doi:10.1309/Y6CY-XF4E-LL1G-KQBU (2004).

237 Buxbaum, J. Mechanisms of disease: monoclonal immunoglobulin deposition. Amyloidosis, light chain deposition disease, and light and heavy chain deposition disease. *Hematology/oncology clinics of North America* **6**, 323-346 (1992).

238 Rocken, C. *et al.* Plasmacytoma of the tonsil with AL amyloidosis: evidence of post-fibrillogenic proteolysis of the fibril protein. *Virchows Archiv : an international journal of pathology* **436**, 336-344 (2000).

239 Picken, M. M., Gallo, G., Buxbaum, J. & Frangione, B. Characterization of renal amyloid derived from the variable region of the lambda light chain subgroup II. *Am J Pathol* **124**, 82-87 (1986).

240 Kiyama, M. *et al.* Immunohistochemical and immunochemical study of amyloid in liver affected by systemic Alambda amyloidosis with antibodies against three different regions of immunoglobulin lambda light chain. *Pathology international* **57**, 343-350, doi:10.1111/j.1440-1827.2007.02106.x (2007).

241 Brumshtein, B. *et al.* Formation of amyloid fibers by monomeric light chain variable domains. *The Journal of biological chemistry* **289**, 27513-27525, doi:10.1074/jbc.M114.585638 (2014).

242 Olsen, K. E., Sletten, K. & Westermark, P. Fragments of the constant region of immunoglobulin light chains are constituents of AL-amyloid proteins. *Biochemical and biophysical research communications* **251**, 642-647, doi:10.1006/bbrc.1998.9508 (1998).

243 Lavatelli, F. *et al.* Amyloidogenic and associated proteins in systemic amyloidosis proteome of adipose tissue. *Molecular & cellular proteomics : MCP* **7**, 1570-1583, doi:10.1074/mcp.M700545-MCP200 (2008).

244 Glenner, G. G. Amyloid deposits and amyloidosis: the beta-fibrilloses (second of two parts). *The New England journal of medicine* **302**, 1333-1343, doi:10.1056/NEJM198006123022403 (1980).

245 Casadonte, R. *et al.* Imaging mass spectrometry analysis of renal amyloidosis biopsies reveals protein co-localization with amyloid deposits. *Analytical and bioanalytical chemistry* **407**, 5323-5331, doi:10.1007/s00216-015-8689-z (2015).

246 Gallo, G. *et al.* Light chain cardiomyopathy. Structural analysis of the light chain tissue deposits. *Am J Pathol* **148**, 1397-1406 (1996).

247 Sethi, S. *et al.* Laser microdissection and mass spectrometry-based proteomics aids the diagnosis and typing of renal amyloidosis. *Kidney international* **82**, 226-234, doi:10.1038/ki.2012.108 (2012).

248 Takahashi, N. *et al.* Establishment of a first-order kinetic model of light chain-associated amyloid fibril extension in vitro. *Biochimica et biophysica acta* **1601**, 110-120 (2002).

249 Lavatelli, F. *et al.* Novel mitochondrial protein interactors of immunoglobulin light chains causing heart amyloidosis. *FASEB journal : official publication of the Federation of American Societies for Experimental Biology* **29**, 4614-4628, doi:10.1096/fj.15-272179 (2015).

250 Olzscha, H. *et al.* Amyloid-like aggregates sequester numerous metastable proteins with essential cellular functions. *Cell* **144**, 67-78, doi:10.1016/j.cell.2010.11.050 (2011).

251 Falk, R. H. & Skinner, M. The systemic amyloidoses: an overview. *Advances in internal medicine* **45**, 107-137 (2000).

252 Dubrey, S. W., Cha, K., Skinner, M., LaValley, M. & Falk, R. H. Familial and primary (AL) cardiac amyloidosis: echocardiographically similar diseases with distinctly different clinical outcomes. *Heart* **78**, 74-82 (1997).

253 Mahmood, S., Palladini, G., Sanchorawala, V. & Wechalekar, A. Update on treatment of light chain amyloidosis. *Haematologica* **99**, 209-221, doi:10.3324/haematol.2013.087619 (2014).

254 Naiki, H. *et al.* Fluorometric examination of tissue amyloid fibrils in murine senile amyloidosis: use of the fluorescent indicator, thioflavine T. *Laboratory investigation; a journal of technical methods and pathology* **62**, 768-773 (1990).

255 LeVine, H., 3rd. Stopped-flow kinetics reveal multiple phases of thioflavin T binding to Alzheimer beta (1-40) amyloid fibrils. *Archives of biochemistry and biophysics* **342**, 306-316, doi:10.1006/abbi.1997.0137 (1997).

256 Sarkar, N., Singh, A. N. & Dubey, V. K. Effect of curcumin on amyloidogenic property of molten globule-like intermediate state of 2,5-diketo-D-gluconate reductase A. *Biological chemistry* **390**, 1057-1061, doi:10.1515/BC.2009.107 (2009).

257 Horwich, A. Protein aggregation in disease: a role for folding intermediates forming specific multimeric interactions. *J Clin Invest* **110**, 1221-1232, doi:10.1172/JCI16781 (2002).

258 Sarkar, N., Kumar, M. & Dubey, V. K. Rottlerin dissolves pre-formed protein amyloid: a study on hen egg white lysozyme. *Biochimica et biophysica acta* **1810**, 809-814, doi:10.1016/j.bbagen.2011.06.012 (2011).

259 Semisotnov, G. V. *et al.* Study of the "molten globule" intermediate state in protein folding by a hydrophobic fluorescent probe. *Biopolymers* **31**, 119-128, doi:10.1002/bip.360310111 (1991).

260 Andrich, K. *et al.* Aggregation of Full Length Immunoglobulin Light Chains from AL Amyloidosis Patients Is Remodeled by Epigallocatechin-3-gallate. *The Journal of biological chemistry*, doi:10.1074/jbc.M116.750323 (2016).

261 Ubeda, A., Montesinos, C., Paya, M., Terencio, C. & Alcaraz, M. J. Antioxidant action of benzylisoquinoline alkaloids. *Free radical research communications* **18**, 167-175 (1993).

262 Nisbet, R. M., Polanco, J. C., Ittner, L. M. & Gotz, J. Tau aggregation and its interplay with amyloid-beta. *Acta neuropathologica* **129**, 207-220, doi:10.1007/s00401-014-1371-2 (2015).

263 Mach, R. H. New targets for the development of PET tracers for imaging neurodegeneration in Alzheimer disease. *Journal of nuclear medicine : official publication, Society of Nuclear Medicine* **55**, 1221-1224, doi:10.2967/jnumed.114.127811 (2014).

264 Kelly, J. W. The alternative conformations of amyloidogenic proteins and their multi-step assembly pathways. *Current opinion in structural biology* **8**, 101-106 (1998).

265 Dobson, C. M. The structural basis of protein folding and its links with human disease. *Philosophical transactions of the Royal Society of London. Series B, Biological sciences* **356**, 133-145, doi:10.1098/rstb.2000.0758 (2001).

266 Wall, J. *et al.* Thermodynamic instability of human lambda 6 light chains: correlation with fibrillogenicity. *Biochemistry* **38**, 14101-14108 (1999).

267 Wilcken, R., Wang, G., Boeckler, F. M. & Fersht, A. R. Kinetic mechanism of p53 oncogenic mutant aggregation and its inhibition. *Proceedings of the National Academy of Sciences of the United States of America* **109**, 13584-13589, doi:10.1073/pnas.1211550109 (2012).

268 Nielsen, L. *et al.* Effect of environmental factors on the kinetics of insulin fibril formation: elucidation of the molecular mechanism. *Biochemistry* **40**, 6036-6046 (2001).

269 Evans, K. C., Berger, E. P., Cho, C. G., Weisgraber, K. H. & Lansbury, P. T., Jr. Apolipoprotein E is a kinetic but not a thermodynamic inhibitor of amyloid formation: implications for the pathogenesis and treatment of Alzheimer disease. *Proceedings of the National Academy of Sciences of the United States of America* **92**, 763-767 (1995).

270 Necula, M. *et al.* Methylene blue inhibits amyloid Abeta oligomerization by promoting fibrillization. *Biochemistry* **46**, 8850-8860, doi:10.1021/bi700411k (2007).

271 Necula, M., Kayed, R., Milton, S. & Glabe, C. G. Small molecule inhibitors of aggregation indicate that amyloid beta oligomerization and fibrillization pathways are independent and distinct. *The Journal of biological chemistry* **282**, 10311-10324, doi:10.1074/jbc.M608207200 (2007).

272 Blanchard, B. J. *et al.* Efficient reversal of Alzheimer's disease fibril formation and elimination of neurotoxicity by a small molecule. *Proceedings of the National Academy of Sciences of the United States of America* **101**, 14326-14332, doi:10.1073/pnas.0405941101 (2004).

273 Pallitto, M. M., Ghanta, J., Heinzelman, P., Kiessling, L. L. & Murphy, R. M. Recognition sequence design for peptidyl modulators of beta-amyloid aggregation and toxicity. *Biochemistry* **38**, 3570-3578, doi:10.1021/bi982119e (1999).

274 Trexler, A. J. & Rhoades, E. Function and dysfunction of alpha-synuclein: probing conformational changes and aggregation by single molecule fluorescence. *Molecular neurobiology* **47**, 622-631, doi:10.1007/s12035-012-8338-x (2013).

275 Arkin, M. R. & Wells, J. A. Small-molecule inhibitors of protein-protein interactions: progressing towards the dream. *Nature reviews. Drug discovery* **3**, 301-317, doi:10.1038/nrd1343 (2004).